# Wide-Area Backup Protection in Power Systems with High Penetration of Renewable Energy Sources


Mohammad Rezaei Jegarluei

University of Leeds

School of Electronic and Electrical Engineering

Submitted in accordance with the requirements for the degree of

*Doctor of Philosophy*

December, 2023

Dedicated to my beloved late father, **Aliasghar Rezaei Jegarluei**, this thesis is a testament to the values he instilled in me - perseverance, determination, and a thirst for knowledge. I will forever hold onto the lessons he taught me, and the unwavering love he showered upon me.

Dad, your presence may be missed, but your spirit lives on in everything I do. It is with profound love with tears in my eyes that I dedicate this thesis to you, my dearest father.

# Intellectual Property Statement

The candidate confirms that the work submitted is his own, except where work that has formed part of jointly authored publications has been included. The contribution of the candidate and the other authors to this work has been explicitly indicated below. The candidate confirms that appropriate credit has been given within the thesis where reference has been made to the work of others.

The work in Chapters 1 and 2 of the thesis has appeared in the following publications:

1. M. R. Jegarluei, J. S. Cortes, S. Azizi and V. Terzija, "Wide-Area Event Identification in Power Systems: A Review of the State-of-the-Art," *2022 International Conference on Smart Grid Synchronized Measurements and Analytics (SGSMA*), Split, Croatia, May 2022, pp. 1-7.

   As the lead author, the candidate performed the literature review, formulated the objective of the review paper, and wrote the paper.

   Dr Sadegh Azizi, my supervisor, supervised the work, modified the text, proof-read the drafts, and made suggestions and corrections to the paper.

   Jesus Sanchez Cortes and Prof. Vladimir Terzija reviewed the final draft of the paper and provided some suggestions.

2. S. Azizi, M. Rezaei Jegarluei, J. Sanchez Cortes, V. Terzija, "State of the Art, Challenges and Prospects of Wide-Area Event Identification on Transmission Systems," *International Journal of Electrical Power and Energy Systems*, Volume 148, 2023, 108937.

This journal paper is an extended version of the previous conference paper. The candidate performed the literature review, wrote the introduction, and contributed to writing the paper.

Dr Sadegh Azizi, my supervisor, supervised the work and helped to write the main body of the paper, modified the text, and made corrections to the paper.

Jesus Sanchez Cortes and Prof. Vladimir Terzija reviewed the final draft of the paper and provided some suggestions.

The work in Chapter 3 of the thesis has appeared in the following publications:

3. M. R. Jegarluei, A. S. Dobakhshari, and S. Azizi, "Reducing the Computational Complexity of Wide-Area Backup Protection in Power Systems," *IEEE Transactions on Power Delivery*, vol. 37, no. 3, pp. 2421-2424, 2022.

   As the lead author, the candidate performed all the computational as well as simulation work and wrote the paper.

   Dr Sadegh Azizi, my supervisor, supervised the work, modified the text, proof-read the drafts, and made suggestions and corrections to the paper.

   Dr Ahmad Salehi Dobakhshari reviewed the final draft of the paper and provided some suggestions.

4. M. R. Jegarluei, T. E. H. El-Gorashi, J. M. H. Elmirghani and S. Azizi, "A Generalized Closed-From Solution for Wide-Area Fault Location by Characterizing the Distributions of Superimposed Errors," *IEEE Transactions on Power Delivery*, vol. 37, no. 6, pp. 5484-5487, Dec. 2022.

   As the lead author, the candidate performed all the computational as well as simulation work and wrote the paper.

   Dr Sadegh Azizi, my supervisor, supervised the work, modified the text, proof-read the drafts, and made suggestions and corrections to the paper.

   Dr Taisir E. H. El-gorashi and Prof. Jaafar M. H. Elmirghani reviewed the final draft of the paper and provided some suggestions.

The work in Chapters 1 and 4 has appeared in the following publications:

5. M. Rezaei Jegarluei, P. Aristidou, S. Azizi, "Wide-Area backup protection against asymmetrical faults in the presence of renewable energy sources," *International Journal of Electrical Power and Energy Systems*, Volume 144, 2023, 108528, ISSN 0142-0615.

   As the lead author, the candidate performed all the computational as well as simulation work and wrote the paper.

   Dr Sadegh Azizi, my supervisor, supervised the work, modified the text, proof-read the drafts, and made suggestions and corrections to the paper.

   Dr Petros Aristidou reviewed the final draft of the paper.

6. M. Rezaei Jegarluei, A. S. Dobakhshari, M. Popov, V. Terzija, and S. Azizi, "PMU-based backup protection in the presence of inverter-based resources," *International Conference on Energy Technologies for Future Grids (ETFG)*, Wollongong, Australia, 2023.

   A full version of this paper will also be submitted to *IEEE Transactions on Industry Applications*.

   As the lead author, the candidate performed all the computational as well as simulation work and wrote the paper.

   Dr Sadegh Azizi, my supervisor, supervised the work, modified the text, proof-read the drafts, and made corrections to the paper.

   Dr Ahmad Salehi Dobakhshari, Prof. Marjan Popov, and Prof. Vladimir Terzija reviewed the final draft of the paper and provided some suggestions.

The work in Chapter 5 of the thesis has appeared in the following publication:

7. M. Rezaei Jegarluei, P. Aristidou, W. Fernandes and S. Azizi, "Wide-Area Backup Protection Using Sparse Synchronized/Unsynchronized PMU Measurements," *IEEE Transactions on Power Delivery*, vol. 38, no. 4, pp. 2630-2640, Aug. 2023.

As the lead author, the candidate performed all the computational as well as simulation work and wrote the paper.

Dr Sadegh Azizi, my supervisor, supervised the work, modified the text, proof-read the drafts, and made suggestions and corrections to the paper.

Dr Petros Aristidou and William Fernandes reviewed the final draft of the paper and provided some suggestions.

# Acknowledgements

I want to express my appreciation and gratitude to my main supervisor, **Dr. Sadegh Azizi**. His insightful guidance has been invaluable throughout my PhD journey. His invaluable advice and research ideas have been instrumental in shaping my work. I feel fortunate to have a mentor who has dedicated so much of their time to supporting me.

I would like to sincerely thank my dear friend **Jesus Sanchez Cortes** for his constant support and encouragement throughout this journey. His friendship and presence made this challenging journey much more bearable. Additionally, I would like to thank all of my co-authors for their contributions, lessons, advice, and comments at various stages of my research. Their input has greatly enriched my work and I am truly grateful for their support.

I would like to express my deepest gratitude to my dear wife, **Niousha Nateghi**, for her tremendous support and understanding during my PhD journey. Her belief in my abilities, patience during long hours of work, and unwavering support in both good and challenging times have been invaluable. She has been my pillar of strength, always cheering me on when I needed it most. Her love and belief in me have been the driving force behind my success. Thank you, my dear wife, for everything you have done for me.

# Abstract

Due to the unique fault behaviours of renewable energy sources (RESs), the growing integration of RESs poses new challenges to the effectiveness of conventional protection systems. Additionally, protection schemes must contend with typical issues such as hardware failures, deficiencies in logic, and measurement errors. One significant benefit of PMUs is their ability to facilitate wide-area backup protection (WABP) to address the shortcomings of local protection schemes. Ensuring the reliability of protection systems in the presence of RESs requires a comprehensive understanding of the unique fault behaviour of RESs as per their various control strategies. This, however, has not been well addressed in the WABP methods in the literature. In this work, this understanding is combined with taking advantage of PMUs for the design of effective WABP methods. This work proposes robust WABP methods for transmission systems with high penetration of RESs. The methods are aimed at addressing practical challenges such as temporary loss of the time-synchronisation signal (LTSS), sparse PMU coverage, and communication failures and latencies without placing any rigid constraints on PMU locations.

Novel formulations with low computational burden are proposed to identify the faulted line in near real-time based on the superimposed-circuit methodology and the weighted least-squares method. The main contributions of the present thesis can be summarised as follows: (*i*) A technique is proposed for reducing the computational complexity of WABP methods that are based on the superimposed-circuit methodology; (*ii*) A rigorous derivation of the equation weights is proposed based on the statistical distributions of the superimposed errors to be used in the weighted least-squares method; (*iii*) Non-linear fault behaviours of RESs are captured while maintaining the linearity of the WABP formulation and accounting for any penetration level, locations, and control strategies for RESs; (*iv*) A new methodology is proposed that can work well with unsynchronised and delayed measurements without imposing a significant computational burden.

Simulation studies conducted on the IEEE 39-bus test system verify the superiority of the proposed methods over existing methods and the robustness of the proposed methods against influential factors such as measurement and parameter errors and other practical challenges, e.g., LTSS, sparse PMU coverage, and communication failures and latencies.

# CONTENTS

# Abbreviations

| | |
|---|---|
| AC | Alternating Current |
| AFDE | Average Fault Distance Error |
| AFLE | Average Fault Location Error |
| CB | Circuit Breaker |
| CT | Current Transformer |
| DD | Dependence Degree |
| DC | Direct Current |
| DFT | Discrete Fourier Transform |
| FL | Fault Location |
| FLC | Fault Location Candidate |
| FLISR | Faulted-Line Identification Success Rate |
| GC | Grid Code |
| LNRT | Largest Normalized Residual Test |
| LIFR | Line Identification Failure Rate |
| LTSS | Loss Of The Time Synchronization Signal |
| LVRT | Low-Voltage Ride-Through |
| MD | Mismatch Degree |
| IBR | Inverter-Based Resource |
| POMISR | Operating Mode Identification Success Rate |
| OLS | Ordinary Least-Squares |
| PC | Personal Computer |
| PMU | Phasor Measurement Unit |
| PCC | Point of Common Coupling |
| PWM | Pulse Width Modulation |
| RAM | Random Access Memory |
| RV | Random Variable |
| RES | Renewable Energy Source |
| SCADA | Supervisory Control And Data Acquisition |
| TVE | Total Vector Error |
| VSC | Voltage Source Converter |
| VT | Voltage Transformer |
| WLS | Weighted Least-Squares |
| WSSR | Weighted Sum Of Squared Residual |
| WABP | Wide-Area Backup Protection |
| WAFL | Wide-Area Fault Location |

# NOMENCLATURE

| | |
|---|---|
| $\boldsymbol{Y}$ | Admittance matrix |
| $\boldsymbol{Z}$ | Bus impedance matrix |
| $\boldsymbol{Z}^{(i,j)}$ | Bus impedance matrix of the network with the line $i-j$ remove |
| $z_l$ | Series impedance of the line |
| $y_l$ | Shunt admittance of the line |
| $Z_{ij}$ | The element in the $i$-th row and $j$-th column of the bus impedance matrix |
| $Z^c_{u,v}$ | Characteristic impedance of line $u-v$ |
| $\gamma_{u,v}$ | Propagation constant of line $u-v$ |
| $l_{u,v}$ | Length of of line $u-v$ |
| $C_{uv,q}$ | Coefficient for $\Delta J_{uv}$ relating to the nodal current source at bus $q$ |
| $Z^{T,s}_{u,f}$ | Transfer impedance between bus $u$ and $f$ in the sequence circuit "$s$" |
| $\boldsymbol{V}^{\text{pre}}$ | Vector of bus voltages before the fault |
| $\boldsymbol{V}^{\text{post}}$ | Vector of bus voltages after the fault |
| $\boldsymbol{I}^{\text{pre}}$ | Vector of nodal currents before the fault |
| $\boldsymbol{I}^{\text{post}}$ | Vector of nodal currents after the fault |
| $\Delta V_i$ | Superimposed voltage of bus $i$ |

| | |
|---|---|
| $\Delta I_j$ | Superimposed nodal current injection at bus $j$ |
| $\Delta J_{uv}$ | Superimposed branch current from bus $u$ to bus $v$ |
| $+$ | Superscript for the positive sequence circuit |
| $-$ | Superscript for the negative sequence circuit |
| $\boldsymbol{m}$ | Measurement vector |
| $\boldsymbol{H}$ | Coefficient matrix |
| $\boldsymbol{\varepsilon}$ | Error vector |
| $\boldsymbol{x}$ | Unknown vector: vector of unknown nodal current injections |
| $\hat{\boldsymbol{x}}$ | Vector of estimates of unknowns |
| $\boldsymbol{R}$ | Covariance matrix of measurement errors |
| $\boldsymbol{W}$ | Weight matrix |
| $\boldsymbol{S}$ | Residual sensitivity matrix |
| $\boldsymbol{r}$ | Vector of residuals |
| $\alpha_{i,j}$ | Fault distance on line $i-j$ |
| $e^{j\theta_k}$ | Phase angle operators for bus $k$ representing LTSS |
| $I_f^+$ | Fault current in the positive sequence circuit |
| $I_f^-$ | Fault current in the negative sequence circuit |
| $y = re^{j\theta}$ | Random variables representing the pre-fault synchrophasors |
| $y' = r'e^{j\theta'}$ | Random variables representing the post-fault synchrophasors |
| $\varepsilon_r$ | Error in the magnitude of the pre-fault synchrophasors |
| $\varepsilon_\theta$ | Error in the angle of the pre-fault synchrophasors |
| $\varepsilon_{r'}$ | Error in the magnitude of the post-fault synchrophasors |

| | |
|---|---|
| $\varepsilon_{\theta'}$ | Error in the angle of the post-fault synchrophasors |
| $\sigma_r^2$ | Variance of the error in the magnitude of the pre-fault synchrophasors |
| $\sigma_\theta^2$ | Variance of the error in the angle of the pre-fault synchrophasors |
| $\sigma_{r'}^2$ | Variance of the error in the magnitude of the post-fault synchrophasors |
| $\sigma_{\theta'}^2$ | Variance of the error in the angle of the post-fault synchrophasors |
| $\mu_{\epsilon_m}^2$ | Mean of superimposed error |
| $\sigma_{\epsilon_m}^2$ | Variance of superimposed error |
| $\mu_r$ | True values of the magnitudes of the pre-fault synchrophasors |
| $\mu_\theta$ | True values of the magnitudes of the pre-fault synchrophasors |
| $\mu_{r'}$ | True values of the magnitudes of the post-fault synchrophasors |
| $\mu_{\theta'}$ | True values of the magnitudes of the post-fault synchrophasors |
| $v_\alpha^+$ , $v_\beta^+$ | Postive sequence voltage in $\alpha\beta$ reference frame |
| $v_\alpha^-$ , $v_\beta^-$ | Negative sequence voltage in $\alpha\beta$ reference frame |
| $v_d^+, v_q^+$ | Postive sequence voltage in $dq$ reference frame |
| $v_d^-$ , $v_q^-$ | Negative sequence voltage in $dq$ reference frame |
| $P_{ref}$ | IBR reference values for the active power |
| $Q_{ref}$ | IBR reference values for the reactive power |
| $z^-$ | Equivalent negative-sequence impedance of the IBR |
| $\theta^-$ | Phase angle of the per-unit equivalent negative-sequence impedance of the IBR |
| $i_{\max}^-$ | IBR's maximum negative-sequence current |
| $i_{\max}^+$ | IBR's maximum positvie-sequence current |
| $i_{\max}$ | IBR's maximum total current |

$i^{+}_{d-ref}, i^{+}_{q-ref}$ dq-axis reference current in the positive-sequence circuit

$i^{-}_{d-ref}, i^{-}_{q-ref}$ dq-axis reference current in the negative-sequence circuit

$S_n$ Nominal power

$S(t)$ Connectivity status of the IBR

$\boldsymbol{x}^{unm}$ Vector of superimposed currents of unmonitored IBRs

$\boldsymbol{m}^{mod}$ Modified measurement vector

$\boldsymbol{m}^{\text{exp,s}}$ Expected superimposed measurement vector

$\boldsymbol{h}^{s}_{f}$ Vector of coefficient at fault location in the sequence circuit "$s$"

$\boldsymbol{h}^{s}_{FLC}$ Vector of coefficient at FLC in the sequence circuit "$s$"

$MD^{mag}$ Mismatch degree of magnitudes

$MD^{ang}$ Mismatch degree of phase-angles

$\theta^{\text{LTSS}}_{k}$ Unknown angle drifts caused by LTSS at substation $k$

$MD_{m,h}$ Mismatch degree between $m$ and $h$

$DD_{h_1,h_1}$ Dependence degree between $h_1$ and $h_2$

$N_{FLC}$ Number of FLCs

$T_{mul}$ Time needed for conducting a multiplication operation

$T_{\text{sum}}$ Time needed for conducting a summation operation

$P$ Number of PMUs

$N_p$ Number of measurements

$N_L$ Number of transmission lines

$Nm$ Number of monitored IBRs

$Nn$ Number of unmonitored IBRs

# LIST OF FIGURES

# LIST OF TABLES

# CHAPTER 1

Introduction

## 1.1 Overview

The reliability of protection schemes is an essential factor to consider for ensuring the secure operation of power systems in the presence of various contingencies. Dependability and security are key aspects characterising the reliability of a well-designed protection scheme [1]. Local protection refers to the use of protective devices within the substation to detect and respond to faults or abnormal conditions in order to prevent damage to equipment and ensure the safety of personnel. Local protection schemes are not ideal and their reliability may occasionally be compromised for different reasons [2]. Besides the typical deficiencies of local protections, they are now dealing with new practical issues. The integration of renewable energy sources (RESs) into the electricity grid is typically achieved through power-electronic inverters. These are also known as inverter-based resources (IBRs). IBRs behave differently during faults compared to synchronous generators, which makes conventional protection systems less reliable [3].

The advent of phasor measurement units (PMUs) has opened a promising avenue to wide-area monitoring, protection, and control in power systems [4]. Such applications present great potential for overcoming the growing complexity of power systems by complementing local protection/control practices and covering for their insufficiencies. The proliferation of PMUs has paved the way for wide-area backup protection (WABP) as a complementary means for addressing shortcomings of local protections [4]. In this context, WABP is defined as the processing of phasors provided by PMUs and other intelligent electronic devices to identify the faulted line and generate appropriate protection commands accounting for local protection failures. The integration of WABP with local protections offers several advantages. WABP can identify faults that may occur in areas where local protection devices have failed to operate or are unable to detect the fault accurately. These faults, if undetected, could propagate and cause widespread power system disruptions.

## 1.2 Research Motivations and Problem Statement

Timely and accurate fault location is beneficial to power system stability and operation. One of the main causes of failures in protection systems lies with the measurement errors of voltage and current phasors during short-circuit faults. Erroneous measurements during a fault incident

are originally caused by the transient behaviour of voltage and current transformers which are installed close to the fault location [2, 5]. As the measurement points for local protection systems could be quite close to the fault location, they are prone to erroneous measurements, which could result in misoperation or maloperation. In case of a failure in the main protection system, backup protection is an indispensable element of protection systems that conduct the last protective actions trying to remove the faulted parts and sustain the operation of the healthy sections of the power system. Therefore, in terms of dependability, backup protection is of critical importance as its failure might cause cascading events and even major blackouts [5, 6].

Moreover, the security of backup protection is also crucial. As power systems are spread over extensive geographical areas with lots of interconnected grids of transmission lines, protection systems are always prone to misoperating over a healthy section of the power system. For example, backup distance relays might make unwanted actions when transmission lines are utilised close to their operational limits [6]. Specifically speaking, undesired operation of the third zone of backup distance relays, has been known as an imposing cause of cascading outages, which potentially can culminate in blackouts [2, 7].

In addition to the typical deficiencies of local primary/backup protections due to hardware failures, incorrect settings, logic deficiency, and measurement errors [2, 8], local protections have recently faced new practical issues. Renewables are usually connected to the rest of the electricity grid through power-electronic inverters as interface. This enables IBRs to offer distinguished controllability characteristics [3]. IBRs exhibit distinctive fault behaviours compared to synchronous generators, thereby making the design logic of conventional protection systems less reliable or even invalid. IBRs are causing pressing protection challenges as evidenced by increasing misoperation and malfunction cases of distance, unbalanced current, and directional protection functions [9, 10].

In response to the above challenges, traditional power system protection practices have received remarkable attention and witnessed some improvements in recent years. It might be conceivable to propose some local protection schemes, i.e., with adaptive features, to overcome any challenges in all situations. However, it is neither economical nor practical to replace or modify all existing local protective relays concerning the ongoing RES installation in the system [11]. Thus, there is a growing need for new wide-area protection schemes to address the inherent concerns of protection systems and overcome challenges in the presence of RESs.

The proliferation of advanced metering devices such as PMUs along with communication systems readiness has opened new horizons for centralised protection of transmission systems. Voltage and current signals taken slightly farther away from the fault location might be more accurate than those taken from the faulted line terminals. This is because the transient response of an instrument transformer will be smaller and less disturbing when the sudden change it undergoes is smaller [2, 4]. In this context, PMU-based protection is one of the numerous applications of PMU data. However, it can hardly be employed for primary protection due to corresponding communication latencies.

A WABP method would be advantageous to the system operators if it can make swift yet reliable decisions and offers the following characteristics [4, 6]:

- **Accounting for high penetration of renewable energy sources:** High penetration of RESs is introducing huge changes into well-established operational and control paradigms of power systems. This is because IBRs demonstrate distinguished dynamic behaviours that significantly differ from those of synchronous generators. Appropriate adjustments to almost all existing WABP methods or the development of new ones are deemed necessary if we are to accommodate the presence of RESs in the system [12].
- **Independence from the operation statuses of circuit breakers and protective relays:** As backup protection, WABP should not rely on the data coming from local protective and control relays. This is necessary as otherwise, the WABP method will not function properly in cases of circuit breaker failures and relay malfunction/misoperation [13].
- **Ability to detect the fault type and faulted phases:** This is to enable single-pole tripping of circuit breakers (CBs) following single-phase-to-ground faults [11].
- **Remaining valid after non-simultaneous single- or three-pole tripping of CBs:** The openings of the CBs at the two line ends rarely occur simultaneously. Instead, one- or three-pole of the CB at one end of the faulted line might be opened shortly after the fault inception. Therefore, the WAFL formulations are to remain reliable after fast single-end, one- or three-pole disconnection of lines [14].
- **Low sensitivity to fault resistance:** Fault resistance is of a random magnitude and

highly nonlinear by nature. To ensure the security and dependability of WABP, the underlying WAFL is to be robust against the magnitude of fault resistance [15].

In addition, a WABP method should be able to tackle the following system-wide practical challenges to stand a chance to be implemented in practice.

- **Sparse PMU coverage:** PMU installation at every substation cannot be guaranteed due to infrastructure and budget limitations. To guarantee reliable continuous service, therefore, full network observability should not be a prerequisite of any WABP methods [4].
- **PMU malfunction and communication failures:** Power systems are subject to the misoperation of metering devices and failures in the communication infrastructure. WABP methods should be robust against these unpredictable and unavoidable challenges [16].
- **Unacceptably long communication latencies:** Even if the power system were fully observable, it could not be assumed that all measurements are received on time. Loss of data and communication latencies occur quite often in power system operations [15].
- **Loss of the time-synchronisation signal (LTSS):** The phasors estimated by a PMU are synchronised to its local time reference. If a PMU temporarily stops receiving the time-synchronisation signal, its phasors might start drifting away from phasors calculated by other time-synchronised PMUs [13, 17].
- **Measurement errors and bad data:** Measurement errors attached to meter accuracy, misconfiguration, and noise. Larger errors can be attributed to biased or wrongly connected meters and cyberattacks that might lead operators to bad decision-making [12].

This research is focused on developing reliable and computationally efficient WABP methods that are able to capture the behaviour of IBRs, offer the required practical characteristics, and cope with system-wide challenges.

## 1.3 Literature Review

Transmission lines are usually protected by local main and backup protection systems. Various schemes for main and backup protection are implemented in protective relays such as distance,

differential, and over-current protection. As shown in Figure 1.1, traditional backup protection systems, or simply backup protective relays, can be categorised into two types. The first type which is usually known as local backup relays, are locally installed in parallel with the main protective relays. For example, in Figure 1.1, relays R1-2 and R2-2 act as backup relays for Line 1 and Line 2, respectively. They usually have distinct circuits and protection philosophy from those of the main relays to avoid mutual failure causes. The second type which is typically known as remote relays, are located at adjacent substations and need to be coordinated with the local relays. For instance, in Figure 1.1, relays R1-1 or R1-2 at line 1 can be considered remote backup relays for Line 2. Typical schemes usually used in traditional remote backup protection are phase overcurrent, earth fault overcurrent, and overreaching zones of distance relays [2, 5]. Since the measurement points for local main and backup protection systems are almost the same, they experience equal short circuit current and voltage dip following a fault incident. As a result, erroneous measurements could result in the maloperation of both the local main and backup protective relays.

WABP methods would be highly advantageous to implement in order to overcome or at least alleviate emerging protection challenges [11, 12]. There has been a growing interest in WABP over recent years to complement local protection schemes. PMU-based protection systems have also been receiving more attention for implementation in practice in recent years, e.g., in Ecuador and India [18]. Due to the inherent limitations of WABP, e.g., originating from communication latencies, WABP is not supposed to replace the local main/backup protection but complement it [4].

Operation philosophies of conventional protection schemes have mainly been developed for power systems dominated by synchronous machines. On the other hand, renewable energy sources demonstrate exclusive fault characteristics that significantly differ from those of synchronous generators. Thus, the high penetration of renewables is making some underlying

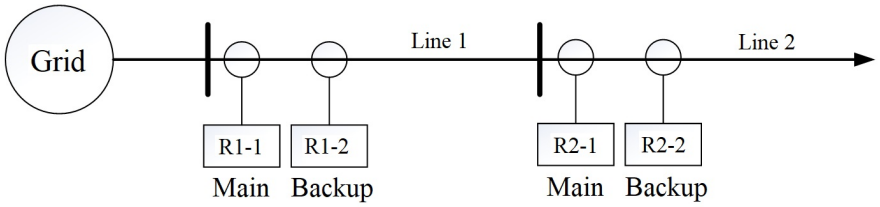


Figure 1.1: Example of local main and backup protection.

assumptions of conventional protection schemes increasingly invalid. This can adversely affect the performance of protection systems, which is demonstrated by more cases of maloperation and malfunction of protective relays [9, 19, 20]. For instance, the distinctive negative-sequence fault current contribution of renewables can easily mislead the negative-sequence overcurrent and communication-assisted protections following asymmetrical faults [21]. In addition, high penetration of RESs can cause instability in voltage and frequency levels, which can impact the performance of local protective relays. Furthermore, the intermittent nature of renewable energy sources can make fault detection and clearance more challenging [9].

Many wide-area fault location (WAFL) methods are only suited to offline purposes [17, 22–25] as they suffer from technical difficulties introduced by iterative solving processes and non-linear formulations. These methods are computationally demanding and not flexible enough to deal with practical challenges. As they are essentially designed for offline calculations, the inherent attributes of these methods make them unsuitable for WABP.

Great efforts have also been made in the literature to develop WABP methods to account for deficiencies of local backup protection. In [26, 27], the operation statuses of CBs and protective relays are used to identify the faulted line. However, the performance of these methods may be impaired in the case of CB failures and relay malfunctions. In [28], an effective WABP method is presented using the residual vector of a synchrophasor state estimator. However, subject to the PMU placement, this method might not be able to infer the presence or absence of a fault on some lines.

The WABP methods presented in [29–42] require the availability of PMUs at certain locations and suffer from one or more of the challenges pointed out in the previous section. Nevertheless, PMUs are normally installed considering financial constraints and the availability of communication infrastructure rather than the necessities of a specific functionality [43]. As these methods need PMU data from certain locations, they cannot tolerate PMU losses. It is worth mentioning that methods presented in [33, 40–42, 44, 45] can only identify the faulted line, and do not provide the exact location of the fault on the faulted line.

The method in [11] is a pioneer superimposed-circuit-based WABP method based on voltage measurements. The work is further developed in [15] by incorporating both voltage and current measurements. Similar to many other WABP methods, these two methods are sensitive to the temporary loss of the time synchronisation signal (LTSS). In response, research works such

as [13] tackle the possibility of unsynchronised input phasors with the cost of the noticeably higher computational burden.

RESs are characterised by their controllability features, which are barely accounted for by the existing WAPB methods. IBRs can rapidly regulate the amplitude and phase angle of their terminal voltage and current to meet their control targets in the steady-state, fault, and post-fault conditions within a few milliseconds [46]. None of the methods mentioned above can account for RESs assuming all generating units are synchronous machines. In these methods, synchronous generators are modelled as an impedance behind an ideal voltage source, which means they are modelled by a constant impedance in the superimposed circuit. However, this modelling technique, cannot be employed for RESs because of their time-variant nature and distinguished fault behaviour, which calls for innovative solutions. To utilise the methods in [11, 13, 15, 17, 34, 38, 39, 47–49], one needs to disregard the presence of RESs in the power system. However, simulations show that this approach might easily lead to misoperation or malfunction of the WABP method.

Table 1.1 summarises some important features of the most effective WAFL/WABP methods in the literature. As can be seen, the linear method of [13] outperforms most of the other methods as they are all sensitive to the loss of the time synchronisation signal. The nonlinear method presented in [17] is another method that can function with unsynchronised measurements but at the expense of an iterative solving process. The method is thus computationally demanding and prone to the multiplicity of solutions. The WABP methods proposed in [29, 30, 32–34, 37, 38, 50, 51] place certain constraints on PMU numbers and locations to be operative.

As will be explained in Section 2.3 single- or three-pole disconnection of the faulted line from one end will not affect the validity of the superimposed-circuit-based WABP. In addition, other WABP methods normally cannot tolerate PMU losses or long communication latencies as they require a specific set of PMU data [34, 39, 54].

The majority of WABP methods proposed thus far have non-linear formulations and have been designed for conventional power systems. These methods do not take renewable generations into account, which makes them less attractive to system operators given the increasing penetration of RESs in power systems. Improving the reliability of local protection schemes in the presence of renewable energy sources has received remarkable attention in recent years

Table 1.1: Performance Comparison Between Different WAFL/WABP Methods

| Reference | [29, 30, 34, 37] | [11, 51, 52] | [17] | [13] | [40] | [41] | [53] | [42] | [44] | [45] |
|---|---|---|---|---|---|---|---|---|---|---|
| Tolerate Loss of PMUs? | No | Yes | Yes | Yes | No | No | No | No | No | Yes |
| Need Time-Synch Signal? | Yes | Yes | No | No | Yes | Yes | Yes | Yes | Yes | Yes |
| Involve Iterative Solution? | No | No | Yes | No | No | Yes | No | Yes | No | No |
| Need Specific PMU Placement? | Yes | No | No | No | Yes | Yes | Yes | Yes | No | No |
| Identify 1-ph-g faults? | No | No | No | Yes | No | No | No | No | Yes | No |
| Accurate over time? | No | No | No | Yes | No | Yes | Yes | Yes | Yes | No |
| Computationally expensive? | No | No | Yes | No | No | Yes | Yes | No | No | Yes |
| Need statuses of CBs /relays? | No | No | No | No | No | No | No | No | No | No |
| Valid for non-sim. CB opening? | No | No | No | Yes | No | No | No | No | No | No |
| Valid for 1-p CB opening? | No | No | No | Yes | No | No | No | No | No | No |
| Sensitivity to fault resistance | Low | Low | Low | Low | N/A | N/A | N/A | N/A | N/A | N/A |
| Identify faults in substations? | No | No | No | No | Yes | No | No | No | Yes | No |
| Identify faults in transformers? | No | No | No | Yes | Yes | Yes | No | No | Yes | Yes |
| Address the presence of RESs? | No | No | No | No | No | No | No | No | No | No |

[55–58]. To overcome the protection challenges introduced by renewables, more sophisticated local/wide-area methods with adaptive features are needed.

The presence of renewable energy sources in the transmission system has been accounted for by a few WABP methods over the previous years [42, 59–63]. The authors in [59] present a method that complements distance protection by WABP. Faulted line identification is accomplished by monitoring the absolute impedance angles of certain lines in the positive-sequence circuit. One major shortcoming of this method is its reliance on specific PMU placements. A communication-free active protection strategy for inverter-dominated power systems is presented in [63], which is only applicable to islanded microgrids. As will be demonstrated in Chapter 4, the superimposed-circuit methodology has proved to be flexible enough to account for the presence of RESs in the power system [12].

## 1.4 Research Objectives

The primary objective of this research is to propose and develop reliable and computationally efficient WABP methods that can effectively identify the faulted line in modern power systems with high penetration of renewable energy sources. The proposed methods are aimed to be applicable in real-time scenarios, be capable of providing essential prerequisites of power system protection, and cope with practical system-wide challenges related to the available wide-area data and measurements. In order to achieve these goals, the following objectives have been defined:

1. To critically analyse the existing WABP/WAFL methods in the literature. The aim is to assess their potential for improving the protection of transmission lines in modern and complex power systems and addressing practical challenges of wide-area applications.

2. To identify and describe the necessary prerequisites for WABP methods as protective elements against short circuit faults in the power systems for their successful implementation in real-world scenarios.

3. To propose a technique that reduces the computational complexity of WABP methods that are based on the superimposed-circuit methodology.

4. To improve the accuracy of the superimposed-circuit-based WABP methods that utilise the weighted least-squares method through a rigorous formulation for determining the weights of the equations.

5. To incorporate the non-linear fault characteristics exhibited by RESs within power systems in superimposed-circuit-based WABP methods by addressing high levels of RES penetration with any geographic locations and various control strategies.

6. To propose a novel methodology that effectively handles unsynchronised and delayed measurements without imposing a significant computational burden.

Given the aforementioned objectives, the subsequent subsection presents a comprehensive overview of the specific contributions made by the thesis.

## 1.5 Performance Evaluation Methodology in the Thesis

The performance of the proposed methods will be evaluated through plenty of Electro-Magnetic Transients (EMT) simulations with an integration step size of 0.1 milliseconds on the New England 39-bus system. DIgSILENT power factory software will be used as the simulator to model the test system and simulate different types of faults on various points of the system. In this project, different control strategies of IBRs in both positive and negative sequence circuits will be modelled by DSL tools in the DIgSILENT power factory software. The extensive simulations are automatised via DPL tools in the DIgSILENT power factory.

Using MATLAB software, simulated time-domain voltage and current waveforms are put through an anti-aliasing Butterworth filter and sampled with a practical sampling frequency, e.g. 2 kHz. The Discrete Fourier Transform (DFT) and a real PMU model [64] are used to estimate phasors of recorded time-domain waveforms. For conducting sensitivity analysis against input errors, the measurement and parameter errors are applied to the vector of measurements and system parameters in MATLAB. The communications failure/latencies and loss of time synchronisation signal are also applied to the vector of measurements in MATLAB.

## 1.6 Thesis Contributions and Related Publications

The main contributions of the present thesis are:

(i) The WABP/WAFL methods in the literature are critically examined for their potential to enhance the protection of transmission lines in modern and complex power systems. Specifically, the superimposed-circuit methodology is elucidated and endorsed as a robust approach capable of mitigating system-wide challenges, including communication latencies, communication failures, sparse PMU coverage, measurement inaccuracies, bad data, and the loss of time synchronisation signals. Additionally, this study identifies and describes certain imperative prerequisites of WABP methods to ensure their feasibility and implementation in real-world scenarios.

Regarding this contribution, the materials presented in Chapters 2 and 3 of this thesis are supported by the following publications [12, 65]:

M. R. Jegarluei, J. S. Cortes, S. Azizi and V. Terzija, "Wide-Area Event Identification in Power Systems: A Review of the State-of-the-Art," *2022 International Conference on Smart Grid Synchronized Measurements and Analytics (SGSMA*), Split, Croatia, May 2022, pp. 1-7.

S. Azizi, M. Rezaei Jegarluei, J. Sanchez Cortes, V. Terzija, "State of the art, challenges and prospects of wide-area event identification on transmission systems," *International Journal of Electrical Power and Energy Systems*, Volume 148, 2023, 108937.

(ii) A technique is proposed for reducing the computational complexity of superimposed-circuit-based WABP methods. A proposition is presented and proved to justify that the system of equations pertaining to every candidate line can be directly obtained from the bus impedance matrix of the pre-fault power system. This is in contrast with existing WABP methods requiring the establishment of as many distinct bus impedance matrices as the number of candidate lines in the power system [11, 13, 15, 34]. The proposed technique limits the foregoing requirement to merely calculating the bus impedance matrix of the pre-fault system.

Regarding this contribution, the materials presented in Chapter 3 of this thesis are sup-

ported by the following publication [66]:

M. R. Jegarluei, A. S. Dobakhshari, and S. Azizi, "Reducing the Computational Complexity of Wide-Area Backup Protection in Power Systems," *IEEE Transactions on Power Delivery*, vol. 37, no. 3, pp. 2421-2424, June 2022.

(iii) To apply the weighted least-squares method for WAFL/WABP, it is necessary to calculate the mean and variance of superimposed errors. This has not been considered in the existing superimposed-circuit-based methods [11, 13, 15, 17, 23, 34, 48, 67, 68]. In this thesis, these errors are determined using statistical distributions based on the errors of pre- and post-fault synchrophasors. By incorporating a carefully derived weight matrix into the formulation and considering both voltage and current synchrophasors, the proposed method significantly improves the accuracy of the results compared to similar WAFL/WABP methods. Furthermore, the linear nature of the formulation and the rigorous derivation of superimposed errors facilitate the application of established bad data detection methods.

Regarding this contribution, the materials presented in Chapter 3 of this thesis are supported by the following publication [69]:

M. R. Jegarluei, T. E. H. El-Gorashi, J. M. H. Elmirghani and S. Azizi, "A Generalised Closed-From Solution for Wide-Area Fault Location by Characterizing the Distributions of Superimposed Errors," *IEEE Transactions on Power Delivery*, vol. 37, no. 6, pp. 5484-5487, Dec. 2022.

(iv) In order to employ the methods presented in [11, 13, 15, 17, 34, 38, 39, 47–49] in modern power systems, it is imperative to overlook the existence of RESs within the system. Nevertheless, simulations indicate that adopting this approach may result in erroneous operation or failure of the WABP method. In this research work, a robust WABP method against asymmetrical faults is proposed for transmission systems with high penetration of renewables. The method, which is based on the negative-sequence circuit, exploits the full potential of available synchrophasors without placing any rigid constraints on PMU locations. To this end, the faulted line and a few appropriately selected RESs are replaced by equivalent current sources using the *Substitution Theorem*. The remaining

RESs are substituted by their equivalent impedances accounting for their response to a fault, considering the control strategies and overcurrent limits of these RESs. This results in a linear system of equations whose solution readily indicates the faulted line on account of the weighted sum of squared residuals concept.

Regarding this contribution, the materials presented in Chapter 4 of this thesis are supported by the following publication [70]:

M. Rezaei Jegarluei, P. Aristidou, S. Azizi, "Wide-Area backup protection against asymmetrical faults in the presence of renewable energy sources," *International Journal of Electrical Power and Energy Systems*, Volume 144, 2023, 108528, ISSN 0142-0615.

(v) A WABP method against all types of faults is proposed for transmission systems with high penetrations of RESs. The method, which is based on the positive-sequence circuit, relies neither on the system's full observability nor the availability of a predetermined set of PMU data. This is made possible by replacing RESs and the candidate line (i.e., a line that is assumed to be faulted) with appropriate nodal current sources in the superimposed circuit. Then, the currents of RESs without PMU measurements are calculated with respect to their power references and low-voltage ride-through (LVRT) characteristics. To find the actual faulted line amongst the set of candidate lines, a residual-based index is proposed based on the notion of superimposed circuits and the weighted least-squares method. A core achievement of the method is accounting for the non-linear fault behaviours of RESs while maintaining the linearity of the formulation. The method performs well with any penetration level, locations, and LVRT characteristics for RESs.

Regarding this contribution, the materials presented in Chapter 4 of this thesis are supported by the following publication [71]: .

M. Rezaei Jegarluei, A. S. Dobakhshari, M. Popov, V. Terzija, and S. Azizi, "PMU-based backup protection in the presence of inverter-based resources," *International Conference on Energy Technologies for Future Grids (ETFG)*, Wollongong, Australia, 2023.

A full version of this paper will also be submitted to *IEEE Transactions on Industry Applications*.

(vi) A WABP method is proposed for transmission systems using sparse synchronised/ unsynchronised PMU measurements. The method is aimed at addressing practical challenges such as temporary loss of the time-synchronisation signal (LTSS), sparse PMU coverage, and communication failures and latencies. A linear and computationally efficient formulation is proposed to identify the faulted line in near real-time based on the superimposed-circuit concept. An index is proposed that quantifies the mismatch degrees between the expected and observed superimposed phasors without requiring full network observability. Only a few methods in the literature account for the unsynchronised measurements caused by LTSS. The most effective method in the literature [13] is highly sensitive to inaccuracies in the superimposed measurements. Additionally, solving the presented system of equations in [13] necessitates inverting and multiplying large matrices, which hampers its efficiency for real-time applications. The proposed method in this thesis can work well with unsynchronised measurements without imposing a significant computational burden. Since no matrix inversion is involved, sparse PMU measurements do not result in singularity, and thus, the unsolvability of the equations. A technique is proposed to assess the feasibility of faulted-line identification by a given set of PMUs. Being robust against measurement and parameter errors, the method performs well with PMUs of different reporting rates regardless of the fault distance, type, and resistance.

Regarding this contribution, the materials presented in Chapter 5 of this thesis are supported by the following publication [16]:

M. Rezaei Jegarluei, P. Aristidou, W. Fernandes and S. Azizi, "Wide-Area Backup Protection Using Sparse Synchronized/Unsynchronized PMU Measurements," *IEEE Transactions on Power Delivery*, vol. 38, no. 4, pp. 2630-2640, Aug. 2023.

## 1.7 Thesis Outline

The rest of this thesis is structured as below

- **Chapter 2** provides a detailed explanation and endorsement of the superimposed circuit methodology for WABP. This methodology is characterised as a robust and effective approach for addressing a wide range of practical challenges encountered in real-world scenarios, including communication latencies and failures, partial network observability, sparse PMUs coverage, measurement errors, bad data, and the loss of time synchronisation signals. Then, the essential criteria for the successful implementation and practicality of WABP techniques are identified and explained.

- **Chapter 3** presents a technique for reducing the computational complexity of superimposed circuit-based WABP methods. A proposition is introduced and proved, showing that the system of equations relating to each potential faulted line can be directly derived from the bus impedance matrix of the power system before the fault occurs. The chapter demonstrates the existence of a one-to-one equivalence between the responses of the superimposed circuit with and without the faulted line. Moreover, a system of linear equations is formulated for the WAFL/WABP, which incorporates both voltage and current synchrophasors. This formulation enables the development of a generalised closed-form solution for identifying the faulted line and calculating the fault distance. The weighted least-squares method is employed to rigorously determine the equation weights, with the statistical distributions of the superimposed errors, i.e., the differences between the errors of the corresponding pre- and post-fault synchrophasors, serving as the basis for weight determination. The method's effectiveness, robustness against different factors, and superiority over existing methods are demonstrated by extensive simulations and comparison studies conducted on the IEEE 39-bus test system.

- **Chapter 4** presents a comprehensive analysis of the integration of RESs in the superimposed circuit-based WABP methods. The chapter starts by describing the configuration of IBRs, along with their relevant power control strategies and Grid Code requirements. Then, a novel WABP method is proposed for transmission systems with a high penetration of renewables, utilizing the negative-sequence circuit to address asymmetrical

faults. The proposed method is then modified to accommodate a large number of RESs, and the details of these modifications are provided. The performance of the method is evaluated through extensive simulations conducted on the IEEE 39-bus test system, demonstrating its effectiveness regardless of the number and location of RESs and their control strategies. Additionally, a novel WABP method is introduced, which is capable of addressing all types of faults by utilizing the positive-sequence circuit. The modifications made to the WABP formulation to handle the challenges posed by high penetration of RESs are then presented. Finally, simulation studies validate the superiority of this method compared to existing approaches and demonstrate its robustness against influential factors such as input inaccuracies.

- **Chapter 5** introduces a new method for WABP that aims to solve practical problems such as temporary loss of the time-synchronisation signal, sparse PMU coverage, and communication failures and latencies. The chapter first suggests an index that measures the discrepancy between expected and observed superimposed phasors. It then proposes a technique to determine if a given set of PMUs can accurately identify any faulted line. The chapter also discusses modifications made to overcome practical challenges. Finally, the results of extensive simulations conducted on the IEEE 39-bus test system are presented and analysed, confirming the effectiveness of the proposed method.

- **Chapter 6** summarises the contribution of this thesis and puts forward several suggestions for future works.

# CHAPTER 2

## Principals of Superimposed-Circuit Methodology and Its Application for WABP

## 2.1 Overview

The superimposed-circuit methodology is a technique used in electrical engineering to analyse complex circuits. It involves breaking down a circuit into simpler circuits and analyzing each one individually. The responses of each circuit are then combined to determine the overall behaviour of the complex circuit. This methodology is especially useful in circuits with multiple sources, as it allows engineers to understand how each source affects the circuit independently. By analyzing each source separately, one can more easily determine interactions and their impact on the overall circuit behaviour. It provides a systematic approach to circuit analysis, simplifying the process of understanding and troubleshooting complex circuits.

## 2.2 Superimposed-Circuit Methodology

Based upon the *Substitution Theorem* [72], any element can be replaced by proper nodal current sources. It is possible to do this such that the pre-disturbance and post-disturbance bus impedance matrices remain the same [13]. This will result in a system of linear equations (KVL and KCL equations) relating the superimposed voltage and current phasors to unknown nodal current sources that replaced the disturbed element. Applying the weighted least-squares method to the developed system of equations would enable the identification of the disturbed element. The disturbance of interest in this thesis is defined as sudden changes in nodal current injections in the circuit. Figures 2.1(a) and 2.1(b) show the corresponding pre- and post-disturbance circuits with the same topology but with nodal current sources of different values. Having the same topology and elements, the circuits of Figures 2.1(a) and 2.1(b) have the same bus impedance matrix denoted by $\boldsymbol{Z}$.

The circuit nodes are indexed 1 to $N$. Let $\boldsymbol{V}^{\text{pre}}$ and $\boldsymbol{V}^{\text{post}}$ represent the vector of node voltages before and after the disturbance, respectively. Then, the nodal equations for the two circuits satisfy the following equations [15]:

$$\boldsymbol{V}^{\text{pre}} = \boldsymbol{Z}\boldsymbol{I}^{\text{pre}} \tag{2.1}$$

$$\boldsymbol{V}^{\text{post}} = \boldsymbol{Z}\boldsymbol{I}^{\text{post}} \tag{2.2}$$

where, $\boldsymbol{I}^{\text{pre}}$ and $\boldsymbol{I}^{\text{post}}$ represent the vectors of nodal currents before and after the disturbance,

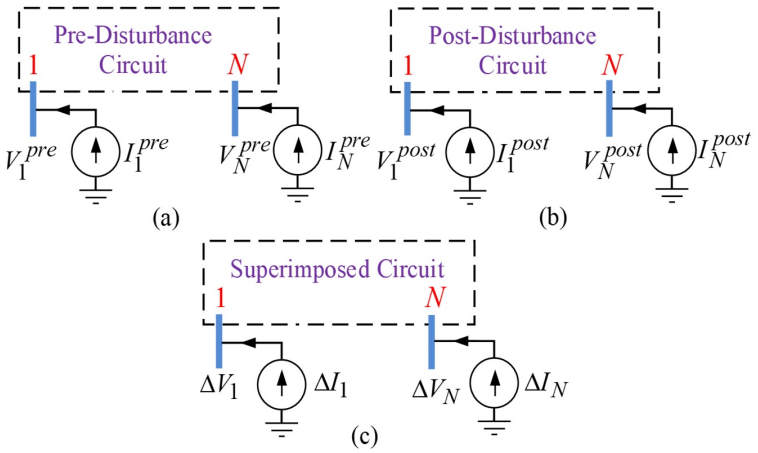


Figure 2.1: (a) Pre-disturbance circuit, (b) Post-disturbance circuit, and (c) Superimposed circuit for a disturbance [65].

respectively. Also, $\boldsymbol{Z}$ denotes the bus impedance matrix of the system. It should be noted that any non-linear elements of the system such as RESs, should be replaced by nodal current sources to be able to easily establish the bus impedance matrix of the system.

By subtracting (2.1) from (2.2), the following equation can be derived:

$$\Delta \boldsymbol{V} = \boldsymbol{Z} \Delta \boldsymbol{I} \tag{2.3}$$

Equation (2.3) can be attributed to a hypothetical superimposed circuit, as shown in Figure 2.1(c), in which all quantities are indicated by the $\Delta$ symbol. The letters $I$ and $J$ are used for nodal current injections and branch currents, respectively, to distinguish between them. If $\Delta I_j$ refers to the superimposed nodal injection at a node $j$, the superimposed voltage at any node $i$ can be obtained from:

$$\Delta V_i = \sum_{j=1}^{N} Z_{i,j} \Delta I_j \tag{2.4}$$

where $Z_{ij}$ denotes the element in the $i$-th row and $j$-th column of the bus impedance matrix of the superimposed circuit with $N$ nodes. Let $\Delta J_{u,v}$ denote the superimposed current of the sending-end of a healthy line $u-v$, which satisfies the following equation:

$$\Delta J_{uv} = \sum_{q=1}^{N} C_{uv,q} \Delta I_q \tag{2.5}$$

where the coefficient $C_{uv,q}$ for a nodal current source at bus $q$ can be obtained as follows [15]:

$$C_{uv,q} = \frac{Z_{u,q}}{Z^c_{u,v}\tanh(\theta_{u,v})} - \frac{Z_{v,q}}{Z^c_{u,v}\sinh(\theta_{u,v})} \tag{2.6}$$

where a line is connected between buses $u$ and $v$, and $Z^c_{u,v}$ is the characteristic impedance of line $u-v$. Let $\theta_{u,v} = \gamma_{u,v} \times l_{u,v}$, where $\gamma_{u,v}$ is its propagation constant, and $l_{u,v}$ is the length of the line. By writing equations of types (2.4) and (2.5) associated with the measured voltage and current synchrophasors, a system of linear equations can be obtained as below:

$$\boldsymbol{m} = \boldsymbol{H}\boldsymbol{x} + \boldsymbol{\varepsilon} \tag{2.7}$$

where $\boldsymbol{m}$, $\boldsymbol{H}$ and $\boldsymbol{\varepsilon}$ are the measurement vector, coefficient matrix, and error vector, respectively. Further, $\boldsymbol{x}$ is the vector of unknown nodal current injections. It should be noted that for the superimposed nodal currents that are directly measured by PMUs, the associated coefficient in $\boldsymbol{H}$ will be 1 or -1, depending on the convention assumed for the direction of the nodal current injection. The system of linear equations (2.7) can be readily solved using the weighted least-squares method as follows

$$\widehat{\boldsymbol{x}} = \left(\boldsymbol{H}^*\boldsymbol{R}^{-1}\boldsymbol{H}\right)^{-1}\boldsymbol{H}^*\boldsymbol{R}^{-1}\boldsymbol{m} \tag{2.8}$$

where the asterisk on $\boldsymbol{H}$ refers to the conjugate transpose of that matrix. The vector $\hat{\boldsymbol{x}}$ contains the estimates of unknowns, obtained by applying the weighted least-squares method to (2.10). These estimates might not be precisely equal to their corresponding true values because of measurement errors incurred in practice. The weighted sum of squared residuals (*WSSR*) is the objective function minimised for solving (2.7) and can be obtained from:

$$WSSR = [\boldsymbol{m} - \boldsymbol{H}\widehat{\boldsymbol{x}}]^*\boldsymbol{R}^{-1}[\boldsymbol{m} - \boldsymbol{H}\widehat{\boldsymbol{x}}] \tag{2.9}$$

where $\boldsymbol{R}$ denotes the covariance matrix of measurement errors, which is an $N_p$-by-$N_p$ diagonal matrix whose $i$-th diagonal entry is the variance of the $i$-th measurement. $N_p$ is the number of measurements. Equation (2.9) can also be represented as below:

$$WSSR = \boldsymbol{m}^*\boldsymbol{S}^*\boldsymbol{R}^{-1}\boldsymbol{S}\boldsymbol{m} \tag{2.10}$$

The matrix $\boldsymbol{S}$ is called the residual sensitivity matrix and can be obtained from [73]:

$$\boldsymbol{S} = \boldsymbol{I} - \boldsymbol{H}\left(\boldsymbol{H}^{*}\boldsymbol{R}^{-1}\boldsymbol{H}\right)^{-1}\boldsymbol{H}^{*}\boldsymbol{R}^{-1} \tag{2.11}$$

where $\boldsymbol{I}$ denotes the identity matrix of appropriate size. The *WSSR* of the actual disturbed element is theoretically zero and non-zero for healthy elements. Accordingly, (2.10) is evaluated for every suspected element to identify the smallest *WSSR*, thus the disturbed element. The estimated unknowns by (2.8) can be used to further investigate the identified disturbed element. For example, it can be used to calculate the fault distance on the faulted line.

### 2.2.1 Conceptual Diagram of the Superimposed-Circuit Methodology

Figure 2.2 provides a conceptual representation of superimposed-circuit-based wide-area applications. In these approaches, the bus impedance matrix of the power system is calculated based on the network topology and the impedance model of the network components, e.g., transmission lines, transformers, loads, generators, and the like. The power system is a dynamic system with varying topology and load flow. Thus, the system's bus impedance matrix will be time-variant. Nevertheless, the most updated data about the load flow and operating topology of the system reported via SCADA can be utilised to calculate the most recently updated bus impedance matrix.

It is assumed that in the short time between fault inception and clearance, the bus impedance matrix of the system (excluding the faulted line and those elements that are replaced by nodal current sources) does not noticeably change, which is quite an acceptable assumption [74]. In superimposed-circuit-based wide-area applications, voltage and current phasor measurements are widely gathered across the power system and the phasors measured by each PMU are time-tagged with GPS signals to establish a synchronised measurement system.

A flowchart of the superimposed-circuit methodology for WABP is shown in Figure 2.3. The product $\boldsymbol{S}^{*}\boldsymbol{R}^{-1}\boldsymbol{S}$ can be calculated and saved in memory a-priory based on the bus impedance matrix of the system. Therefore, the real-time calculations are mainly limited to calculating *WSSR*s by (2.10).

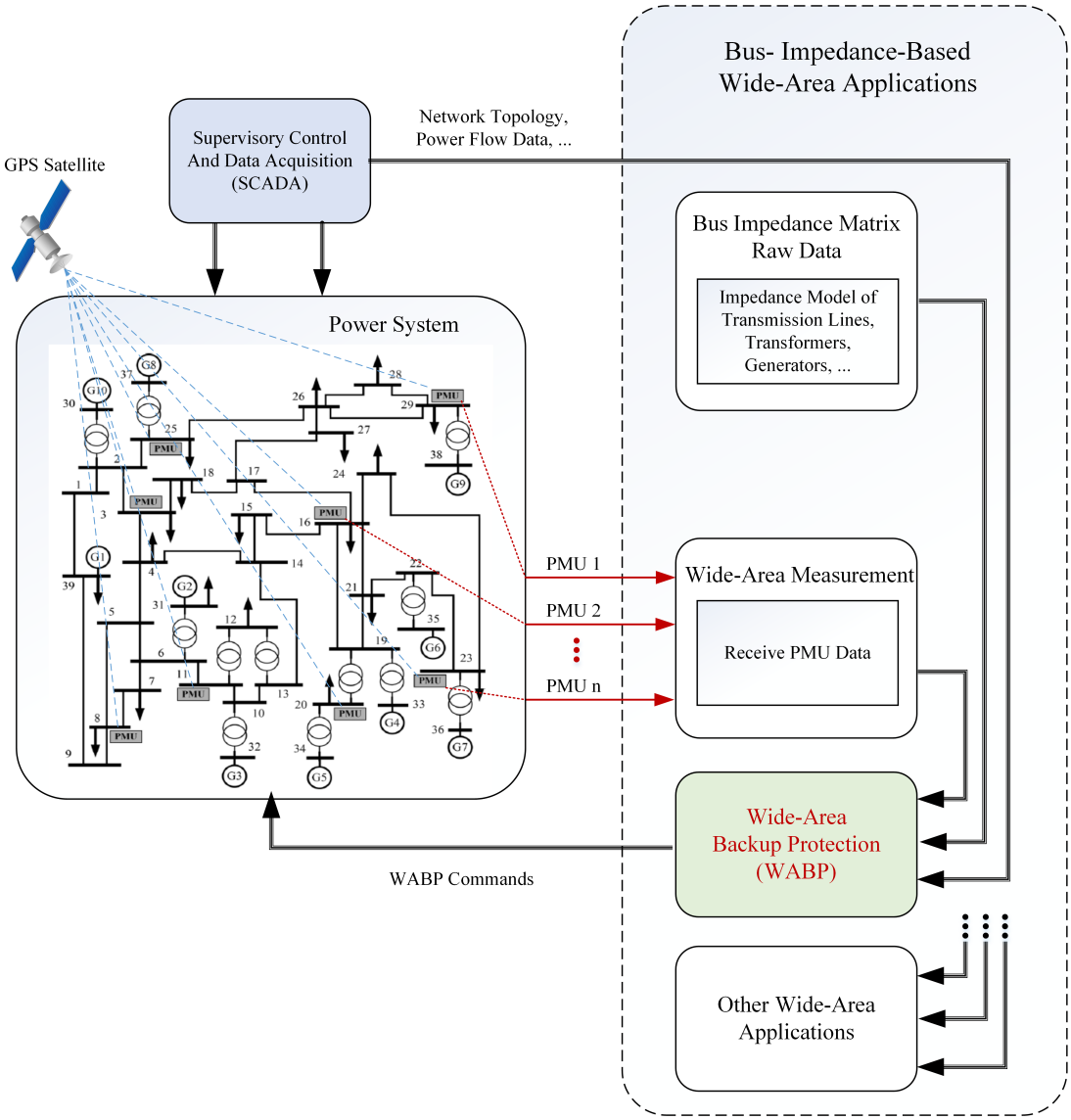


Figure 2.2: Conceptual representation of superimposed-circuit-based wide-area applications.

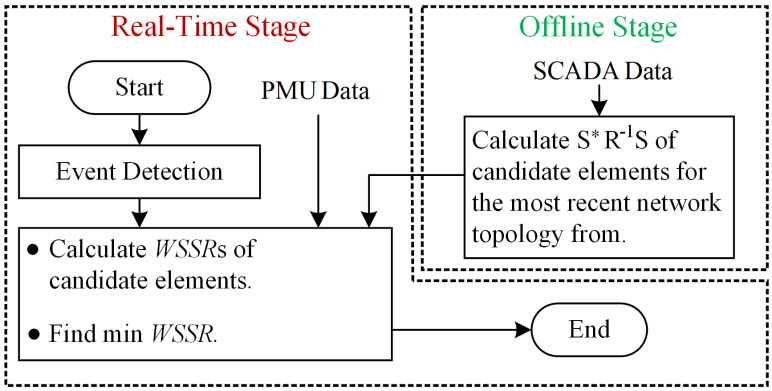


Figure 2.3: Flowchart of a superimposed-circuit-based method [65].

## 2.3 Superimposed-Circuit Methodology for WABP

Based on the *Substitution Theorem*, an element or a set of elements in a system could be replaced with a properly adjusted current source that injects the same amount of current. This substitution will not change the phasors of currents flowing in lines of the remaining network as well as its node voltages. According to the *Substitution Theorem*, voltage and current phasors in the remaining network of the original network, in which no element is substituted, and those of equivalent network model would be analogous as shown in Figure 2.4(a) and 2.4(b).

In order to form the nodal equivalent circuit, every voltage source in series with an impedance needs to be replaced by a proper current source in parallel with the same impedance [75]. Accordingly, the following equation stands for the original network in Figure 2.4(a).

$$\boldsymbol{V}^{pre} = \boldsymbol{Z}\boldsymbol{I}^{pre} \tag{2.12}$$

The vector $\boldsymbol{I}^{pre}$ is a vector of nodal currents, the $k$-th element of which, $I_k$, is the sum of all source current phasors entering bus $k$, as follows:

$$\boldsymbol{I}^{pre} = \left[I_1^{pre}, ..., I_k^{pre}, ..., I_N^{pre}\right]^T \tag{2.13}$$

For the equivalent network in Figure 2.4(b), the relation between bus voltage phasors and

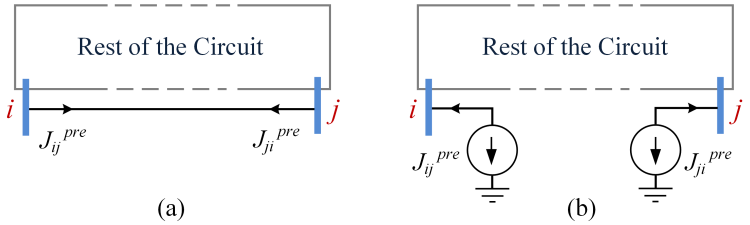


Figure 2.4: (a) Original, and (b) equivalent models under normal operating conditions.

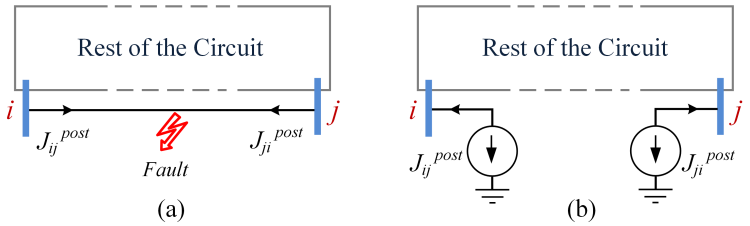


Figure 2.5: (a) Original, and (b) equivalent models under fault conditions.

nodal current phasors is as follows:

$$\boldsymbol{V}^{pre} = \boldsymbol{Z}\boldsymbol{I}^{pre} \tag{2.14}$$

In which, $\boldsymbol{Z}$ is the bus impedance matrix of the remaining network with the line $i-j$ removed. The vector $\boldsymbol{I}^{pre}$ would be as follows:

$$\boldsymbol{I}^{pre} = \left[I_1^{pre}, ..., I_i^{pre} - J_{i,j}^{pre}, ..., I_j^{pre} - J_{j,i}^{pre}, ..., I_N^{pre}\right]^T \tag{2.15}$$

As shown in Figure 2.5(a), let us assume that a fault has occurred at line $i-j$. According to the *Substitution Theorem*, the faulted line can be substituted with two equivalent current sources as shown in Figure 2.5(b). For the voltage and current phasors of the equivalent circuit 2.5(b), a matrix equation can be made similar to equation (2.12) as follows:

$$\boldsymbol{V}^{post} = \boldsymbol{Z}\boldsymbol{I}^{post} \tag{2.16}$$

In which

$$\boldsymbol{I}^{post} = \left[I_1^{post}, ..., I_i^{post} - J_{i,j}^{post}, ..., I_j^{post} - J_{j,i}^{post}, ..., I_N^{post}\right]^T \tag{2.17}$$

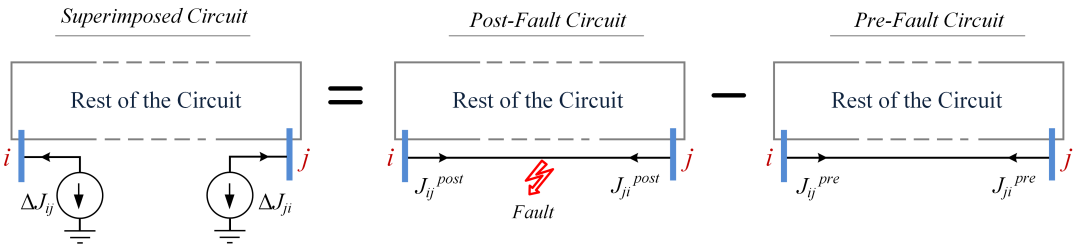


Figure 2.6: The concept of the superimposed circuit.

Regardless of the fault distance at the faulted line, the remaining network would be similar to the pre-fault network if the substituted line $i-j$ is actually the faulted line. As a result, the matrix $\boldsymbol{Z}^{(i,j)}$, which is constructed by the pre-fault topology of the remaining network, will be valid during the fault condition. In this way, the non-linear impedance matrix, which is a function of the exact fault distance on the faulted line is avoided.

The differences between the voltage and current phasors following the fault can be attributed to the corresponding voltages and currents in the superimposed circuit, as shown in Figure 2.6. The nodal equations for the superimposed form of the remaining network considering a fault at line $i-j$ are obtained by subtracting equation (2.14) from (2.16) as follows:

$$\Delta \boldsymbol{V} = \boldsymbol{Z}\Delta \boldsymbol{I} - \begin{bmatrix} Z_{1,i} & Z_{1,j} \\ \vdots & \vdots \\ Z_{N,i} & Z_{N,j} \end{bmatrix} \begin{bmatrix} \Delta J_{i,j} \\ \Delta J_{j,i} \end{bmatrix} \tag{2.18}$$

in which, $\Delta \boldsymbol{V}$ is the vector of superimposed bus voltages, $\Delta \boldsymbol{I}$ is the vector of superimposed nodal current injections, and $\Delta J_{i,j}$ and $\Delta J_{j,i}$ are superimposed terminal currents of the faulted line. The negative sign in equation (2.18) is because the reference directions of substituted current sources exit the connected buses.

The detailed system of equations used for WABP is presented here. Let $Nv$, $Nc$, and $Nb$ denote the number of PMU-measured bus voltages, PMU-measured nodal current injections, and PMU-measured branch currents whose associated measurement errors are respectively denoted by $e_V$, $e_I$, and $e_J$. In addition, let $Nu$ stand for the number of unknown nodal current sources in the power system. The overdetermined system of linear equations (2.7) can be formed using (2.5) and (2.18) as follows, where coefficients $C$ can be obtained by (2.6).

$$\overbrace{\begin{bmatrix} \Delta V_1 \\ \vdots \\ \Delta V_{Nv} \\ \\ \Delta I_1 \\ \vdots \\ \Delta I_{Nc} \\ \\ \Delta J_1 \\ \vdots \\ \Delta J_{Nb} \\ \\ \Delta J_{i,j} \\ \Delta J_{j,i} \end{bmatrix}}^{\boldsymbol{m}} = \overbrace{\begin{bmatrix} \begin{bmatrix} Z_{1,i} & Z_{1,j} \\ \vdots & \vdots \\ Z_{Nv,i} & Z_{Nv,j} \end{bmatrix} & \begin{bmatrix} Z_{1,1} & \cdots & Z_{1,Nu} \\ \vdots & \ddots & \vdots \\ Z_{Nv,i} & \cdots & Z_{Nv,Nu} \end{bmatrix} \\ [0]_{(Nc\times 2)} & -[I]_{(Nc\times Nu)} \\ \begin{bmatrix} C_{1,i} & C_{1,j} \\ \vdots & \vdots \\ C_{Nb,i} & C_{Nb,j} \end{bmatrix} & \begin{bmatrix} C_{1,1} & \cdots & C_{1,Nu} \\ \vdots & \ddots & \vdots \\ C_{Nb,i} & \cdots & C_{Nb,Nu} \end{bmatrix} \\ -[I]_{(2\times 2)} & [0]_{(2\times Nu)} \end{bmatrix}}^{\boldsymbol{H}} \times \overbrace{\begin{bmatrix} \Delta J_{i,j} \\ \Delta J_{j,i} \\ \Delta I_1 \\ \vdots \\ \Delta I_{Nu} \end{bmatrix}}^{\boldsymbol{x}} + \overbrace{\begin{bmatrix} e_{V_1} \\ \vdots \\ e_{V_{Nv}} \\ e_{I_1} \\ \vdots \\ e_{I_{Nc}} \\ e_{J_1} \\ \vdots \\ e_{J_{Nb}} \\ e_{J_{i,j}} \\ e_{J_{j,i}} \end{bmatrix}}^{\boldsymbol{\varepsilon}} \tag{2.19}$$

It is worth noting that in this modeling, only linear elements such as transmission lines and synchronous generators are included in the bus impedance matrix. As a result, non-linear elements such as RESs shall be excluded from the bus impedance matrix and be modelled as an unknown nodal current source in the superimposed circuit. This point will be further clarified in Chapter 4.

### 2.3.1 Individual Analysis of the Sequence Circuits

Some events, such as asymmetrical faults and single-pole opening of CBs make the three-phase power system unbalanced. The method of symmetrical components replaces the solution of an unbalanced three-phase circuit with the solution of three balanced circuits connected to each other in a particular way satisfying the event constraints [5]. Based on the sequence theorem, in the superimposed circuit methodology, each sequence circuit can be analysed independently regardless of the event type. This is possible if other sequence circuits are replaced by

proper current or voltage sources imitating the omitted circuits' behaviour following the event [11, 13, 15, 47]. Hence, all known and unknown variables and parameters in (2.1) to (2.11) can be addressed with the superscripts "+", "−", and "$z$" representing them in the positive, negative, and zero sequence circuit, respectively. For instance, $\Delta V_i^+$, $\Delta J_j^+$, $C_{h,q}^+$, and $\boldsymbol{Z}^+$ can be obtained for the positive-sequence circuit.

During asymmetrical faults to the ground, the sum of three-phase currents of transmission lines runs into the ground mainly via overhead line shield wires and towers grounds or directly to the ground at the fault point and returns mostly at transformers star points [75]. Regarding such current flowing paths, the impedances of the tower grounds, shield wires, and ground resistance at the fault point are included in the zero-sequence impedances of transmission lines. Moreover, the zero-sequence current may flow into different routes with various impedances. For instance, in case of a short circuit fault ensuing from a lightning flash, fault current passes through the shield wires and a bunch of tower ground in parallel. Conversely, during a direct ground fault, the fault current goes into the ground at the fault point. The zero-sequence impedance of the line is also affected by the soil resistivity, which is irregularly non-uniform along the whole line route. It is also influenced by the soil humidity and weather conditions. Accordingly, the zero-sequence impedance of transmission lines cannot be calculated precisely. Thus, the zero-sequence bus impedance matrix will contain noticeable inaccuracies [76, 77] and is better to be excluded from fault location equations. This is easily achievable by the superimposed circuit methodology as each sequence circuit can be analysed independently.

### 2.3.2 Fault Location Feasibility Analysis

The equation (2.7) for wide-area application is usually formed as an overdetermined system of equations. So, there might be no solution, one unique solution, or indefinite solutions for the unknown vector $\boldsymbol{x}$. The fault location feasibility analysis pertains to the evaluation of whether the superimposed currents and voltage at the faulted line terminals can be uniquely calculated from equation (2.10) from available measurements.

Providing that the coefficient matrix $\boldsymbol{H}$ is full rank, the vector of unknowns $\boldsymbol{x}$ composed of substituted superimposed currents of the faulted line and all other superimposed nodal current measurements, can be uniquely obtained. The feasibility analysis is to assess the solvability of the fault location problem when $\boldsymbol{H}$ is rank deficient. It might happen if the system of equations

(2.7) does not involve enough independent equations. The situation gets worse if some of the measurements are also excluded as bad data. For example, assume that a fault occurs on a line by which the network is separated into two distinct sub-networks. If there is no PMU at one of these sub-networks, matrix (2.7) would be rank deficient because there is no dependant equation for calculating superimposed voltage and current of a line terminal which is a part of PMU-lacking sub-network [15].

An overdetermined system of equations might not have a unique solution for all of its unknowns. Recall from matrix algebra, the first element with a value of 1 in each non-zero row of the reduced row echelon form of a matrix is called a pivot, which is a helpful tool for feasibility assessment. In the reduced echelon form of matrix $\boldsymbol{H}$, the corresponding variable to each pivot has a unique solution if and only if all other entries in the same row are zero [73]. This might not be the case for all pivots but some of them. Accordingly, it is possible to obtain unique solutions for the corresponding unknowns of those pivots while there is no unique solution for the whole system. As per the substitution theorem, any element can be replaced by a nodal current source and its superimposed values can be considered as an unknown in the formulation. However, from the viewpoint of superimposed fault location equations and regardless of the rank of $\boldsymbol{H}$, as long as superimposed currents at the faulted line terminals from equation (2.7) are uniquely obtained, the fault distance can be easily computed [15], as detailed in the next section.

### 2.3.3 Fault Location Calculation

Once the faulted line is identified, in each sequence circuit, superimposed currents calculated from equation (2.8) can be put into (2.4) to obtain the superimposed voltages at the faulted line terminals. Let us assume that line $i-j$ is the faulted line. Having obtained $\Delta V_i$, $\Delta V_j$, $\Delta J_{i,j}$, and $\Delta J_{j,i}$ and using the equivalent $\pi$ model derived from the distributed model of the faulted line, the fault distance $\alpha_{i,j}$ at line $i-j$ can be readily calculated. The closed-form equation for the fault distance $\alpha_{i,j}$ is obtained as follows [78]:

$$\alpha_{i,j} = \frac{1}{\theta_{i,j}} \times \tanh^{-1}\left(\frac{\cosh(\theta_{i,j})\Delta V_j - Z^c_{i,j}\sinh(\theta_{i,j})\Delta J_{j,i} - \Delta V_i}{\sinh(\theta_{i,j})\Delta V_j - Z^c_{i,j}\cosh(\theta_{i,j})\Delta J_{j,i} - Z^c_{i,j}\Delta J_{i,j}}\right) \tag{2.20}$$

As will be further explained, the fault distance is calculated to ensure that it lies within the

acceptable range [0,1], thereby reinforcing the security of the method. In addition, accurate fault location can help to minimize the costs associated with fault repair. It allows for targeted repair efforts, reducing the need for extensive troubleshooting and unnecessary equipment replacement.

### 2.3.4 PMU Coverage and Data Loss

PMUs are normally placed in power systems with respect to the availability of infrastructure and budget restrictions rather than the requirements of particular functionality [43]. Wide-area methods that need synchrophasor measurements from specific locations are essentially vulnerable to losses of PMU data and long communication latencies. This is while the superimposed-circuit-based methods do not impose rigid limitations on the number and locations of PMUs. The reason is that in the superimposed-circuit-based methods, a highly over-determined system of equations is established. An important implication of the foregoing feature is that the loss of PMU data or long communication latencies will not render superimposed circuit-based methods unfeasible, as long as the coefficient matrix is not rank deficient. Indeed, the system of (2.7) is normally overdetermined to a great extent, thanks to the multitude of measurements provided by PMUs. It follows that the solvability of (2.7) is not dependent on the availability of any specific equations. Therefore, excluding the equations corresponding to a few PMUs whose data have not been received in the control centre for any reason would not compromise the functionality of the proposed WABP method. It is an easy offline task to determine the simultaneous losses of which measurements can make (2.7) unsolvable [15] by checking the rank of the coefficient matrix. This is because the coefficient matrix for any sets of received PMU data can be easily calculated prior to a fault onset.

### 2.3.5 Considerations for Loss of Time-Synchronising Signal

Synchrophasors reported by a PMU will be all time-stamped with respect to the time reference of that device. The time drift of locally measured phasors can be confined in the order of 1 $\mu$s over one second [79]. Therefore, the phase angles of phasors measured by a PMU at the same substation can be considered highly accurate with respect to each other [15]. To model the impact of the loss of time synchronisation signal, phasors provided by $\text{PMU}_1$ to $\text{PMU}_{N_{pmu}}$ may be multiplied by unknown phase angle operators, $e^{j\theta_1}, \ldots, e^{j\theta_{N_{pmu}}}$. These

multiplications make the formulation nonlinear in terms of the new unknowns. Rearranging the equations of (2.7) as a linear combination of nodal current sources and angle drifts can help maintain the system's linearity [13]. In doing so, the unknown angle drift operators can be moved from the measurement vectors to the vector $\boldsymbol{x}$, while their coefficient will be added to the $\boldsymbol{H}$ matrix with the cost of a noticeable higher computational burden. Another method to deal with unsynchronised measurements is presented in Chapter 5, in which the impact of angle drifts is totally disregarded in the formulations with a minor computation burden.

### 2.3.6 Bad Data Detection and Identification

Due to the inclusion of bad data in the measurement set, the event identification results might become unreliable from time to time. This will be the case unless bad data is spotted and eliminated from the measurement set. As presented in Chapter 3, the superimposed errors, i.e., the differences between the errors of the corresponding pre- and post-fault synchrophasors errors, can be characterised based on the statistical distributions of the errors of pre- and post-fault synchrophasors. The linearity of the formulation, along with the derivations of superimposed errors, allows for the application of well-established bad data detection and identification methods. The largest normalised residual test (LNRT) [80, 81] is a common technique that can be used to deal with erroneous measurements, e.g., current measurements of saturated CTs during close-in faults. Finally, thanks to the overdetermined nature of the system of equations (2.7), the detected bad data can be excluded from the vector of measurements.

### 2.3.7 Accounting for Non-Simultaneous One- or Three-Pole Tripping of CBs

Following a fault on a line, CBs at the line ends will be tripped by protective relays. However, the opening of CBs at the two line-ends may not be simultaneous [12]. It is vital for WABP formulations to remain valid after single-end line disconnection. In other words, WABP formulations should not be affected by the status of CBs at the faulted line end. One end of the faulted line might be rapidly tripped in less than a couple of power frequency cycles following the fault. Phasors estimated within that time will not be accurate due to the transient response of phasor estimation algorithms. Hence, the WABP method might fail by using inexact phasors.

A faulted line $i-j$ is represented by two equivalent current sources in each sequence circuit. Upon any new event on this line, the measurement vector and the values of the unknown current

Table 2.1: Criteria for Fault Type Identification

| Comparison Result | $I_f^+ = I_f^-$ | $I_f^+ = -I_f^-$ | $\left\|I_f^+\right\| \neq \left\|I_f^-\right\|$ | $I_f^- = 0$ |
|---|---|---|---|---|
| Fault Type | 1-ph-g | 2-ph | 2-ph-g | 3-ph |

sources replaced for the line change while the bus impedance matrix remains unchanged. Thus, (2.10) holds at any moment, e.g., from a fault onset to the disconnection of one and finally both ends of the line. Indeed, every event on the line can be entirely translated into an equivalent modification in the vector of unknowns. The system of linear equations (2.10) can also be formed for the negative- and zero-sequence circuits, if the event is asymmetrical and involves these circuits, i.e., one-pole tripping of faulted line's CBs. Therefore, non-simultaneous single- or three-pole disconnection of the faulted line from one end will not affect the validity of the superimposed-based WABP formulations [15].

### 2.3.8 Fault Type and Faulted Phases Identification

As explained, in the superimposed circuit methodology, each sequence circuit can be analysed independently regardless of the event type. As detailed in Table 2.1, all types of faults can be identified by comparing positive- and negative-sequence fault currents [13]. It is worth noting that the fault type is merely identified based on the estimated fault current. The types and locations of fault current sources (including synchronous machines and RESs) do not impact this judgment as long as they are correctly modelled in the superimposed circuit.

### 2.3.9 Low Sensitivity to Fault Resistance

In the superimposed circuit methodology, the faulted line is replaced by two appropriate nodal current sources based on the *Substitution Theorem*. Therefore, the faulted line and fault resistance are not included in the bus impedance matrix, while their effects are reflected in the current sources. In other words, the superimposed-circuit-based WABP infers the currents and voltages at both terminals of the faulted line [11, 13, 15]. This simplifies the problem of wide-area fault location to a two-terminal fault location. One of the inherent advantages of the two-terminal fault location methods is their low sensitivity to fault resistance [78].

## 2.4 Summary

In this chapter, the superimposed-circuit methodology and its application for WABP were detailed and promoted as a powerful methodology with great potential for addressing real-world challenges such as communication latencies/failures, temporarily incomplete network observability, sparse PMU coverage, measurement errors, bad data, and the loss of the time synchronisation signal. Furthermore, this chapter highlighted the essential prerequisites for ensuring the viability of WABP methods for implementation in practice.

# CHAPTER 3

## Improvement to the Superimposed-Circuit Methodology for WABP

## 3.1 Overview

This chapter proposes a technique for reducing the computational complexity of superimposed-circuit-based WABP methods. This chapter demonstrates the existence of a one-to-one equivalence between the responses of the superimposed circuit with and without the faulted line. A proposition is presented and proved to justify that the system of equations pertaining to every candidate line can be directly obtained from the bus impedance matrix of the pre-fault power system without removing the faulted line from the bus impedance matrix. This is in contrast with existing WABP methods requiring the establishment of as many distinct bus impedance matrices as the number of candidate lines in the power system.

Furthermore, a system of linear equations is formulated for WAFL/WABP, taking advantage of both voltage and current synchrophasors. This results in a generalised closed-form solution for the fault distance calculation using the weighted least-squares method. In doing so, the equation weights related to superimposed measurements are rigorously derived based on the statistical distributions of the superimposed errors, i.e., the differences between the errors of the corresponding pre- and post-fault synchrophasors.

## 3.2 Reducing the Computational Complexity of WABP

A prerequisite for applying superimposed methodology for WABP is that the pre-fault and post-fault circuits have the same bus impedance matrix. This can easily be realised by removing the faulted line from the circuit and replacing it by suitable current sources before and after the fault onset. To identify the faulted line, the replacement procedure is carried out for all candidate lines. A system of equations is derived for each case relating the measurements to the candidate line under study. The weighted sum of squared residuals (*WSSR*) is calculated for the developed system of equations. The candidate line with the least *WSSR* is identified as the faulted line [11, 13, 15].

If $l$ denotes the number of lines in a power system, WABP methods introduced in [11, 13, 15] require the calculation of $l$ distinct bus impedance matrices upon any changes in the power system's topology/operating point. Given the dynamic nature of power systems, this translates to a continuous need for calculating and updating $l$ coefficient matrices, which can be highly demanding for large-scale power systems.

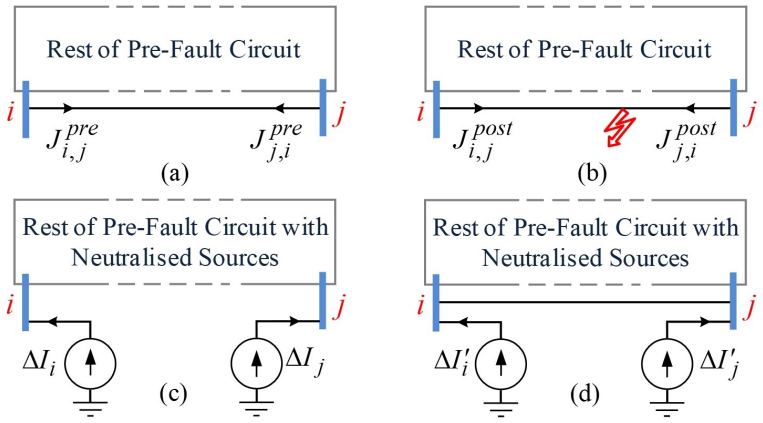


Figure 3.1: (a) Pre-fault circuit. (b) Post-fault circuit. (c) Superimposed circuit with line $i$-$j$ removed. (d) Superimposed circuit with line $i$-$j$ connected [66].

In this section it will be asserted that the coefficient matrix corresponding to every candidate line can be directly calculated from the bus impedance matrix of the pre-fault power system, irrespective of the faulted line, fault type, and fault location. A proposition is presented with analytical proof justifying the validity of the proposed technique. This removes the need for numerous modifications of the bus impedance matrix with respect to the candidate lines under study. Extensive simulations are conducted to confirm that the proposed technique reduces the computational burden without impacting the success rate of WABP.

### 3.2.1 WABP Based on the Superimposed-Circuit Methodology

Let us assume line $i$-$j$ in a power system is faulted. Figures 3.1(a) and 3.1(b) show the pre-fault and post-fault circuits of this power system with $N$ buses. The differences between the voltage and current phasors following the fault can be attributed to the corresponding voltages and currents in the superimposed circuit shown in Figure 3.1(c). The topology of the superimposed circuit is independent of the fault location on the line, yet different from that of the pre-fault circuit as line $i$-$j$ is excluded from the former. Let $\Delta I_i$ and $\Delta I_j$ refer to the superimposed nodal injections at buses $i$ and $j$, respectively. As synchronous generators can be modelled as constant impedances in the superimposed circuit [11], $\Delta I_i$ and $\Delta I_j$ are the only non-zero injections in the superimposed circuit of Figure 3.1(c). Thus, the superimposed voltage at an arbitrary bus $q$ can be obtained from

$$\Delta V_q = Z_{qi}\Delta I_i + Z_{qj}\Delta I_j \tag{3.1}$$

where $Z_{qi}$ is the entry in the $q$-th row and $i$-th column of the bus impedance matrix. Let $\Delta J_{uv}$ denote the sending-end superimposed current of line $u$-w. It can be easily shown that

$$\Delta J_{uv} = C_{uv,i}\Delta I_i + C_{uv,j}\Delta I_j \tag{3.2}$$

where the derivation of $C_{uv,k}$ is obtained by (2.6). Every voltage and current measurement provided by PMUs can be substituted in (3.1) and (3.2), respectively, to form an equation in $\Delta I_i$ and $\Delta I_j$. These equations together form an overdetermined system of equations as below

$$\boldsymbol{m} = \boldsymbol{H}\begin{bmatrix} \Delta I_i \\ \Delta I_j \end{bmatrix} + \boldsymbol{\varepsilon} \tag{3.3}$$

where $\boldsymbol{m}$ and $\boldsymbol{H}$ are the measurement vector and the coefficient matrix. The vector $\boldsymbol{\varepsilon}$ also stands for measurement errors. The residuals of a system of equations are defined as the discrepancy between the measured quantities and their corresponding estimations [80]. The *WSSR* for (3.3) can be calculated from the closed-form solution of (2.10).

As explained, to form (3.3), it is assumed that line $i$-$j$ is the faulted line; a hypothesis whose truth is unknown upon receiving PMU data. Nonetheless, if this hypothesis is true, the *WSSR* corresponding to (3.3) will be quite negligible (ideally zero if measurements were error-free). This feature has been employed in several research works to identify the faulted line [11, 13, 15]. In doing so, (3.3) is built for every candidate line, and a *WSSR* is calculated for each. The line corresponding to the smallest *WSSR* is identified as the faulted line.

It is worth noting that (3.3) remains functional even if the faulted line is a double-circuit line. The reason is that the whole faulted line can still be modelled by proper current sources from the viewpoint of the remainder of the power system. As a result, the *WSSR* index can still pinpoint the faulted line regardless of whether it is single- or double-circuit. However, a PMU at one of the faulted line terminals is necessary if we are to determine which of the two circuits is faulted [25].

### 3.2.2 Proposed Technique to Reduce the Computational Complexity

To determine which candidate line is faulted, (3.3) is built for every line to obtain the associated *WSSR* [15]. This requires the removal of the candidate line from the pre-fault circuit to calculate the entities of the corresponding coefficient matrix $\boldsymbol{H}$. If there are $l$ candidate lines in the system, $\boldsymbol{H}$ must be obtained for $l$ different circuits that differ from one another in the presence/absence of the candidate line. This section asserts that $\boldsymbol{H}$ can be directly built from the pre-fault circuit for all candidate lines, with no modifications with respect to the candidate line under study. The argument follows from the proposition below:

**Proposition**: *Consider the response of the circuit of Figure 3.1(c) for given nodal injections $\Delta I_i$ and $\Delta I_j$ at buses $i$ and $j$, respectively. There are unique injections $\Delta I_i'$ and $\Delta I_j'$ that produce the same response in the circuit of Figure 3.1(d) if applied respectively at buses $i$ and $j$ of that circuit.*

The converse of the above proposition is also true. For any response in the circuit of Figure 3.1(d) resulting from non-zero injections $\Delta I_i'$ and $\Delta I_j'$, there are unique $\Delta I_i$ and $\Delta I_j$ that will produce the same response in the circuit of Figure 3.1(c).

It can be concluded from the above proposition and its converse that any response that can be achieved for either of the two circuits is achievable for the other one. A conditional statement that follows from this is that if the *WSSR* for the circuit of Figure 3.1(c) is zero, the *WSSR* for the circuit of Figure 3.1(d) will be zero, as well. The converse of this conditional statement is also true. The reason is that the *WSSR* being zero means the observed measurements could be the response of the superimposed circuit for which (3.3) has been built [13]. Therefore, we assert that building $\boldsymbol{H}$ based upon the pre-fault circuit can reduce the computational complexity while maintaining the capability of indicating the faulted line.

### 3.2.3 Mathematical Proof of the Proposition

Let us assume that the two non-zero nodal injections $\Delta I_i$ and $\Delta I_j$ result in superimposed voltages $\Delta V_1, \Delta V_2, \ldots, \Delta V_N$ in the circuit of Figure 3.1(c). Now, let us reorder buses as $i, j, 1, \ldots, N$. The admittance matrix of the circuit of Figure 3.1(c) after this reordering is denoted by $\boldsymbol{Y}$. By partitioning $\boldsymbol{Y}$, the nodal equations for this circuit can be written as follows

$$\begin{bmatrix} \Delta I_i \\ \Delta I_j \\ - \\ 0 \\ \vdots \\ 0 \end{bmatrix} = \overbrace{\left[\begin{array}{c|c} \boldsymbol{A}_{2\times 2} & \boldsymbol{B}_{2\times(N-2)} \\ - - - - - & - - - - - \\ \boldsymbol{C}_{(N-2)\times 2} & \boldsymbol{D}_{(N-2)\times(N-2)} \end{array}\right]}^{\boldsymbol{Y}} \begin{bmatrix} \Delta V_i \\ \Delta V_j \\ - \\ \Delta V_1 \\ \vdots \\ \Delta V_N \end{bmatrix} \tag{3.4}$$

In virtue of the invertibility of the nodal admittance matrix [82], the superimposed voltages $\Delta V_i$ and $\Delta V_j$ can be uniquely calculated from (3.1) as follows

$$\begin{bmatrix} \Delta V_i \\ \Delta V_j \end{bmatrix} = \begin{bmatrix} Z_{ii} & Z_{ij} \\ Z_{ij} & Z_{jj} \end{bmatrix} \begin{bmatrix} \Delta I_i \\ \Delta I_j \end{bmatrix} \tag{3.5}$$

Let $z_l$ and $y_l$ denote the series impedance and shunt admittance of line $i$-$j$, which can be accurately calculated from the distributed parameter model of line $i$-$j$. Now let us define nodal injections $\Delta I_i'$ and $\Delta I_j'$ as below

$$\begin{bmatrix} \Delta I_i' \\ \Delta I_j' \end{bmatrix} = \begin{bmatrix} \frac{1}{z_l}+\frac{y_l}{2} & \frac{-1}{z_l} \\ \frac{-1}{z_l} & \frac{1}{z_l}+\frac{y_l}{2} \end{bmatrix} \begin{bmatrix} Z_{ii} & Z_{ij} \\ Z_{ij} & Z_{jj} \end{bmatrix} \begin{bmatrix} \Delta I_i \\ \Delta I_j \end{bmatrix} + \begin{bmatrix} \Delta I_i \\ \Delta I_j \end{bmatrix} \tag{3.6}$$

One can conclude from (3.4), (3.5), and (3.6) that

$$\begin{bmatrix} \Delta I_i' \\ \Delta I_j' \end{bmatrix} = \overbrace{\left(\begin{bmatrix} \frac{1}{z_l}+\frac{y_l}{2} & \frac{-1}{z_l} \\ \frac{-1}{z_l} & \frac{1}{z_l}+\frac{y_l}{2} \end{bmatrix} + \boldsymbol{A}\right)}^{\boldsymbol{A}'} \begin{bmatrix} \Delta V_i \\ \Delta V_j \end{bmatrix} + \boldsymbol{B} \begin{bmatrix} \Delta V_1 \\ \vdots \\ \Delta V_N \end{bmatrix} \tag{3.7}$$

Combining (3.7) with the lower part of (3.4) gives

$$\begin{bmatrix} \Delta I_i' \\ \Delta I_j' \\ 0 \\ \vdots \\ 0 \end{bmatrix} = \overbrace{\left[\begin{array}{c|c} \boldsymbol{A'}_{2\times 2} & \boldsymbol{B}_{2\times(N-2)} \\ \boldsymbol{C}_{(N-2)\times 2} & \boldsymbol{D}_{(N-2)\times(N-2)} \end{array}\right]}^{\boldsymbol{Y}'} \begin{bmatrix} \Delta V_i \\ \Delta V_j \\ \Delta V_1 \\ \vdots \\ \Delta V_N \end{bmatrix} \tag{3.8}$$

The only difference between the circuits of Figures 3.1(c) and 3.1(d) is that line $i$-$j$ does not exist in the former but in the latter. It can be confirmed that the matrix $\boldsymbol{Y}'$ is the admittance matrix of the circuit of Figure 3.1(d) in which the buses are reordered as $i$, $j$, $1, \ldots, N$. Since the shunt/series elements of line $i$-$j$ are only connected to buses $i$ and $j$, the submatrices $\boldsymbol{B}, \boldsymbol{C}$, and $\boldsymbol{D}$ in $\boldsymbol{Y}$ and $\boldsymbol{Y}'$ are identical. Accounting for these elements, $\boldsymbol{A}$ needs to be replaced by $\boldsymbol{A}'$ to form the admittance matrix of the circuit of Figure 3.1(d). Therefore, (3.8) implies that injecting $\Delta I_i'$ and $\Delta I_i'$ in the circuit of Figure 3.1(d), results in the same superimposed voltages as those in the circuit of Figure 3.1(c).

The voltage response equivalence between the two circuits guarantees that the superimposed branch currents in both circuits are identical. This is because identical lines will carry the same currents if subjected to the same terminal voltages. This ends the proof. The converse of the Propostion can be proved in a similar way, as well. It is worth noting that (3.3) is formed for conventional power systems, in which generators are all synchronous and can be modelled by constant impedances in the superimposed circuit. For modern power systems, as will be explained in Chapter 4, renewables can be modelled by nodal current sources in the superimposed circuit. With the same approach, it can be shown that the Propostion is still valid in the presence of other nodal current sources.

### 3.2.4 Analysis of the Computation Time

The computation time of WABP using the proposed technique for every candidate line includes the time needed to build the matrix $\boldsymbol{H}$ related to the candidate lines and the calculation time for the *WSSR* of the line. Let $N_p$ denote the number of measurements. The big O notation of the computation time of the method represents the asymptotic curve that refers to the computation complexity with a very large $N_p$ [83]. As detailed in [15], three multiplications are needed to calculate every entry of $\boldsymbol{H}$. Therefore, $T_H$ can be presented as $O\left(6N_p\right)$ for all $2N_p$ entries in $\boldsymbol{H}$. Big $O$ notation for multiplication of a $n \times p$ matrix to a $p \times q$ matrix is $O(npq)$ [83]. Accordingly, Table 3.1 shows the big O notation of *WSSR* calculations in detailed steps. The terms $O\left(N_p^2\right)$ dominate the $O\left(N_p\right)$ ones, and thus, the total computation time can be presented as $O\left(5{N_p}^2\right)$ for every candidate line. The constant scalar 5 can be dropped in big O notation for a very large $N_p$. It should be noted that Table 3.1 only represents the total computation burden of the proposed method and does not compare it with that of the existing method.

Table 3.1: Bio $O$ Notation Representation for *WSSR* Calculation

| Operation | Big O notation |
|---|---|
| $\boldsymbol{Y1}_{2\times N_p} = \boldsymbol{H}_{2\times N_p}{}^{*}\boldsymbol{R}^{-1}_{N_p\times N_p}$ | $O\left(2N_p^2\right)$ |
| $\boldsymbol{Y2}_{2\times 2} = \left(\boldsymbol{Y1}_{2\times N_p}\boldsymbol{H}_{N_p\times 2}\right)^{-1}$ | $O\left(4N_p\right)$ |
| $\boldsymbol{Y3}_{N_p\times 2} = \boldsymbol{H}_{N_p\times 2}\boldsymbol{Y2}_{2\times 2}$ | $O\left(4N_p\right)$ |
| $\boldsymbol{S}_{N_p\times N_p} = \boldsymbol{I} - \boldsymbol{Y3}_{N_p\times 2}\boldsymbol{Y1}_{2\times N_p}$ | $O\left(2N_p^2\right)$ |
| $\boldsymbol{y4}_{N_p\times 1} = \boldsymbol{S}_{N_p\times N_p}\boldsymbol{m}_{N_p\times 1}$ | $O\left(N_p^2\right)$ |
| $WSSR = \boldsymbol{y4}_{1\times N_p}{}^{*}\boldsymbol{y4}_{N_p\times 1}$ | $O\left(N_p\right)$ |

### 3.2.5 Performance Evaluation

The performance of the proposed technique is evaluated by conducting extensive simulations on the IEEE 39-bus test system. Buses 3, 5, 8, 11, 14, 16, 19, 23, 25, 27, 29 and 39 are equipped with PMUs [84]. The real PMU model of [64] is used to extract the phasors of generated time-domain waveforms in PowerFactory following a wide variety of short-circuit faults.

To validate the capability of the proposed technique in identifying the faulted line, an arbitrary 1-ph-g fault at 95% of line 17-18 is investigated for up to 300 ms following the fault onset. The fault distance is also estimated using the closed-form solution proposed in [13] by obtaining the superimposed currents and voltages of the faulted line from (3.3), (3.5), and (3.6). Figure 3.2 shows the *WSSR*s calculated for the faulted line, and the fault distance estimation using the proposed technique and the method proposed in [13]. As expected, the *WSSR*s calculated by both methods are quite similar with a difference in the order of $10^{-6}$, which correctly identify the faulted line. The estimated fault distance on the line is practically the same.

Now, the general performance of the proposed technique is examined and compared with that of other methods for various fault types and locations on every line. To compare the sensitivity of WABP methods to measurement and parameter errors, these quantities are assumed to have errors with normal distribution with mean zero. Measurement errors account for different sources of errors such as instrument transformers error, phasor estimation, and measurement noises [85]. The error ranges are reported based on the three-sigma criterion [13]. Table 3.2 summarises the results obtained from 20,000 simulated cases, in terms of faulted-line iden-

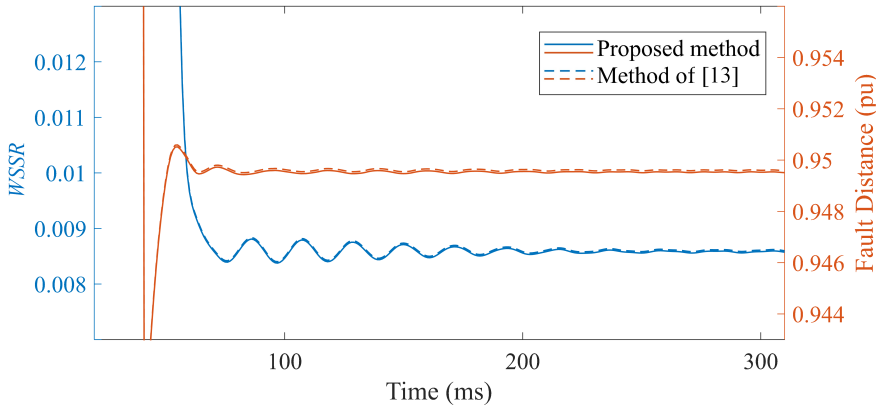


Figure 3.2: *WSSR* and estimated fault distance using different methods [66].

Table 3.2: Comparison Between Different WABP Methods

| Error Type | | Measurement Error | | | Line Parameter Error | | |
|---|---|---|---|---|---|---|---|
| Error Range (%) | | ± 0 | ± 4 | ± 8 | ± 0 | ± 4 | ± 8 |
| FLISR (%) | Proposed | 99.88 | 99.03 | 98.49 | 99.88 | 97.29 | 94.22 |
| | [15] | 99.93 | 99.15 | 98.47 | 99.93 | 97.59 | 93.75 |
| | [13] | 99.43 | 99.26 | 98.83 | 99.43 | 97.73 | 92.92 |
| AFLE (%) | Proposed | 0.63 | 0.96 | 1.21 | 0.63 | 1.41 | 2.11 |
| | [15] | 0.65 | 1.00 | 1.11 | 0.65 | 1.11 | 2.01 |
| | [13] | 0.67 | 1.01 | 1.48 | 0.67 | 1.02 | 3.23 |

tification success rate (FLISR) and average fault location error (AFLE). Table 3.3 shows the method's performance for different fault resistances. The minor difference in *WSSR*s and estimated nodal currents in the presence of parameter/measurement error and different fault resistances do not noticeably affect WABP's success rate nor the accuracy of fault location.

The computational burden of WABP by the methods investigated can be divided into two parts, namely building $\boldsymbol{H}$ and (3.3) for different candidate lines and calculating the *WSSR*s for the developed systems of equations. On average, the first part takes around 25 ms by the methods in [13, 15], which is reduced to 12 ms using the proposed technique. The second part is identical in all methods and takes around 5 ms for the IEEE 39-bus system. Thus, the proposed and existing method takes 17 ms and 30 ms in total, respectively. This demonstrates about 40% reduction in the whole computational burden.

Table 3.3: Sensitivity of the Proposed Method to Fault Resistance

| Fault Resistance | 0Ω | 5Ω | 10Ω | 15Ω | 25Ω |
|---|---|---|---|---|---|
| FLISR (%) | 99.88 | 99.82 | 99.63 | 99.47 | 99.34 |
| AFLE (%) | 0.63 | 0.65 | 0.67 | 0.71 | 0.74 |

## 3.3 Characterising the Distributions of Superimposed Errors

Accurate fault location reduces the outage time and enhances power system reliability. The WAFL methods proposed in [11, 67] can only utilise voltage synchrophasors. Nevertheless, voltage transformers located far from the fault location are likely to experience small voltage variations following a fault. Hence, the resulting superimposed synchrophasors could be of the order of noise and phasor estimation error. Thus, the relative errors of voltage-related equations might be exceedingly high, making them counterproductive. In contrast, the amounts of currents flowing through transmission lines greatly increase in fault conditions [15]. It follows that the relative errors of superimposed current synchrophasors are, in general, smaller than those of voltage synchrophasors. On the other hand, one can derive only a single equation for the voltage synchrophasor at a substation, while several equations can typically be formed based on current synchrophasors (for the multiplicity of the lines connected to each substation). The inclusion of current measurements has great potential to significantly improve the fault location accuracy by adding a greater number of equations in the equation set [80].

In the proposed method described in this section, both voltage and current synchrophasors are incorporated into the WAFL formulation while maintaining its linearity. The weighted least-squares (WLS) method is used to solve the system of linear equations to provide a closed-form solution for the fault distance. The derivations of the mean and variance of superimposed errors enable a rigorous establishment of the weight matrix required for the WLS estimation. To achieve this, the statistical distributions of the magnitude and phase-angle errors of pre- and post-fault synchrophasors are taken into account.

In principle, CTs located farther from the fault location experience smaller current variations upon a fault. Hence, the accuracy of current measurements taken farther away from the fault location would be hardly affected by saturation [86]. The linearity of the formulation,

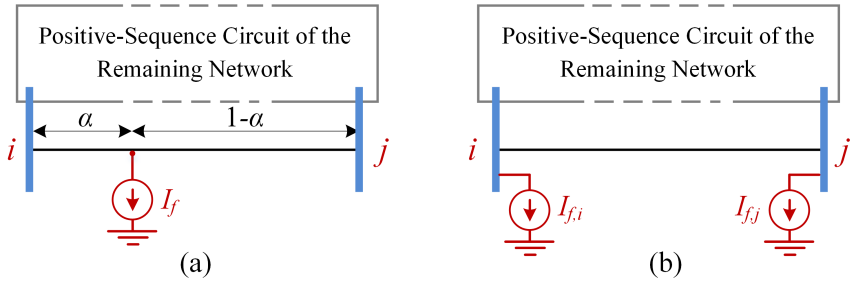


Figure 3.3: (a) Superimposed positive-sequence circuit of the faulted power system with one current source, and (b) its equivalent circuit with two current sources.

along with the derivations of superimposed errors, allows for the application of well-established bad data detection and identification methods to deal with erroneous measurements, e.g., current measurements of saturated CTs during close-in faults. Extensive simulations confirm that the fault location accuracy is considerably improved by incorporating current synchrophasors into the formulation and taking account of the distributions of superimposed errors.

### 3.3.1 Generalised Expression for Fault Location

Figure 3.3(a) shows the superimposed positive-sequence circuit of a network with a fault on line $i$-$j$ at the distance $\alpha$ from bus $i$. A nodal current injection is used to represent the fault current in this superimposed circuit. As shown in Figure 3.3(b), the current source $I_f$ can be resolved into two nodal current injections placed at the faulted line terminals, i.e., $I_{f,i}$ and $I_{f,j}$, where [67]

$$I_{f,i} = \frac{\sinh\left(l_{ij}\gamma_{ij}(1-\alpha)\right)}{\sinh\left(l_{ij}\gamma_{ij}\alpha\right)} I_{f,j} \tag{3.9}$$

in which $l_{ij}$ and $\gamma_{ij}$ are the length and propagation constant of the faulted line, respectively. As per the circuit of Figure 3.3(b), the superimposed voltage at an arbitrary bus $u$ is obtained from

$$\Delta V_u = Z_{ui} I_{f,i} + Z_{uj} I_{f,j} \tag{3.10}$$

where $Z_{ui}$ is the $(u, i)$ th entry of the bus impedance matrix. To take advantage of the information provided by current measurements, they are also incorporated into the formulation. Let $\Delta J_{uv}$ denote the sending-end superimposed current of line $u$-$v$, which satisfies the following equation:

$$\Delta J_{uv} = C_{uv,i} I_{f,i} + C_{uv,j} I_{f,j} \tag{3.11}$$

where the derivation of $C_{uv,q}$ is obtained by (2.6). Writing (3.10) and (3.11) for the synchrophasors provided by PMUs, one can form the following system of equations:

$$\boldsymbol{m} = \begin{bmatrix} \Delta J_1 & \cdots & \Delta J_L & \Delta V_1 & \cdots & \Delta V_N \end{bmatrix}^T = \boldsymbol{H} \begin{bmatrix} I_{f,i} & I_{f,j} \end{bmatrix}^T + \boldsymbol{\varepsilon} \tag{3.12}$$

where indices 1 to $L$ and 1 to $N$ refer to the PMU-measured superimposed currents and voltages, respectively. Moreover, $\boldsymbol{m}, \boldsymbol{H}$, and $\boldsymbol{\varepsilon}$ are the measurement vector, coefficient matrix, and vector of measurement errors, respectively. The unknowns can be estimated using the WLS method as

$$\left[\hat{I}_{f,i}, \hat{I}_{f,j}\right]^T = \left(\boldsymbol{H}^* \boldsymbol{W} \boldsymbol{H}\right)^{-1} \boldsymbol{H}^* \boldsymbol{W} \boldsymbol{m} \tag{3.13}$$

where the asterisk refers to the conjugate transpose of the matrix and $\boldsymbol{W}$ is the weight matrix. Let $\beta$ denote the ratio between $\hat{I}_{f,i}$ and $\hat{I}_{f,j}$ obtained from (3.13). With proper mathematical manipulations, a generalised closed-form solution for the fault distance can be derived from (3.9) as below [67]

$$\alpha = \frac{1}{2 l_{ij} \gamma_{ij}} \ln \left[ \frac{e^{l_{ij}\gamma_{ij} + \beta}}{e^{-l_{ij}\gamma_{ij} + \beta}} \right] \tag{3.14}$$

### 3.3.2 Faulted Line Identification

Fault location is carried out offline, and the faulted line may or may not be known to the process [67, 87]. If not, one can easily use the superimposed-circuit technique to indicate the faulted line from available PMU data. In this technique, the system of equations (3.12) is derived and solved for every faulted line candidate using (3.13). Let $\widehat{\boldsymbol{x}}$ denote the vector of estimated nodal current injections at the fault line terminals obtained by (3.13), i.e., $\widehat{\boldsymbol{x}} = \left[\hat{I}_{f,i}, \hat{I}_{f,j}\right]^T$. The vector of residuals can be calculated as $\boldsymbol{r} = \boldsymbol{m} - \boldsymbol{H}\widehat{\boldsymbol{x}}$. Finally, the weighted sum of squared residuals can be easily obtained using the closed-from expression below

$$WSSR = \boldsymbol{r}^* \boldsymbol{W} \boldsymbol{r} \tag{3.15}$$

The *WSSR* of the faulted line would be ideally zero as all measurements hold true in equations of types (3.10) and (3.11). In contrast, the *WSSR*s of non-faulted lines take non-eligible values

because these lines have a set of incorrect equations with no meaningful connections to the measurements taken [11, 15]. For a set of incorrect equations, the equation residuals, and thus the corresponding *WSSR*, will be non-zero [73]. To identify the faulted line, thus, it is only needed to evaluate the *WSSR*s for all candidate lines as the smallest one refers to the faulted line.

### 3.3.3 Weight Matrix and Superimposed Errors

Due to measurement errors, there may be more confidence in some synchrophasors than others. WLS is a generalisation of ordinary least-squares (OLS) in which measurement errors are incorporated into the estimation to achieve the best linear unbiased prediction of unknowns [80]. If the measurements are independent, the weight of each measurement will be set equal to the reciprocal of its variance [80]. In the context of the proposed formulation, the term superimposed error refers to the error of a superimposed synchrophasor, which is the difference between the random errors of the corresponding post- and pre-fault synchrophasors. Thus, the superimposed error is a function of the error of the corresponding pre- and post-fault synchrophasors. A salient contribution of this research is formulating the mean and variance of the superimposed error with respect to the statistical distributions of the errors of pre- and post-fault synchrophasors.

As verified in [67, 88], synchrophasors have independent distributions of errors in magnitude and phase-angle. Pre- and post-fault synchrophasors, in general, can have different distributions of errors. Let $y = re^{j\theta}$ and $y' = r'e^{j\theta'}$ denote random variables (RVs) representing the pre- and post-fault fundamental-frequency synchrophasors of a variable. Similar to many other studies, errors are assumed to have normal distributions [67]. Measurement errors account for different sources of errors, such as instrument transformer errors and measurement noises [85]. The errors in the magnitudes and phase-angles of $y$ and $y'$ can be defined by four real-valued independent Gaussian random variables as $\varepsilon_{r'} \sim \mathcal{N}\left(0, \sigma_{r'}^2\right), \varepsilon_{\theta'} \sim \mathcal{N}\left(0, \sigma_{\theta'}^2\right)$, $\varepsilon_r \sim \mathcal{N}\left(0, \sigma_r^2\right)$, and $\varepsilon_\theta \sim \mathcal{N}\left(0, \sigma_\theta^2\right)$, where $\sigma$ denotes the standard deviation of errors. Let $y_m = r_m e^{j\theta_m}$ and $y'_m = r'_m e^{j\theta'_m}$ denote the measured samples of these RVs. Let us denote the expected value of the error of the superimposed synchrophasor $\Delta y_m = y'_m - y_m$, i.e., the mean of superimposed error, by $\mu_{\epsilon_m}$. As will be justified in the following subsection, this can

be obtained from

$$\mu_{\epsilon_m} = y'_m \left(e^{-\sigma^2_{\theta'}} - e^{-\sigma^2_{\theta'}/2}\right) - y_m \left(e^{-\sigma^2_{\theta}} - e^{-\sigma^2_{\theta}/2}\right) \tag{3.16}$$

It follows from (3.16) that although the mean of $\varepsilon_{r'}, \varepsilon_{\theta'}, \varepsilon_r$, and $\varepsilon_\theta$ are zero, the mean of the superimposed error can be nonzero. This means WLS estimation using superimposed synchrophasors will be biased [80, 89]. To counteract this, the means should be subtracted from the corresponding superimposed synchrophasors in [86]. As will be demonstrated in the following, the variance of superimposed errors will be

$$\sigma^2_{\Delta y_m} = \sigma^2_{\epsilon_m} = r'^2_m \left(1 - e^{-\sigma^2_{\theta'}}\right) + \sigma^2_{r'} \left(2 - e^{-\sigma^2_{\theta'}}\right) + r^2_m \left(1 - e^{-\sigma^2_{\theta}}\right) + \sigma^2_r \left(2 - e^{-\sigma^2_{\theta}}\right) \tag{3.17}$$

The weight associated with each equation in [88] is equal to the reciprocal of the variance of its superimposed error. The knowledge of the variance of superimposed errors, given in (3.17), is also a prerequisite for effective bad data detection [80].

### 3.3.4 Mathematical Proof for the Equations Derived

Let $\mu_r, \mu_\theta, \mu_{r'}$, and $\mu_{\theta'}$ denote the true values of the magnitudes and phase-angles of the pre- and post-fault synchrophasors. The RV for the corresponding superimposed synchrophasor can be expressed as

$$\Delta y = (\mu_{r'} + \varepsilon_{r'})\, e^{j(\mu_{\theta'} + \varepsilon_{\theta'})} - (\mu_r + \varepsilon_r)\, e^{j(\mu_\theta + \varepsilon_\theta)} \tag{3.18}$$

Equation (3.18) can be rewritten as

$$\Delta y = \mu_{r'} e^{j\mu_{\theta'}} - \mu_r e^{j\mu_\theta} + \epsilon \tag{3.19}$$

where $\mu_{r'} e^{j\mu_{\theta'}} - \mu_r e^{j\mu_\theta}$ is the true value of $\Delta y$, and

$$\epsilon = \mu_{r'} e^{j\mu_{\theta'}} \left(e^{j\varepsilon_{\theta'}} - 1\right) + \varepsilon_{r'} e^{j(\mu_{\theta'} + \varepsilon_{\theta'})} - \mu_r e^{j\mu_\theta} \left(e^{j\varepsilon_\theta} - 1\right) - \varepsilon_r e^{j(\mu_\theta + \varepsilon_\theta)} \tag{3.20}$$

It is well known that for two independent RVs, any function of one RV is independent of any function of the other RV. Since $\varepsilon_r$ and $\varepsilon_\theta$ are independent,

$$\mathbb{E}\left(f\left(\varepsilon_r\right)\cdot g\left(\varepsilon_\theta\right)\right)=\mathbb{E}\left(f\left(\varepsilon_r\right)\right)\mathbb{E}\left(g\left(\varepsilon_\theta\right)\right) \tag{3.21}$$

As $\mathbb{E}\left(\varepsilon_r\right)=0$, the expected value of the multiplication of $\varepsilon_r$ by any function of $\varepsilon_\theta$ is zero. Accordingly, the expected values of the second and the fourth terms in (3.20) are zero. Moreover, for a Gaussian random variable, e.g., $\varepsilon_\theta$, we have [89]

$$\mathbb{E}\left(e^{j\varepsilon_\theta}\right)=\mathbb{E}\left(e^{-j\varepsilon_\theta}\right)=e^{-\sigma_\theta^2/2} \tag{3.22}$$

Using (3.21) and (3.22), the expected value of $\epsilon$ is obtained as

$$\mu_\epsilon=\mu_{r'}e^{j\mu_{\theta'}}\left(e^{-\sigma_{\theta'}^2/2}-1\right)-\mu_r e^{j\mu_\theta}\left(e^{-\sigma_\theta^2/2}-1\right) \tag{3.23}$$

The variance of $\epsilon$ can be obtained by (3.20) and (3.23) as [89]

$$\sigma_\epsilon^2=\mathbb{E}\left(\left|\epsilon-\mu_\epsilon\right|^2\right)=\mathbb{E}\left(\left[\epsilon-\mu_\epsilon\right]\left[\epsilon-\mu_\epsilon\right]^*\right) \tag{3.24}$$

Using (3.21) to (3.24) and some mathematical manipulations, one can obtain the variance of $\epsilon$ as below

$$\sigma_\epsilon^2=\mu_{r'}^2\left(1-e^{-\sigma_{\theta'}^2}\right)+\sigma_{r'}^2+\mu_r^2\left(1-e^{-\sigma_\theta^2}\right)+\sigma_r^2 \tag{3.25}$$

Since the values of $\mu_{r'}$, $\mu_{\theta'}$, $\mu_r$, and $\mu_\theta$ are not available in practice, (3.23) and (3.25) cannot be directly utilised to calculate the mean and variance of the error of a superimposed phasor measurement. Therefore, the expected values of $\mu_\epsilon$ and $\sigma_\epsilon^2$ should be obtained conditioned on the measured values, i.e., $y_m=r_m e^{j\theta_m}$ and $y'_m=r'_m e^{j\theta'_m}$. We have $\mu_{r'}=r'_m-\varepsilon_{r'}$, $\mu_{\theta'}=\theta'_m-\varepsilon_{\theta'}$, $\mu_r=r_m-\varepsilon_A$, and $\mu_\theta=\theta_m-\varepsilon_\theta$. These equations are replaced in (3.23) and (3.25) to calculate the expected values of the resulting expressions. Using (3.21) and (3.22) and after some mathematical manipulations, the mean and the variance of the superimposed error associated with the superimposed synchrophasor $\Delta y_m=y'_m-y_m$, conditioned on the measured values, are obtained as (3.16) and (3.17), respectively. It is worth noting that these formulations are derived based on having a normal distribution for the RVs. Otherwise, the formulations should be accordingly adjusted to the considered distributions of RVs.

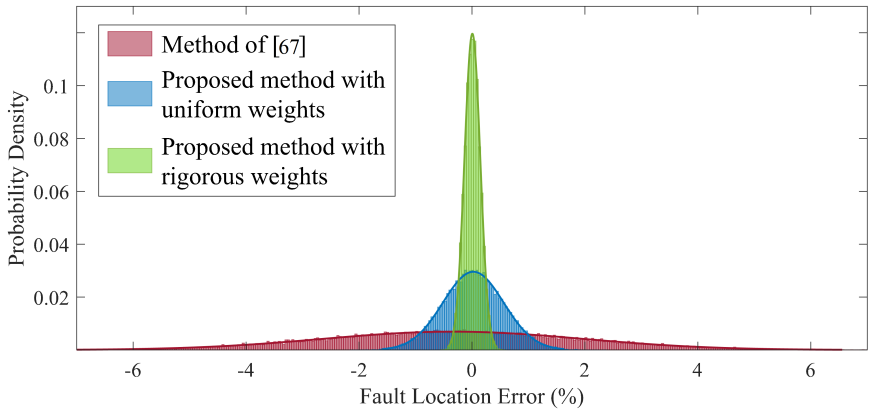


Figure 3.4: Distribution of the fault location error using different methods [69].

### 3.3.5 Performance Evaluation

Extensive simulations are conducted on the IEEE 39-bus test system to evaluate the performance of the proposed method. The phasors of the time-domain waveforms generated in PowerFactory are estimated using a real PMU model [64]. PMUs are typically placed in power systems to provide network observability [84]. Thus, using the method of [84], 12 PMUs are placed at buses 3, 5, 8, 11, 14, 16, 19, 23, 25, 27, 29, and 39 to make the network fully observable. However, the method does not require full network observability. The performance with partial network observability and different numbers of PMUs will also be studied.

The errors of magnitudes and phase angles of synchrophasors are assumed to have a variation range of $\pm 1\%$ with normal distribution. The variation ranges of errors are reported based on the three-sigma criterion [89]. In other words, the variation range of a normally distributed error with standard deviation $\sigma$ is $[-3\sigma, +3\sigma]$. In principle, one phasor reported before and one after the fault onset would be sufficient to obtain the superimposed phasors [67]. In the simulations conducted, these are calculated at 60 ms following the fault onset.

First, the method's performance is studied for an arbitrary 1-ph-g fault at 20% of line 3-18. To obtain solid results, the fault case is repeated 50,000 times. Figure 3.4 shows the distribution of the fault location error by different methods, i.e., that of [67] (which ignores current measurements), the proposed method with uniform weights (OLS), and the proposed method with rigorous weights (WLS). It can be seen that the standard deviation of fault location errors by OLS is smaller than that by the method of [67]. This demonstrates that the inclusion

Table 3.4: Fault Location Error (%) by Different Methods

| Fault Location Method | Fault Distance | | | |
|---|---|---|---|---|
| | 97.5% | 95% | 90% | 80% |
| Conventional [78] | 9.88 | 9.53 | 8.75 | 7.92 |
| Proposed | 0.43 | 0.41 | 0.39 | 0.38 |

Table 3.5: WAFL Results with Different Numbers of PMUs

| Number of PMUs | | 12 | 9 | 6 | 12 | 9 | 6 |
|---|---|---|---|---|---|---|---|
| Fault Case | Fault Location Error (%) | Proposed Method | | | Method of [67] | | |
| 2-ph-g at 25% Line 26-28 | Mean | 0.04 | 0.06 | 0.09 | 0.07 | 0.08 | 0.12 |
| | Standard Deviation | 0.22 | 0.21 | 0.25 | 1.38 | 1.77 | 2.35 |
| 3-ph-g at 95% Line 10-13 | Mean | 0.38 | 0.44 | 0.64 | 1.04 | 1.56 | 2.45 |
| | Standard Deviation | 0.36 | 0.75 | 0.97 | 2.56 | 3.96 | 5.45 |

of current synchrophasors, even without the knowledge of variances of superimposed errors, enhances the accuracy of FL. As expected, the fault location accuracy is significantly improved when the WLS is minimised using the rigorous weights obtained in the previous section.

To demonstrate the method's capability in dealing with CT saturation and close-in faults, all 12 PMUs are connected to magnetic-core CTs/VTs with an accuracy class of 0.5. A solid 1-ph-g fault at different locations of line 7-8 is considered. For faults near bus 8, the CT feeding the PMU at this bus becomes saturated, resulting in an erroneous current measurement. Accordingly, the largest normalised residual test is used for bad data detection and elimination [80]. Table 3.4 compares the fault location error by the proposed method and the well-known two-terminal method of [78]. As seen, the presence of extra data (redundant equations) in the proposed method enables it to reduce the impact of erroneous measurements to a great extent.

Now, the impact of the number of PMUs on the fault location error is investigated. To this end, 20 random PMU placements leading to a solvable system of equations are considered for each certain number of PMUs. The simulation is repeated 10,000 times for each PMU placement. Table 3.5 reports the mean and standard deviation of the fault location errors for faults on two arbitrary lines using various methods. As can be seen, the proposed method outperforms the method of [67], especially with fewer PMUs.

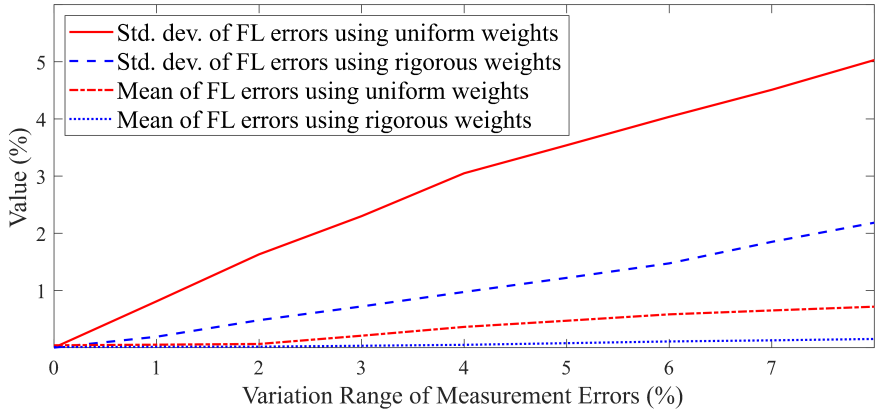


Figure 3.5: Mean and standard deviation of the fault location error by different methods [69].

Table 3.6: Sensitivity to the Presence of PMU at the Faulted Line Terminals

| Faulted Line Terminals with PMUs | Neither | One | Both |
|---|---|---|---|
| Mean of Fault Location Errors (%) | 0.10 | 0.09 | 0.06 |
| Standard Deviation of Fault Location Errors (%) | 0.56 | 0.53 | 0.45 |

Here, a total of 2,000 fault cases of different types are simulated at different locations in the system. For each fault case, the fault resistance is varied between 0 Ω to 50 Ω in 10 Ω steps. Measurement errors are set to have normal distributions, and each fault case is repeated 10,000 times. The voltage and current phasors from the 12 PMUs [84] are contaminated with up to 8% errors before calculating the fault distance from (3.14). Figure 3.5 shows the results obtained by the proposed method using uniform weights and the rigorous weights derived. As seen, the mean and standard deviation of the fault location (FL) errors are noticeably smaller using the rigorously established weight matrix. This confirms that accounting for the distributions of superimposed errors can considerably improve WAFL accuracy.

Two independent equations are sufficient to solve (3.12) by (3.13). The method does not require any specific set of PMU data, such as PMUs at either or both terminals of the faulted line. To demonstrate this, simulations are repeated for the lines with no PMUs at either terminal by adding PMUs at their terminals. In this study, the variation range of the errors is considered to be $\pm 1\%$. The results are tabulated in Table 3.6, showing that the proposed WAFL method can provide accurate results with and without PMUs at the faulted line terminals.

## 3.4 Summary

This chapter focused on the improvement of the superimposed circuit methodology for WAFL and WABP. A technique was proposed to reduce the computational complexity of WAFL/WABP methods that are based on the superimposed circuit methodology. A proposition was put forward and proved to demonstrate that there is a one-to-one equivalence between the responses of the superimposed circuit with and without the faulted line. This removes the need for calculating as many bus impedance matrices as the number of candidate lines in the system to identify the faulted line. The proposed technique limits the foregoing requirement to merely calculating the bus impedance matrix of the pre-fault power system. Extensive simulations conducted confirm that the proposed technique can reduce the computational burden without impacting the success rate of WABP.

Furthermore, to enhance the application of the weighted least-squares method for WAFL and WABP, the mean and variance of superimposed errors were rigorously calculated based on the statistical distributions of the errors of pre- and post-fault synchrophasors. In doing so, a generalised closed-form solution for WAFL/WABP using sparse PMU measurements was presented. Incorporating the established weight matrix into the formulation, and taking advantage of both voltage and current synchrophasors make the results considerably more accurate than that of similar WAFL methods. The linearity of the formulation and the rigorous derivations of superimposed errors facilitate the application of well-established bad data detection methods. Extensive simulations conducted confirm the effectiveness of the proposed method and its robustness against different factors such as fault type and resistance.

# CHAPTER 4

## WABP in the Presence of Renewable Energy Sources

## 4.1 Overview

Renewable energy sources possess distinctive controllability features that are not adequately accounted for in WAPB methods found in the literature. The inverter-based resources (IBRs) are capable of swiftly adjusting the amplitude and phase angle of their terminal voltage and current in order to fulfil their control objectives during steady-state, fault, and post-fault conditions in a matter of milliseconds [46]. To develop a dependable WABP method, it is crucial to accurately capture the behaviour of IBRs while simultaneously minimising the computational burden. This chapter aims to address these challenges without imposing any restrictions on the number or locations of IBRs, as well as their control strategies. It is worth noting that the techniques proposed in Chapter 3 for improving the speed and accuracy of superimposed-circuit methodology can also be applied to the proposed method in this Chapter.

## 4.2 IBR Configuration and Power Control Strategy

Various types of IBRs are being used in power systems, including full converter wind turbines, photovoltaic generators, and doubly-fed induction generators. Two things are common between them, an internal DC link and a DC-to-AC converter. The internal DC link functions as a bridge to deliver active power from an AC-to-DC converter or directly from the renewable power source to the DC-to-AC converter connected to the grid. The fault behaviour of IBRs differs from that of synchronous machines. IBRs can rapidly modify the phasors of their current/voltage based on some control strategies for steady-state, fault conditions, and post-fault conditions quite faster than conventional generators. The speed of response and available control strategies are mainly related to the technology used in the converters.

This section presents the IBR's configuration studied and the power control strategies scrutinised in the following sections. It is assumed that a standard three-phase voltage source converter (VSC) is connected to the point of common coupling (PCC) and the grid through an LCL filter, as shown in Figure 4.1. Such IBRs are typically controlled by a three-level control structure, including the outer control loops, inner current control loop, and the PWM controller [46]. The outer control loops determine current references for the inner current control loop, which translates these to voltage references for the PWM controller.

It is worth noting that the type of renewable energy source, e.g., solar, and wind, is not

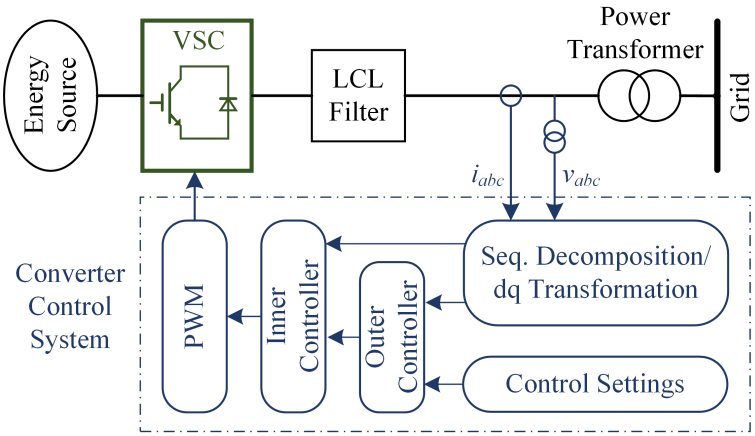


Figure 4.1: IBR's configuration and power control scheme.

of interest in this study since it does not have any influence on the subject of this research. Indeed, the DC voltage source stands for the active power generated by the IBR. In this study, the behaviour of IBRs during fault conditions for the power system protection concerns is of interest. Accordingly, the internal control mechanism of switching devices is not of interest as their response time is much shorter than that of concerned by WABP methods [3, 15].

Fully controllable VSCs allow handling active and reactive power independently in all four-quadrant control areas. The decoupled control algorithm enables us to adjust active and reactive terminal currents during both steady-state and transient conditions. In the steady state, the active current control loop is responsible for adjusting the active power delivered by the energy source. In other words, the active current controller is in charge of regulating the voltage of the DC link. Moreover, the reactive current control loop regulates the voltage at the PCC, i.e., reactive power delivered to the grid. During fault conditions, a control system is responsible for tuning active and reactive currents according to the grid code requirements. It should be noted that in order to avert undesirable damage to the equipment, the terminal current must be limited within the operational range [3].

Without loss of generality, in this thesis, the dual reference frame scheme presented in [90] is used for the outer control loops of IBRs. In this approach, the positive rotating synchronous frame is utilised to control the positive-sequence components. The negative rotating synchronous frame is also used to control the negative-sequence components. In doing so, the converter voltages and currents in the stationary $abc$ frame are first expressed in terms of the stationary

$\alpha\beta$ reference frame [46, 90]. Then, the positive- and negative-sequence quantities in the $\alpha\beta$ frame are obtained. For example, voltage quantities are calculated as shown below

$$\begin{bmatrix} v_\alpha^+ \\ v_\beta^+ \end{bmatrix} = \frac{1}{2}\begin{bmatrix} 1 & -i \\ i & 1 \end{bmatrix}\begin{bmatrix} v_\alpha \\ v_\beta \end{bmatrix}$$
$$\begin{bmatrix} v_\alpha^- \\ v_\beta^- \end{bmatrix} = \frac{1}{2}\begin{bmatrix} 1 & i \\ -i & 1 \end{bmatrix}\begin{bmatrix} v_\alpha \\ v_\beta \end{bmatrix} \tag{4.1}$$

where the operator $i$ represents a $90^\circ$ phase shift in the time domain, and the superscripts $+$ and $-$ refer to positive- and negative- sequence components, respectively. Finally, the $\alpha\beta$ stationary frame quantities are transformed into their respective sequence rotating *dq*-frames, i.e., $v_d^+, v_q^+, v_d^-$, and $v_q^-$ [46]. The *dq*-frame transformation is further detailed in Appendix A.

Within the three-level control structure, the outer control loops have the duty of adjusting the average active and reactive power of the IBR in normal operating conditions [46]. However, some extra control loops can be appended to the outer control loop to appropriately respond to fault conditions in the positive- and negative-sequence circuits.

### 4.2.1 Control Strategies in the Negative-Sequence Circuit

While the Grid Code typically dictates positive-sequence control references, negative-sequence quantities may be controlled as appropriate with no strict requirements in place. Popular control objectives for the negative-sequence circuit are suppressing the negative-sequence current, eliminating the active power ripple, eliminating the reactive power ripple, or imitating an impedance in the negative-sequence circuit [61, 91]. These control strategies aimed at unbalanced voltage conditions are detailed below.

#### A. Suppressing Negative-Sequence Current

If the negative-sequence voltage at the VSC terminal is not controlled, it remains zero in all operating conditions. This can result in a large damaging negative-sequence current passing through the VSC upon an asymmetrical fault. A reasonable preventative strategy is to eliminate the negative-sequence current passing through the VSC. To this end, the negative-sequence references are set to zero, while the positive-sequence current references are regulated by the

Grid Code. A key feature of this strategy is the retention of the maximum current capacity of the IBR for control purposes in the positive-sequence circuit [61].

### B. Eliminating the Active or Reactive Power Ripple

The power ripple refers to the oscillating components of active or reactive power during faults. It is possible to remove the power ripple using appropriate negative-sequence control strategies. To this end, the reference currents are calculated as below [61]:

$$\begin{bmatrix} i_d^+ \\ i_q^+ \\ i_d^- \\ i_q^- \end{bmatrix}_{ref} = \begin{bmatrix} v_d^+ & v_q^+ \\ v_q^+ & -v_d^+ \\ -Kv_d^- & Kv_q^- \\ -Kv_q^- & -Kv_d^- \end{bmatrix} \begin{bmatrix} \frac{P_{ref}}{D} \\ \frac{Q_{ref}}{E} \end{bmatrix} \tag{4.2}$$

where $P_{ref}$ and $Q_{ref}$ are the reference values for the active and reactive power, and the coefficients $D$ and $E$ are calculated based on the IBR control strategy and quantities in the rotating *dq*-frames as below

$$\begin{cases} D = \left(v_d^+\right)^2 + \left(v_q^+\right)^2 - K\left(v_d^-\right)^2 - K\left(v_q^-\right)^2 \\ E = \left(v_d^+\right)^2 + \left(v_q^+\right)^2 + K\left(v_d^-\right)^2 + K\left(v_q^-\right)^2 \end{cases} \tag{4.3}$$

The coefficient $K$ in the forgoing formulas is set to -1 when the control strategy is eliminating the active power ripple. This coefficient is set to 1 when the control strategy is eliminating the reactive power ripple.

### C. Imitating an Impedance in the Negative-Sequence Circuit

The most recent German Grid Code [92] requires the negative-sequence current to be injected in proportion to the negative-sequence voltage. This would help directional protection elements operate reliably by providing sufficient negative-sequence current and a noticeable phase angle difference between negative-sequence voltage and current [93]. If the negative-sequence current is maintained proportional to negative-sequence voltage, the IBR demonstrates a constant negative-sequence impedance, i.e., $|z^-|\angle\theta^-$. To achieve this, the reference currents are obtained from

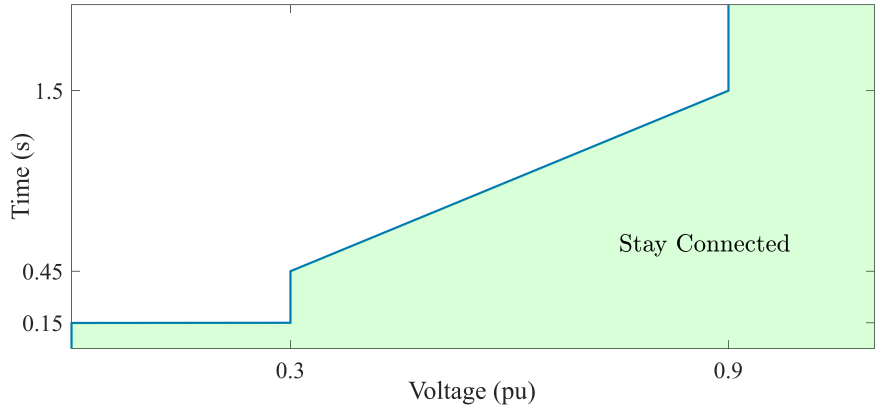


Figure 4.2: Time-voltage profile requirements for wind turbines.

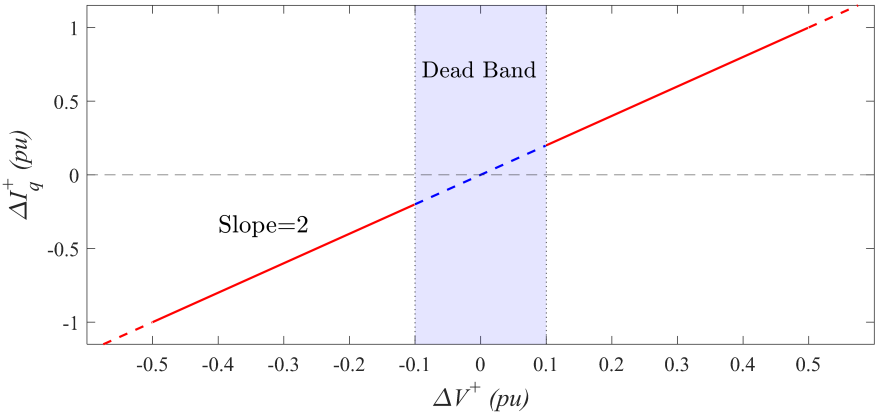


Figure 4.3: Reactive current injection requirements for wind turbines.

$$\begin{bmatrix} i_d^- \\ i_q^- \end{bmatrix}_{ref} = \begin{bmatrix} v_d^- & v_q^- \\ v_q^- & -v_d^- \end{bmatrix} \begin{bmatrix} \frac{\cos(\theta^-)}{|z^-|} \\ \frac{\sin(\theta^-)}{|z^-|} \end{bmatrix} \tag{4.4}$$

### 4.2.2 Control Strategies in the Positive-Sequence Circuit

In the IBR's control strategy shown in Figure 4.1, the outer controller is responsible for adjusting the power references in normal and fault conditions [3]. The operating strategy of IBRs during fault conditions is standardised by Grid Codes under low-voltage ride-through (LVRT) requirements [94–96]. These requirements are set to ensure that IBRs remain connected to the grid during transient voltage deviations based on a time-voltage profile. To this end, these

sources inject additional positive-sequence reactive current to provide voltage support. Various LVRT requirements are defined in Grid Codes. For example, Figures 4.2 and 4.3 show the time-voltage profile and the reactive current injection of a wind turbine, respectively, as mandated by [95]. As can be seen, wind turbines are needed to provide positive-sequence reactive current proportional to the voltage drop during faults. In this regard, they should inject at least 1 pu of reactive current for up to 150 ms during extremely low voltage conditions.

## 4.3 The Proposed Superimposed Circuit Technique

In this subsection, the superimposed circuit technique presented in [15] is extended to derive a linear system of equations for WABP concerning the fault incident. Synchronous generators can be modelled as constant impedances in the superimposed circuit within the time frame of interest [11, 34]. However, this is not valid for renewables due to their time-variant nature induced by their control strategies. Therefore, IBRs are replaced by proper current sources in this study. As a result, the superimposed circuit will include two nodal current injections representing the faulted line and a nodal current injection for each IBR to represent its behaviour with reference to the fault. Then, *WSSR* is used to pinpoint the faulted line.

### 4.3.1 Individual Analysis of the Sequence Circuits

The interconnection of sequence circuits is dictated by the fault type [2]. Nonetheless, as explained in Chapter 2, each sequence circuit can also be studied independently regardless of the fault resistance, type, and location. This is possible so long as the other sequence circuits and fault resistance are replaced by a proper current source based on the *Substitution Theorem* [15]. Asymmetrical faults are the most frequent type of short-circuit faults on transmission systems [2]. The focus of this section is WABP against asymmetrical faults by taking advantage of the unique characteristics of the negative-sequence circuit [13]. The negative-sequence circuit is the most suitable circuit for fault location analysis under asymmetrical faults. This is due to the absence of negative-sequence components in the pre-fault condition, the time-invariant behaviour of synchronous machines in the negative-sequence circuit, and its higher accuracy compared to that of the zero-sequence circuit [13]. As will be described, the positive-sequence circuit will only be employed for identifying the operating modes of IBRs.

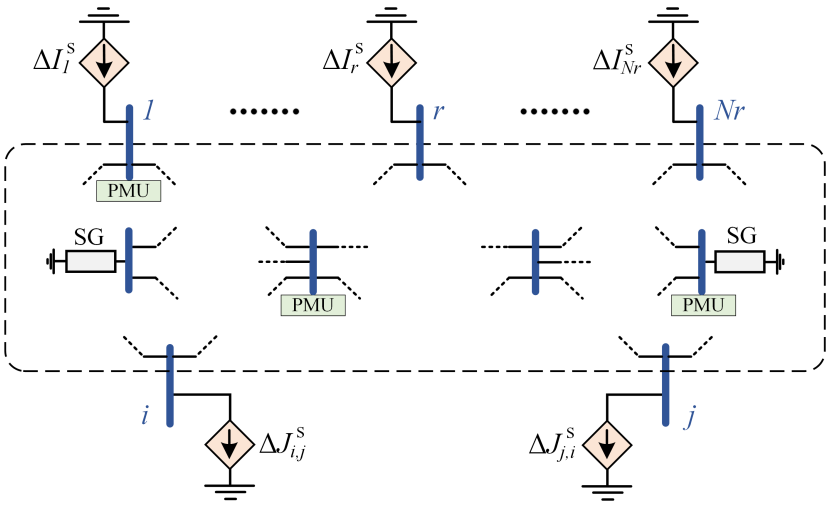


Figure 4.4: Superimposed sequence circuit "$s$" for a fault at line *i*-*j*.

### 4.3.2 Systems of Equations Representing the Fault

As shown in Figure 4.4, let us assume that line $i$-$j$ is the faulted line and $\boldsymbol{Z}^s$ denotes the bus impedance matrix of the sequence circuit "$s$" excluding line $i$-$j$ and all IBRs. The superscript $s$ refers to the corresponding sequence circuit and takes a value of "$+$" or "$-$" for the positive- and negative-sequence circuits, respectively. Let $\Delta I_r^s$, $\Delta J_{i,j}^s$, and $\Delta J_{j,i}^s$ represent the superimposed current of an IBR at bus $r$ and those of the sending- and receiving-end of the faulted line $i$-$j$ in sequence circuit "s", respectively. The superimposed voltage measured by a PMU at an arbitrary bus $k$ satisfies the following equation

$$\Delta V_k^{s,m} = \sum_{r=1}^{Nr} Z_{k,r}^s \Delta I_r^s - Z_{k,i}^s \Delta J_{i,j}^s - Z_{k,j}^s \Delta J_{j,i}^s + e_{V(k)} \tag{4.5}$$

where the superscript "$m$" refers to measured quantities, 1 to $Nr$ are the indices of buses connected to an IBR, and $e_{V(k)}$ represents the associated measurement error.

Let $\Delta J_{u,v}^s$ denote the PMU-measured superimposed current of the sending-end of a non-faulted line $u$-$v$. This current can be expressed as a function of the nodal current sources as below

$$\Delta J_{uv}^{s,m} = \sum_{r=1}^{Nr} C_{uv,r}^s \Delta I_r^s - C_{uv,i}^s \Delta J_{i,j}^s - C_{uv,j}^s \Delta J_{j,i}^s + e_{J(uv)} \tag{4.6}$$

where $e_{J(uv)}$ stands for the corresponding measurement error, and the derivation of $C_{uv}^s$ is

obtained by (2.6). if $\Delta I_r^s, \Delta J_{i,j}^s$, and $\Delta J_{j,i}^s$ are directly mby PMUs, the equations below can also be established

$$\begin{cases} \Delta I_r^{s,m} = \Delta I_r^s + e_{I(r)} \\ \Delta J_{i,j}^{s,m} = -\Delta J_{i,j}^s + e_{J(ij)} \\ \Delta J_{j,i}^{s,m} = -\Delta J_{j,i}^s + e_{J(ji)} \end{cases} \tag{4.7}$$

where the negative signs on the right-hand side of the equations result from the convention assumed for the direction of nodal injections and transmission line currents. It should be noted that Figure 4.4 is only an exemplary representation of the superimposed circuit. Equations (4.5) to (4.7) remain valid even when either or both of buses $i$ and $j$ is connected to an IBR.

Let us assume PMUs provide $Np$ voltage and current measurements from across the grid. By writing equations (4.5) to (4.7) based on available PMU measurements, a system of linear equations can be obtained as below

$$\boldsymbol{m}_{Np\times 1} = \boldsymbol{H}_{Np\times(2+Nr)}\boldsymbol{x}_{(2+Nr)\times 1} + \boldsymbol{\varepsilon}_{Np\times 1} \tag{4.8}$$

where $\boldsymbol{m}, \boldsymbol{H}$, and $\boldsymbol{\varepsilon}$ are the measurement vector, coefficient matrix, and error vector, respectively. Further, $\boldsymbol{x}$ is the vector of current sources replaced for the faulted line and IBRs, as below

$$\boldsymbol{x} = \begin{bmatrix} \Delta J_{i,j}^s & \Delta J_{i,j}^s & \Delta I_1^s \dots & \Delta I_{Nr}^s \end{bmatrix}^T \tag{4.9}$$

The linear system of equations (4.8) can be readily solved using the weighted least-squares method. In this regard, the unknowns can be estimated by (2.8). As explained, these estimates might not be precisely equal to their corresponding true values because of measurement errors incurred in practice.

### 4.3.3 Identifying the Faulted Line

The system of equations (4.8) is derived assuming that the line $i-j$ is the faulted line. The (*WSSR*) is the objective function minimised for solving (4.8) by the least-squares method and can be obtained by (2.9) and (2.10). The *WSSR* of the faulted line would be ideally zero as all measurements hold true in equations (4.5) to (4.7). However, due to measurement/parameter imperfections, the *WSSR* of the faulted line might not be exactly zero but very small [15]. Accordingly, (4.8) should be solved for different suspected lines to identify the smallest *WSSR*,

thus the faulted line. Once unknowns in $\boldsymbol{x}$ are estimated, the superimposed voltages at any buses, including the faulted line terminals, can be obtained by (4.5). Having calculated the superimposed voltage and current phasors at the faulted line terminals, the closed-form expression introduced in [78] can be used to obtain the fault distance on the faulted line. The calculated fault distance is checked to ensure it lies within the acceptable range to enhance the security of the proposed method.

## 4.4 WABP in the Presence of IBRs Using the Negative Seq. Circuit

In this section, using the negative-sequence circuit, a novel WABP method is proposed against asymmetrical faults on transmission systems with high penetration of IBRs. The proposed method leverages the full potential of available synchrophasors without placing any strict constraints on PMU locations. The method performs well under a wide variety of control strategies employed by IBRs in the negative-sequence circuit. To enable this, IBRs are appropriately modelled to capture their fault behaviour, thus formulating their impact on the WABP.

### 4.4.1 Accounting for the High Penetration of RESs

As explained, every IBR circuit can be modelled as an unknown current source in each superimposed sequence. As suggested by [15], this current can be directly measured by a PMU. However, it may not be practical to install a PMU at every bus with an IBR. Even if there is a PMU at all IBR buses, WABP must not be contingent on the availability of a specific set of PMU measurements. As discussed in IEEE standard C37.118.2 [97], communication latency is unavoidably unpredictable and may vary from a few milliseconds to even seconds due to factors such as error checking, forwarding, and routing. Therefore, some PMU measurements might not be received within the action time necessary for successful WABP. On the other hand, having a large number of non-measured unknown currents representing IBRs in the vector $\hat{\boldsymbol{x}}$ might lead to an unsolvable system of equations, thus, no *WSSR*s to act upon [15, 73].

It is fair to assume that the control strategies of IBRs and their corresponding settings are available to the control centre. The knowledge of these may be used to overcome the foregoing unsolvability challenge. The goal is to reduce the number of unknowns to the extent that (4.8) becomes solvable with a unique solution. To this end, a sufficient number of unmonitored IBRs

(IBRs without PMUs) can be replaced by their equivalent superimposed impedances in the negative-sequence circuit. In doing so, the operating modes of IBRs are first determined using the superimposed technique and SCADA data. Next, the equivalent superimposed impedances of the selected IBRs are calculated and incorporated into the superimposed circuit. Since IBRs exhibit different equivalent impedances after reaching their overcurrent limits, their estimated output currents are to be checked, as well. As will be described, appropriate modifications will then be applied in order to update their equivalent superimposed impedances.

### A. IBR's Operating Mode Following a Fault

Following a short-circuit fault, IBRs may work in either steady-state or fault mode. In the steady-state mode, they inject active and reactive power equal to pre-set references. In the fault mode, the operating references are adjusted based on the Grid Code requirements to support the grid in fault conditions. The amount of positive-sequence voltage dip at an IBR terminal determines the IBR's operating mode. For instance, if the balanced voltage dip is larger than 10%, the IBR should operate in the fault mode (as instructed by the GB and Tennet Grid Codes). As detailed in [61], the equivalent positive-sequence impedance of an IBR in the superimposed circuit depends on the pre-fault voltage and current phasors. Hence, IBRs with no PMUs at their terminals cannot be easily modelled in the superimposed positive-sequence circuit.

To determine IBRs' operating modes, the following steps are taken in the proposed method to estimate positive-sequence voltage dips whilst maintaining the computational burden low:

(*i*) IBRs whose currents are not directly measured by PMUs are firstly disregarded in the superimposed circuit. This is to approximately estimate positive-sequence superimposed voltages using the described superimposed circuit technique.

(*ii*) Approximate post-fault bus voltages are calculated in this step. Based on the *Superposition Theorem*, post-fault bus voltages can be obtained from the pre-fault and superimposed bus voltages, i.e., $\boldsymbol{V}^{+}_{post} = \boldsymbol{V}^{+}_{pre} + \Delta\boldsymbol{V}^{+}$. Superimposed bus voltages are estimated in step (i). Pre-fault bus voltages are assumed to be known in the control centre. This can be easily achieved by effective state estimation methods employing existing synchronised/ unsynchronised measurements [68].

(*iii*) Ignoring IBR contributions to the fault current introduces some errors in the estimated

post-fault voltage quantities. The contributions of IBRs operating in the fault mode are more significant to the inaccuracy introduced than that of IBRs operating in the steady-state mode. This is because IBRs operating in steady-state mode continue to inject the same active and reactive power even after the fault inception. Accordingly, the IBRs are arranged in descending order with respect to voltage dips at their terminals. The IBRs on top of the list can be replaced by unknown current sources and included in the vector $\boldsymbol{x}$ to increase accuracy. This will be applied to as many IBRs as possible as long as the matrix $\boldsymbol{H}$ remains of full rank, which is a sufficient condition for the solvability of (4.8) [73]. This helps to obtain more accurate approximations for post-fault bus voltages.

(*iv*) Let us assume that for voltage dips larger than $\alpha\%$, the IBR is set to operate in the fault mode by injecting extra reactive power. The value of $\alpha$ is dictated by the Grid Code requirements. The estimated post-fault voltages in step (*iii*) might not be quite accurate because some IBRs have not been replaced by a current source.

(*v*) All IBRs experiencing voltage dips close to $\alpha$ are considered to have an uncertain operating mode. Special care should be taken to determine the upper and lower bounds of the uncertain voltage range. As demonstrated in [98], however, the impact of control strategies of an IBR connected to the grid barely exceeds $5\%$ of its terminal voltage. This means that we are almost certain that IBRs with estimated voltage dips less than $(\alpha - 5)\%$ will continue to operate in the steady-state mode. On the other hand, those with estimated voltage dips greater than $(\alpha + 5)\%$ can be assumed to be operating in the fault mode. Next, an additional step is needed to confirm the operating mode of IBRs with estimated voltage dips between the thresholds mentioned above.

The fault behaviour of the IBR (from the power system point of view) is dependent on the converter control strategies and settings and feasible bounds rather than the type of energy source [46]. Various types of renewables might demonstrate slightly different transient behaviour for a few milliseconds following the fault inception. Regardless of the type of renewable sources, however, they will be able to regulate the amplitude and phase angle of their terminal voltage and current to meet their control targets in the steady-state, fault, and post-fault conditions within a few milliseconds [46]. Therefore, the proposed formulation is not impacted by the type of renewable sources. On the other hand, the proposed method is expected to come into

effect in case the primary protection has failed to operate. Thus, a few hundred milliseconds is available for WABP to account for the time that IBRs need to completely switch to their final operating modes before making a trip decision [1, 2].

### B. Incorporating IBRs Models

If an IBR operates in the steady-state mode, e.g. an IBR electrically far enough from the fault location, it does not generate a post-fault negative-sequence current. Due to the absence of the pre-fault negative-sequence components, the superimposed negative-sequence current of that IBR will be zero and can be removed from (4.9). Accordingly, the corresponding column in the matrix $\boldsymbol{H}$ is removed. The negative-sequence behaviour of an IBR operating in the fault mode depends on its control strategy. If there is no information about the control strategies of an IBR at the control centre, it will be modelled as an unknown nodal current source in the WABP formulations (4.8). Otherwise, it is incorporated in the superimposed circuit based on its control strategy, as described below.

*1) Suppressing negative-sequence current*

As described in Section 4.2, an IBR with this control strategy eliminates the negative-sequence current during an asymmetrical fault. Similar to the IBR operating in the steady-state mode, the IBR can be omitted from the circuit, i.e., modelled by an open circuit.

*2) Eliminating the active or reactive power ripple*

IBRs operating in the fault mode can be modelled as an impedance in the superimposed circuit. As detailed in [61], the magnitude and phase angle of the per-unit equivalent negative-sequence impedance of an IBR, i.e., $|z^-|$ and $\theta^-$, with these control strategies, can be calculated as:

$$|z^-| = \frac{1}{\sqrt{\left(\frac{P_{ref}}{(V^+)^2 - K(V^-)^2}\right)^2 + \left(\frac{Q_{ref}}{(V^+)^2 + K(V^-)^2}\right)^2}} \tag{4.10}$$

$$\theta^- = \arctan\left(\frac{Q_{ref}}{P_{ref}} \cdot \frac{(V^+)^2 - K(V^-)^2}{(V^+)^2 + K(V^-)^2}\right) - (K+1) \times 90^\circ \tag{4.11}$$

where $V^-$ and $V^+$ are the positive- and negative-sequence terminal voltages of the IBR. The inclusion of the equivalent impedances of IBRs with this control strategy is not straight-

forward because their equivalent impedance is not always known a priori. As (4.10) and (4.11) demonstrate, the equivalent negative-sequence impedance of an IBR is determined by its control strategy, active and reactive power reference values, and the voltage dip it undergoes due to the fault. That is why we need to resort to an iterative method here. An approximate value for $V^+$ can be calculated as described in part $A$ of this section. It is assumed that the control strategy and reference values are received from SCADA. According to (4.10) and (4.11), $z^-$ is represented as a function of $\Delta V^-$, i.e., $f_1\left(\Delta V^-\right)$. Based on (4.5), the value of $\Delta V^-$ is affected by $z^-$ itself. Thus, it is represented as a function of $z^-$, i.e., $f_2\left(z^-\right)$. Herein, a numerical iterative method is utilised to estimate the values of $Z^-$ and $\Delta V^-$ as follows:

(*i*) The IBR is first removed from the superimposed circuit. Then, the initial value of $\Delta V^-$ is estimated using the described superimposed circuit technique.

(*ii*) The amount of $z^-$ is calculated using (4.10) and (4.11).

(*iii*) The IBR is replaced with impedance $z^-$ in the superimposed circuit. Then, the value of $\Delta V^-$ is updated.

(*iv*) The previous two steps are repeated until the new value of $z^-$ lies within $1\%$ proximity of its previous value.

*3) Imitating an impedance in the negative-sequence circuit*

The IBR operating in this mode represents a constant impedance, say $z^- = |z^-| \angle\theta^-$, in the negative-sequence circuit during an asymmetrical fault. Due to the absence of pre-fault negative-sequence components, the post-fault negative-sequence circuit is equivalent to its superimposed circuit. Therefore, the IBR can be substituted by the preset impedance $z^-$ in the superimposed circuit.

### 4.4.2 Considering Overcurrent Limits of IBRs

Once an IBR reaches its overcurrent limit in the negative-sequence circuit, the reference currents calculated in (4.2) and (4.4) will no longer be valid. This results in an equivalent impedance differing from what it was before reaching the overcurrent limit. Therefore, it is necessary to check if the overcurrent limit of an IBR is reached during a fault. If this is the case, proper modification to the obtained equivalent impedance will be applied.

Reference-current saturation is a common current limiting logic [61], which is considered for limiting the negative-sequence current of IBRs in this section. If the negative-sequence current exceeds a threshold, $i^{-}_{\max}$, the corresponding reference currents are tunned as

$$\begin{cases} i^{-,new}_{d-ref} = \dfrac{i^{-}_{\max}}{\sqrt{\left(i^{-}_{d-ref}\right)^2+\left(i^{-}_{q-ref}\right)^2}} \times i^{-}_{d-ref} \\ \\ i^{-,new}_{q-ref} = \dfrac{i^{-}_{\max}}{\sqrt{\left(i^{-}_{d-ref}\right)^2+\left(i^{-}_{q-ref}\right)^2}} \times i^{-}_{q-ref} \end{cases} \tag{4.12}$$

As a result, if an IBR reaches its negative-sequence current limit, the magnitude of its equivalent negative-sequence impedance can be obtained as follows

$$\left|z^{-}\right|_{\min} = \frac{\left|\Delta V^{-}\right|}{i^{-}_{\max}} \tag{4.13}$$

The values of $\Delta V^{-}$ is itself a function of $z^{-}$ as in (4.5). Thus, an algorithm is needed to incorporate the overcurrent limit of IBRs operating in the fault mode. The detailed procedure used in the proposed WABP methods is as follows

(*i*) The amplitude of the current of the IBR is obtained via $I^{-}_{IBR} = \left|\Delta V^{-}\right| / \left|z^{-}\right|$. If $I^{-}_{IBR}$ exceeds $i^{-}_{\max}$, the magnitude of the $z^{-}$ representing the IBR is replaced by $\left|z^{-}\right|_{\min}$.

(*ii*) The new value of $\Delta V^{-}$ is estimated.

(*iii*) Equation (4.13) is employed to update $\left|z^{-}\right|_{\min}$.

(*iv*) The previous two steps are repeated until the new value of $\left|z^{-}\right|_{\min}$ lies within $1\%$ proximity of its previous value.

### 4.4.3 Checking IBRs with Uncertain Mode

From IBRs experiencing voltage dips within the uncertain range $(\alpha \pm 5)\%$, those with voltage dips closer to $\alpha\%$ at their terminals are replaced by nodal current sources. This means they are incorporated into the vector $\boldsymbol{x}$ as extra unknown variables and are removed from the bus impedance matrix. This will be applied to as many IBRs as possible to the extent that the matrix $\boldsymbol{H}$ still remains of full rank. Next, the remaining IBRs with uncertain operating modes are scrutinised to determine their true operating modes.

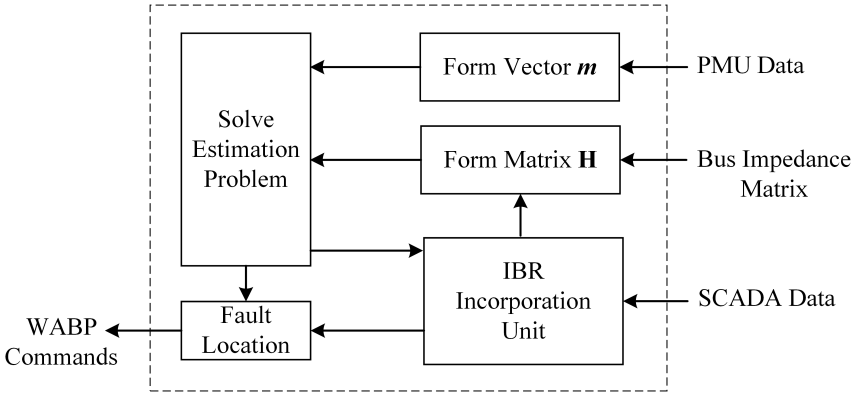


Figure 4.5: Conceptual diagram of the proposed WABP method [70].

As explained in [15], the more accurate the $\boldsymbol{H}$ matrix, the smaller the minimum *WSSR* obtained. Therefore, the targeted IBR is temporarily assumed to be operating in the opposite (fault or steady-state) mode. Accordingly, the required amendments are applied to the $\boldsymbol{H}$ matrix. Then, the new value of the minimum *WSSR* is calculated. If the minimum *WSSR* is reduced, it follows that the IBR under consideration is truly operating in the opposite mode. Otherwise, it is operating in the predefined mode found in Section 4.2.

### 4.4.4 Conceptual Diagram

Figure 4.5 shows a conceptual diagram of the proposed WABP method for transmission systems. The *IBR Incorporation Unit* module is in charge of dealing with uncertainties in the bus-impedance matrix due to the operating status of IBRs and regulating $\boldsymbol{H}$ matrix based on their different control strategies. A flowchart of the functions of the *IBR Incorporation Unit* is shown in Figure 4.6, which has already been detailed in parts A to D. Once the operating modes of all IBRs in the power system are determined, the *WSSR* is updated for the candidate line. Finally, the transmission line corresponding to the minimum *WSSR* is identified as the faulted line. To enhance the security of the proposed method, the calculated fault distance on the pinpointed line is checked to ensure it is real and lies within the acceptable range [0,1].

### 4.4.5 Performance Evaluation

The performance of the proposed WABP method is evaluated by conducting more than 80,000 simulations on the IEEE 39-bus test system with different penetration levels of IBRs. For each

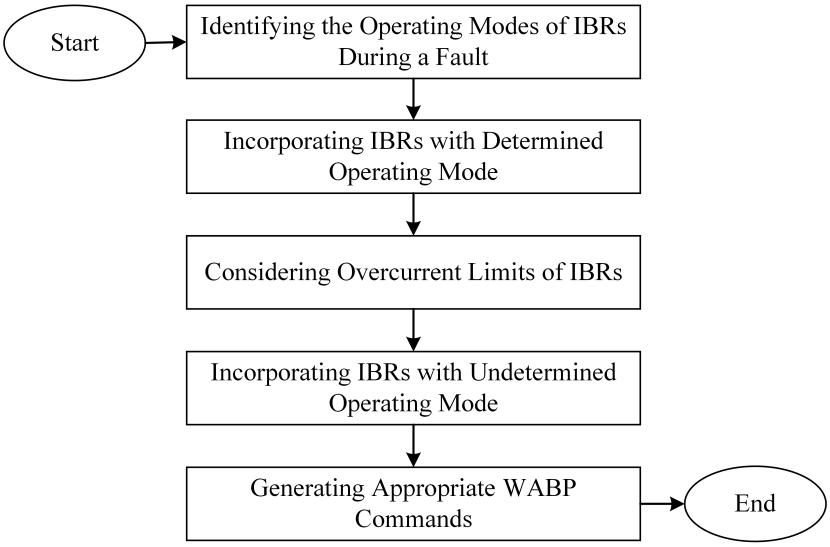


Figure 4.6: Flowchart of the functions of the *IBR Incorporation Unit* [70].

set of IBRs added to the system, their total active power is proportionally deducted from the active power produced by the existing synchronous generators so that the total active power generation (around 6200 MW) is maintained constant. A general performance evaluation for different asymmetrical fault types at various locations with an arbitrary set of IBRs is presented first. Next, the sensitivity of the proposed method to measurement errors, line/generator parameters errors, and pre-fault negative-sequence components is examined. The impact of different numbers and locations of PMUs is also scrutinised. Finally, the performance of the proposed method is tested for various penetration levels and locations of IBRs with different control strategies and settings. For the IBR control loops, a second-order generalised integrator [98] is used to apply $i$ representing a $90^\circ$ phase shift in the time domain in (4.1).

Using DIgSILENT PowerFactory, time-domain voltage and current waveforms are captured and filtered by an anti-aliasing Butterworth filter with a cut-off frequency of 400 Hz. The current measurements for generation transformers are taken from their high-voltage sides, e.g., the delta winding side of the step-up transformer of IBRs. Accordingly, the angle displacements caused by the transformers are incorporated in equations (4.5) to (4.7). Time-domain measurements are then sampled with a frequency of 2 kHz. The DFT is used to estimate the phasors of the recorded time-domain waveforms. Any other effective phasor estimation methods, such as the real PMU model in [64], could be used to provide more accuracy if needed.

Table 4.1: Control Strategies/Settings and Locations of IBRs

| Location (Bus No.) | Control Strategy | Control Setting |
|---|---|---|
| 1,17 | Suppressing Negative Sequence Current | $i^{-}_{\max} = 0, \mathrm{Sn} = 100\mathrm{MVA}$ $P_{ref} = 0.8\mathrm{pu}, Q_{ref} = 0.2\mathrm{pu}$ |
| 2, 6, 9, 13, 14, 18, 22 | Mitigating Active Power Ripple | $i^{-}_{\max} = 0.3, \mathrm{Sn} = 150\mathrm{MVA}$ $P_{ref} = 0.9\mathrm{pu}, Q_{ref} = 0.1\mathrm{pu}$ |
| 3, 7, 10, 15, 19, 28 | Mitigating Reactive Power Ripple | $i^{-}_{\max} = 0.4, \mathrm{Sn} = 150\mathrm{MVA}$ $P_{ref} = 0.9\mathrm{pu}, Q_{ref} = 0.1\mathrm{pu}$ |
| 4, 5, 8, 12, 20, 21, 24 | Imitating an Impedance | $i^{-}_{\max} = 0.4, \mathrm{Sn} = 150\mathrm{MVA}$ $P_{ref} = 0.9\mathrm{pu}, Q_{ref} = 0.1\mathrm{pu}, z^{-} = 0.3\angle 90°$ |

Table 4.2: Model and Parameters of IBRs

| Plant Category | Renewable Generation |
|---|---|
| Technology | Three phase |
| Number of Parallel Units | 30 |
| Proportional Gain of PLL | 10 |
| Integration Gain of PLL | 30 |
| Proportional Gain of Current Controller (d- and q-axis) | 1 |
| Time Constant of Current Controller (d- and q-axis) | 4 ms |
| Impedance of the Series Reactor | 0.1 pu |
| Positive-Sequence Control Strategy | Based on the GB Grid Code |
| Positive-Sequence Maximum Current | 1 pu |

### A. General Evaluation of the Proposed Method

An arbitrary set of 22 IBRs with different control strategies and settings are added to the 39-bus system, as detailed in Table 4.1. This set of IBRs is also applied for parts B, C, D, and E in this subsection. Buses 3, 5, 8, 11, 14, 16, 19, 23, 25, 27, 29, and 39 are equipped with PMUs [84], which are also valid for parts B, C, D, and F. IBRs are modelled as static generators in DIgSILENT PowerFactory. The parameters of simulated IBRs and the applied controllers, other than those in Table 4.1, are listed in Table 4.2.

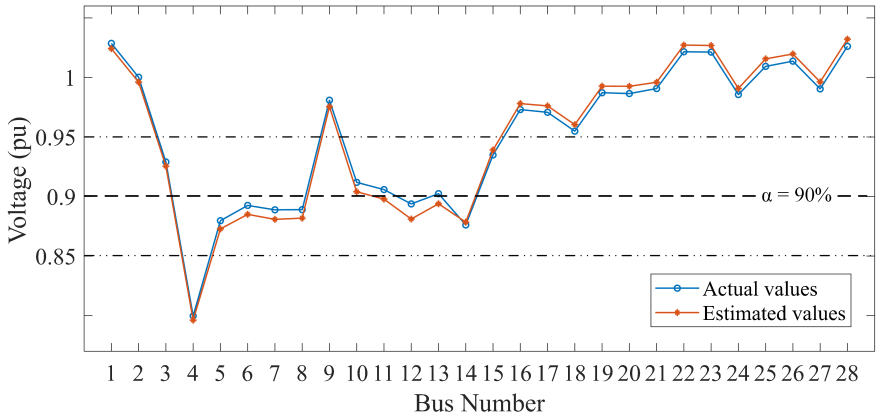


Figure 4.7: Actual and initial estimation of post-fault voltage at IBRs' terminals [70].

Table 4.3: Performance of the Proposed Method for a Solid 1-ph-g Fault at 95% of Line 3-4

| Detected Operating Mode | Incorporation Method | IBR Bus No. | TVE (Ave., Max.) |
|---|---|---|---|
| Steady-State Mode | N/A | 1, 2, 3, 9, 10, 15, 17, 18, 19, 20, 21, 22, 24, 28 | N/A |
| Fault Mode | Replace by a current source | 5, 8, 13, 14 | 1.82%, 2.74% |
| | Replace by an impedance | 4, 6, 7, 12 | 4.08%, 7.75% |

The method estimates the voltage dips at IBRs to determine their operating modes and the way they are incorporated, i.e., by a current source or an equivalent impedance. To demonstrate the capability of the proposed method for doing so, a solid 1-ph-g fault at 95% of line 3-4 is explored. As per the GB Grid Code, IBRs undergoing voltage dips of more than 10% are set to operate in the fault mode. Figure 4.7 shows the initial estimation of the post-fault voltage profile and the actual voltage profile at 80 ms following the fault inception. Accordingly, Table 4.3 reports the identified operating modes of IBRs and the way that each one is incorporated in the WABP formulation. As can be seen from Figure 4.7, the estimated voltage dips of some IBRs are within the uncertain range. However, the operating modes of all IBRs are finally identified correctly.

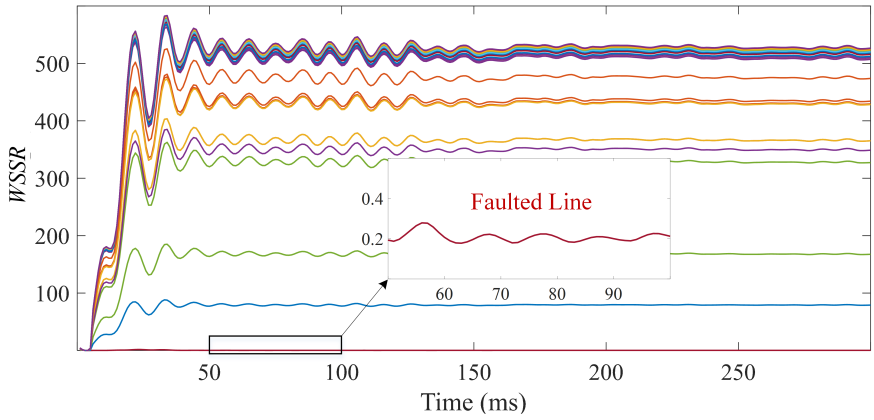


Figure 4.8: *WSSR*s of different candidate lines calculated over time following a solid 1-ph-g fault at 95% of line 3-4 [70].

The amplitude and angle errors between the real and the estimated negative-sequence current or impedance of IBRs are combined into a single error quantity referred to as total vector error (TVE) [97], and listed in the last column of Table 4.3. Figure 4.8 depicts the *WSSR*s of all lines for up to 300 milliseconds after the fault inception. As can be seen, the smallest *WSSR* correctly indicates the true faulted line with sufficient distinction from other candidate lines. The fault location result for this case has only 0.19% error from its actual value.

Due to indefinite wide-area communication latencies, the proposed method cannot be employed for primary protection but for backup protection. As mentioned, a few hundred milliseconds is available for WABP before making a trip decision [1, 2]. Nonetheless, WABP should be fast enough and be able to make a reliable decision once enough PMU data are received at the control centre. A limited number of multiplication and addition operations is needed to calculate the required IBR equivalent impedances and the scalar index *WSSR* for each candidate line. According to extensive simulations conducted, less than three iterations are required for every iterative step on average. The average computation time of the whole procedure is about 50 ms, on a 2.8 GHz processor with 8 GB of RAM, which is less of a concern than communication latencies in the context of decision time available for WABP. It should be noted that for bigger power systems, the proposed WABP can be efficiently limited to the disturbed area whose boundaries are observed by PMUs. This approach has already been presented and successfully tested in [15]. Besides, the related process can also be effectively parallelised on software/hardware levels. Further progress in communication technology to reduce latencies

Table 4.4: Comparison between the Main Characteristics of Different WABP Methods

| Comparison aspect | [34, 38] | [11, 39] | [17] | [15] | Proposed |
|---|---|---|---|---|---|
| Tolerate PMU losses? | No | Yes | Yes | Yes | Yes |
| Need specific PMU placement? | Yes | No | No | No | No |
| Computation burden | Low | Low | High | Low | Low |
| Need statuses of local relays? | No | No | No | No | No |
| Sensitivity to fault resistance | Low | Low | Low | Low | Low |
| Address the presence of IBRs? | No | No | No | No | Yes |

can allow the implementation of the proposed method for the main protection in the future.

Table 4.4 summarises the main characteristics of the most effective WABP methods in the literature that are insensitive to fault resistance and independent of local protective relays. As can be seen, the proposed method can account for the presence of IBRs while outperforming other methods in many aspects, such as tolerance against PMU losses, low computational burden, and independence of specific PMU placement. According to Table 4.4, since the method presented in [15] has better characteristics than other methods listed, the performance of the proposed method is only compared with that of [15].

The method does not operate for symmetrical faults as no significant negative-sequence quantity is present under such conditions. To show the effectiveness of the proposed method, various types of asymmetrical faults are applied at different locations in the system with fault resistances of 0 $\Omega$, 20 $\Omega$, and 100 $\Omega$. In each case, the calculated fault location is averaged over 80-300 ms following the fault inception. The performance of the method is compared to that of the method presented in [15]. Simulations show that the presence of IBRs has a more significant influence on the success rate of faulted-line identification for faults closer to substations. Thus, only results for faults on the first and last 20% of line lengths are reported. Table 4.5 summarises obtained results in terms of faulted-line identification success rate (FLISR) and average fault location error (AFLE). As explained, the operating modes of the IBR are automatically identified by the method. Accordingly, another index reported in Table 4.5 is IBR operating mode identification success rate (POMISR). It can be seen that the proposed method successfully pinpoints the faulted line irrespective of the fault resistance with a success rate of

Table 4.5: General Performance of the Proposed WABP Method

| Fault Type | Results | Proposed Method | | | Method in [15] Ignoring IBRs | | |
|---|---|---|---|---|---|---|---|
| | | 0Ω | 20Ω | 100Ω | 0Ω | 20Ω | 100Ω |
| Single Phase to Ground | FLISR (%) | 99.64 | 99.78 | 100 | 85.22 | 91.25 | 95.3 |
| | AFLE (%) | 0.56 | 0.61 | 0.74 | 6.89 | 4.23 | 2.74 |
| | POMISR (%) | 99.63 | 99.83 | 99.86 | N/A | N/A | N/A |
| Phase to Phase | FLISR (%) | 100 | 100 | 100 | 87.43 | 90.85 | 94.92 |
| | AFLE (%) | 0.44 | 0.48 | 0.56 | 6.58 | 4.63 | 3.04 |
| | POMISR (%) | 99.08 | 99.45 | 99.58 | N/A | N/A | N/A |
| Two Phase to Ground | FLISR (%) | 98.53 | 99.07 | 99.32 | 85.96 | 90.56 | 94.81 |
| | AFLE (%) | 0.54 | 0.61 | 0.69 | 7.11 | 5.84 | 3.21 |
| | POMSR (%) | 99.08 | 99.57 | 99.66 | N/A | N/A | N/A |

Table 4.6: WABP Sensitivity to Measurement Errors

| Results | Variation Range of Errors (%) | | | | |
|---|---|---|---|---|---|
| | ±1 | ±2 | ±3 | ±4 | ±5 |
| FLISR (%) | 99.42 | 99.36 | 99.21 | 99.14 | 98.81 |
| AFLE (%) | 0.57 | 0.60 | 0.64 | 0.72 | 0.83 |

more than 99% on average. As expected, the method presented in [15] demonstrates a noticeably lower accuracy and success rate for not considering the presence of IBRs. This clearly demonstrates the superiority of the proposed method over the existing method in the presence of IBRs, given the reliability requirements for protection applications [1, 2].

### B. Sensitivity to Measurement Errors

To simplify the compliance specification of PMUs, amplitude, and angle error bounds are combined into TVE quantities. Here, TVE is a measure of the difference between the phasor reported by the PMU and the true phasor. The performance of the proposed method with input phasors having different ranges of TVEs is studied in this subsection. To this end, 100 arbitrary

Table 4.7: WABP Sensitivity to Line Parameter Errors

| Results | Variation Range of Errors (%) | | | | |
|---|---|---|---|---|---|
| | ± 1 | ± 2 | ± 3 | ± 4 | ± 5 |
| FLISR (%) | 99.21 | 98.82 | 98.35 | 97.77 | 97.33 |
| AFLE (%) | 0.72 | 1.15 | 1.76 | 2.32 | 3.07 |

Table 4.8: WABP Sensitivity to Generator Parameter Errors

| Results | Variation Range of Errors (%) | | | | |
|---|---|---|---|---|---|
| | ± 1 | ± 2 | ± 3 | ± 4 | ± 5 |
| FLISR (%) | 99.42 | 99.34 | 99.13 | 98.92 | 98.73 |
| AFLE (%) | 0.54 | 0.62 | 0.78 | 0.96 | 1.09 |

asymmetrical faults are applied at different locations throughout the transmission system. The fault resistance is set to have a random value between 0 Ω to 50 Ω. Measurement errors are assumed to have a normal distribution around the true value of corresponding phasors. Each simulated case is repeated 100 times for reporting FLISR and AFLE. The obtained results are tabulated in Table 4.6, where the three-sigma criterion is used for reporting the error range [15]. As expected, larger measurement errors result in less success rate for the proposed method. The proposed method proves to have sufficient robustness against measurement errors as it functions correctly for more than 98.81% of the cases with up to 5% measurement errors.

### C. Sensitivity to Parameter Errors

The impact of transmission line and generator parameter errors on the success rate of the WABP method is scrutinised here. Tables 4.7 and 4.8 summarise obtained results when lines and generators are considered to have random parameter errors within different ranges. The same faults as those in the previous subsection are examined in this study. Each simulated case is repeated 100 times for reporting FLISR and AFLE. As expected, the success rate of the method decreases as the variation range of parameter errors increases. Practically speaking, the success rate still remains in an acceptable range, even for errors of up to 5%.

Table 4.9: WABP Sensitivity to Pre-Fault Negative-Sequence Components

| Results | Up to 1.5% Pre-Fault Voltage Unbalance | | | No Pre-Fault Voltage | | |
|---|---|---|---|---|---|---|
| | 0Ω | 20Ω | 100Ω | 0Ω | 20Ω | 100Ω |
| FLISR (%) | 99.06 | 98.83 | 99.74 | 99.39 | 99.62 | 99.77 |
| AFLE (%) | 0.73 | 0.84 | 0.91 | 0.51 | 0.57 | 0.67 |

### D. Sensitivity to Pre-Fault Negative-Sequence Components

Grid Codes dictate the maximum negative-sequence voltage caused by voltage unbalance to be maintained below certain small values [99]. For instance, the maximum permissible voltage unbalance allowed by the GB Grid Code is 1.5% in the transmission grid. This requirement is to be strictly followed by system operators to avoid the damaging impact of the negative-sequence components on rotating machines. To scrutinise the impact of the pre-fault negative-sequence components, up to 1.5% negative-sequence voltages are induced at different buses in the pre-fault condition by making load and line parameters slightly unbalanced. The success rate of the proposed algorithm in this condition with fault resistances of 0 Ω, 20 Ω, and 100 Ω is reported in Table 4.9. As can be seen, permissible pre-fault negative-sequence components do not noticeably impair the performance of the proposed method.

### E. Observability and PMU Coverage

Full network observability is not a prerequisite for the proposed method to function properly. However, the variance of the estimated unknowns can be obtained by $\left(\boldsymbol{H}^{*}\boldsymbol{R}^{-1}\boldsymbol{H}\right)^{-1}$ [100], which means a greater number of PMUs provides higher accuracy.

Further simulations show that installing a PMU in poorly PMU-covered areas increases the success rate of faulted line identification. To demonstrate this, the performance of the proposed method is studied with different numbers of PMUs. For each specific number of PMUs, 50 randomly created placements leading to a solvable system of equations with a unique solution have been considered. The FLISR and AFLE indices obtained for the foregoing set of asymmetrical faults are summarised in Table 4.10. As can be seen, larger numbers of PMUs result in more accurate and reliable results. It can be concluded that the more intensely PMUs

Table 4.10: WABP Sensitivity to the Number of PMUs

| Results | Number of PMUs | | | | |
|---|---|---|---|---|---|
| | 12 | 11 | 10 | 9 | 8 |
| FLISR (%) | 98.92 | 98.02 | 97.60 | 96.84 | 96.01 |
| AFLE (%) | 1.10 | 1.26 | 1.47 | 1.76 | 1.82 |

cover the fault area, the bigger the *WSSR*s of other candidate locations. This also shows that missing data from a few PMUs would not adversely affect the method's performance.

**F. Impact of IBRs' Locations and Control Strategies**

This subsection studies the impact of the number, location, and control strategies of IBRs on the method's performance. The total active power generated in the system is maintained constant to obtain different penetration levels of IBRs. For each number of IBRs, 50 randomly created placements have been considered. To examine the impact of IBR control strategies, five different scenarios are defined for each IBR placement. For the first to fourth scenarios, one of the control strategies described in Section 4.2 is selected and applied to all IBRs. In the fifth scenario, the control strategy of each IBR is randomly selected. The control settings of each IBR, i.e., $S_n, P_{ref}, Q_{ref}, i^-_{\max}$, $|z^-|$, and $\theta^-$ are randomly selected within [100,150] MVA, [0.85,0.95] pu, [0.1,0.3] pu, [0.2,0.4] pu, [0.2,0.6] pu, and $[60^\circ, 90^\circ]$, respectively.

The FLISR and AFLE indices obtained for a set of 100 asymmetrical short-circuit faults are summarised in Table 4.11. In the proposed method, all IBRs are accurately modelled by an impedance or replaced by a current source. As a result, the number, location, and control strategies/settings of IBRs do not have a noticeable adverse effect on the performance of the method. The scenarios numbered in Table 4.11 are described below

1) All IBRs are set to suppress neg. seq. current.
2) All IBRs are set to mitigate active power ripple.
3) All IBRs are set to mitigate reactive power ripple.
4) All IBRs are set to imitate an impedance.
5) Every IBR is randomly set to one of the foregoing control strategies.

Table 4.11: WABP Sensitivity to Control Strategy/Settings, Number, and Locations of IBRs

| Scenario No. | Results | Number of IBRs | | | | |
|---|---|---|---|---|---|---|
| | | 28 | 24 | 20 | 16 | 12 |
| 1 | FLISR (%) | 99.46 | 99.50 | 99.68 | 99.68 | 99.72 |
| | AFLE (%) | 0.66 | 0.64 | 0.52 | 0.50 | 0.50 |
| | POMISR (%) | 99.51 | 99.56 | 99.69 | 99.68 | 99.71 |
| 2 | FLISR (%) | 99.36 | 99.40 | 99.46 | 99.56 | 99.56 |
| | AFLE (%) | 0.63 | 0.61 | 0.59 | 0.59 | 0.58 |
| | POMISR (%) | 99.62 | 99.31 | 99.39 | 99.42 | 99.42 |
| 3 | FLISR (%) | 99.38 | 99.46 | 99.48 | 99.54 | 99.54 |
| | AFLE (%) | 0.56 | 0.55 | 0.55 | 0.53 | 0.52 |
| | POMISR (%) | 99.54 | 99.33 | 99.36 | 99.43 | 99.45 |
| 4 | FLISR (%) | 99.32 | 99.36 | 99.38 | 99.42 | 99.50 |
| | AFLE (%) | 0.67 | 0.62 | 0.58 | 0.57 | 0.55 |
| | POMISR (%) | 99.77 | 99.76 | 99.78 | 99.79 | 99.78 |
| 5 | FLISR (%) | 99.34 | 99.36 | 99.44 | 99.47 | 99.50 |
| | AFLE (%) | 0.62 | 0.60 | 0.59 | 0.58 | 0.56 |
| | POMISR (%) | 99.71 | 99.71 | 99.73 | 99.74 | 99.76 |

## 4.5 WABP in the Presence of IBRs Using the Positive Seq. Circuit

As described in the previous section, the utilisation of the negative-sequence circuit for WABP has many merits. However, it is not applicable to symmetrical faults, and it can only handle certain negative-sequence control strategies, which IBRs may or may not employ in practice. This section proposes an innovative yet straightforward PMU-based method for backup protection of transmission lines using the positive-sequence circuit. The original contribution of the proposed method is the accommodation of any LVRT characteristics for IBRs into the superimposed-circuit-based WABP, irrespective of the IBRs' number, locations, and pre-fault injections.

In the proposed method, the monitored IBRs (those whose terminals are monitored by PMUs) are substituted by known current sources based on the *Substitution Theorem* [15]. The unmonitored IBRs (those with no PMU measurements at their terminals) are modelled by cur-

rent sources with respect to their pre-fault operating points and control settings satisfying the requirements of pertinent Grid Codes [94–96]. The candidate faulted line is also represented by two unknown nodal current sources. A closed-form residual-based index is developed to indicate the actual faulted line from the set of candidate lines.

### 4.5.1 Accounting for the High Penetration of RESs

In Chapter 2, a system of equations was formulated for every candidate line for nodal analysis of the system. Based on the superimposed methodology [15], the candidate faulted line can be represented by two appropriate nodal current sources. Within WABP's action time, synchronous generators may also be replaced by their sub-transient impedances in the superimposed circuit [13, 15, 23, 34]. Modelling IBRs as an impedance in the positive-sequence superimposed circuit is neither advantageous nor straightforward because their equivalent impedances depend on their pre- and post-fault currents and terminal voltages [61]. To overcome this problem, IBRs are to be substituted by unknown current sources. This helps to find the faulted line using the notion of the *WSSR*, as will be explained. It is shown that replacing all IBRs with unknown current sources might unnecessarily increase unknown variables in the system of equations. To minimise the possibility of rank deficiency and ensure the uniqueness of the solution [73], an effective method is proposed for reducing the number of unknowns.

In the formulation put forward in Section 4.3, every IBR is modelled by its equivalent current source in the superimposed circuit. The current sources representing the IBRs whose terminals are monitored by PMUs appear in both vectors $\boldsymbol{m}$ and $\boldsymbol{x}$ in (4.8). From linear algebra, including such variables in $\boldsymbol{x}$ does not compromise the uniqueness of the solution as its corresponding row in the matrix $\boldsymbol{H}$ has only one non-zero entry [73]. This nonzero entry represents a pivot in the matrix $\boldsymbol{H}$ in its row-echelon form. Therefore, the inclusion of such a row in the matrix $\boldsymbol{H}$ will not make it rank deficient [73]. However, assuming a PMU at every IBR terminal may not be practical. Even if PMUs measure the terminal voltages of all IBRs, it is not guaranteed that all these PMU data will be received within the desired action time of WABP due to communication latency and missing data possibilities, as discussed in [15].

### Rearranging the System of Equations

In this study, IBRs are classified as either monitored or unmonitored depending on whether their terminal voltages and current injections are measured by PMUs. An IBR is called monitored if a PMU at its terminal measures its current and voltage phasors. An unmonitored IBR refers to an IBR whose current/voltage synchrophasors are not taken by PMUs. If the measurements of an IBR are not received in the control centre (e.g., for communication latencies or PMU failures), that IBR is still classified as unmonitored. The current sources replacing the faulted line and unmonitored IBRs are the only unknowns in (4.8) to be estimated by (4.9). This, however, will not be feasible when the number of unknowns in $\boldsymbol{x}$ exceeds the rank of $\boldsymbol{H}$, as it makes (4.8) not uniquely solvable and thus ineffective [15]. The knowledge of the LVRT characteristics of IBRs (explained in Section 4.2) can be exploited to overcome the preceding solvability issue by reducing the number of unknowns. Let $Nm$ and $Nn$ denote the number of monitored and unmonitored IBRs, respectively. The system of equations (4.8) can be rearranged as follows:

$$\boldsymbol{m}^{mod}_{Np\times 1} = \boldsymbol{H}^{mon}_{Np\times(2+Nm)}\boldsymbol{x}^{mon}_{(2+Nm)\times 1} + \boldsymbol{\varepsilon}_{Np\times 1} \tag{4.14}$$

where

$$\boldsymbol{m}^{mod}_{Np\times 1} = \boldsymbol{m}_{Np\times 1} - \boldsymbol{H}^{unm}_{Np\times Nn}\boldsymbol{x}^{unm}_{Nn\times 1} \tag{4.15}$$

where $\boldsymbol{x}^{mon}$ contains the nodal current sources representing the monitored IBRs plus those current sources representing the candidate line, and $Np$ is the number of measurements. The matrix $\boldsymbol{H}^{mon}$ contains the coefficients corresponding to the variables in $\boldsymbol{x}^{mon}$. The vector $\boldsymbol{m}^{mod}$ is the modified measurement vector from which the contributions of unmonitored IBRs are excluded. Moreover, the vector $\boldsymbol{x}^{unm}$ only includes the superimposed currents of unmonitored IBRs, whose related coefficients are arranged in the matrix $\boldsymbol{H}^{unm}$.

In the proposed method, the superimposed currents of unmonitored IBRs are initially disregarded, which means $\boldsymbol{m}^{mod}$ is set equal to $\boldsymbol{m}$ in the first step. This enables us to obtain an initial estimate for the superimposed currents representing the candidate line by solving (4.14). Then, an initial estimate for the superimposed terminal voltages of unmonitored IBRs is obtained from (4.5). As will be detailed, the superimposed currents of unmonitored IBRs in $x^{unm}$ can be approximated using their terminal voltage and LVRT characteristics. Then,

$\boldsymbol{m}^{mod}$ is updated by (4.15). Next, the vector $\boldsymbol{x}^{mon}$ is also updated by solving (4.14). This process is repeated until the changes in the vector $\boldsymbol{x}^{unm}$ caused by an iteration become insignificant. Finally, the *WSSR* for every line is obtained to indicate the actual faulted line. The whole algorithm is further described in Subsection 4.5.2.

### Modelling Unmonitored IBRs

The modified system of equations (4.14) only includes the superimposed currents of the monitored IBRs and those representing the candidate line. The solution of (4.14) gives the *WSSR* indices. This is irrespective of the number of unmonitored IBRs, whose contributions will be estimated separately based on their LVRT characteristics and incorporated in the formulation by (4.15). As a result, only two actual unknowns remain in (4.14) that represent the candidate line in the superimposed circuit. This is because other variables in $\boldsymbol{x}^{mon}$ are also present in the measurement vector. This approach eliminates the solvability issues introduced by the presence of unmonitored IBRs in the power system.

In normal conditions, an IBR injects active and reactive power as per its pre-defined references. The control references of IBRs during a fault are adjusted based on their terminal voltages and LVRT characteristics. In this regard, the LVRT characteristics of IBRs should meet the Grid Code requirements [94–96]. As can be seen in Figures 4.2 and 4.3, the amount of voltage drop at an IBR terminal determines the duration in which it should stay connected to the grid and the required modification the IBR should apply to its reactive current injections. The knowledge of the LVRT characteristics of unmonitored IBRs and their pre-fault power references in the control centre enables the approximation of their superimposed currents following a fault. It is reasonable to assume that these data are available in the control centre with no technical difficulties. If this is not the case for an IBR, its superimposed current should be moved into the unknown vector in (4.14) and will be estimated using the WLS method. Otherwise, as will be described below, this can be approximated and then used to form (4.15).

The positive-sequence superimposed current of an IBR connected to bus $r$ is derived by subtracting the IBR's pre-fault current, denoted by $I_r^{+,pre}$, from its post-fault current, denoted by $I_r^{+,post}$. These currents can be obtained from:

$$I_r^{+,pre} = \frac{\left(P_{ref}^{pre} - jQ_{ref}^{pre}\right)}{\left(V_r^{+pre}\right)^*} \tag{4.16}$$

$$I_r^{+,post} = \frac{\left(P_{ref}^{post} - jQ_{ref}^{post}\right)}{\left(V_r^{+post}\right)^*} \tag{4.17}$$

where $V_r^{+,pre}$, $P_{ref}^{pre}$, and $Q_{ref}^{pre}$ represent the pre-fault positive-sequence voltage at bus $r$, and the IBR's active and reactive power references, respectively. The superscript "$pre$" and "$post$" refer to the pre- and post-fault values, respectively. The pre-fault bus voltages are typically available in the control centre as the output of state estimation methods [68]. The control centre is assumed to know the pre-fault power references. Therefore, $I_r^{+,pre}$ can be readily obtained from (4.16).

Obtaining $I_r^{+,post}$ from (4.17), however, is trickier as the postfault voltage and power references are to be calculated. The post-fault positive-sequence voltage at bus $r$ can be calculated using the pre-fault and the estimated positive-sequence superimposed voltage, i.e., $V_r^{+,post} = V_r^{+,pre} + \Delta V_r^{+}$. If $V_r^{+,post}$ lies within the dead band shown in Figure 4.3, the post-fault power references $\left(P_{ref}^{post} \text{ and } Q_{ref}^{post}\right)$ will be the same as their pre-faults values $\left(P_{ref}^{pre} \text{ and } Q_{ref}^{pre}\right)$. Otherwise, the post-fault power references should be calculated using the IBR's LVRT characteristics as follows.

Let us assume the phase-locked loops align the grid voltage to the $d$-axis. Thus, except for a short transient period following a fault, the positive-sequence $q$-axis voltage, $v_q^+$, will be zero in the pre- and post-fault conditions [3]. Hence, the $d$-axis positive-sequence pre- and post-fault voltage can be calculated as:

$$\begin{cases} v_d^{+,pre} = \left|V_r^{+,pre}\right| \\ v_d^{+,post} = \left|V_r^{+,post}\right| \end{cases} \tag{4.18}$$

where the operator $|.|$ returns the amplitude of a phasor. The IBR's pre-fault reactive current, i.e., $i_q^{+,pre}$, can be obtained as:

$$i_q^{+,pre} = \frac{-Q_{ref}^{pre}}{\left|V_r^{+,pre}\right|} \tag{4.19}$$

Let $f^t(V)$ denote the time-voltage profile of an IBR's LVRT characteristic. As shown

in Figure 4.2, $f^t(V)$ represents the time that the IBR remains connected to the grid during different terminal voltage drops. Moreover, let $f^I(V)$ denote the voltage support characteristic, which represents the change in the IBR's positive-sequence reactive current during faults, as shown in Figure 4.3. Different IBRs might have different $f^t(V)$ and $f^I(V)$ characteristics. For example, the slope of the $f^I(V)$ characteristic could be between 2 and 6 for different types of IBRs [96]. It is assumed in this thesis that these characteristics are known and available in the control centre. Using $f^t(V)$, $f^I(V), \Delta V_r^{+,post}$, and $i_q^{+,pre}$ obtained by (4.19), the post-fault reactive currents of the IBR at the instant $t$ following the fault onset can be obtained as:

$$i_q^{+,post}(t) = S(t) \cdot \text{Min}\left\{ i_q^{+,pre} + \overbrace{f^I\left(\Delta V_r^{+,post}\right)}^{\Delta i_q^+}, i_{\max}^+ \right\} \tag{4.20}$$

where $i_{\max}^+$is the IBR's largest permissible current in the positive-sequence circuit, and $S(t)$ represents the connectivity status of the IBR and can be obtained as follows:

$$S(t) = \begin{cases} 1, & \text{if } t < f^t\left(V_r^{+,post}\right) \\ 0, & \text{otherwise} \end{cases} \tag{4.21}$$

The remaining current capacity of the IBR is used for generating active power. Due to the IBR's overcurrent limits, the active power generation of the IBR may have to be decreased to be able to inject the reactive current imposed by Grid Code requirements [94–96]. Accordingly, the post-fault active current of the IBR at instant $t$ can be obtained as:

$$i_d^{+,post}(t) = S(t) \cdot \text{Min}\left\{ \frac{P_{ref}^{pre}}{\left|V_r^{+,post}\right|}, \sqrt{{i_{\max}^+}^2 - {i_q^{+,post}}^2} \right\} \tag{4.22}$$

The first term in the braces ensures that $P_{ref}^{post}$ does not exceed $P_{ref}^{pre}$, whereas the second term ensures that the overcurrent limit of the IBR is not violated. Using (4.18), the post-fault active and reactive power references of the IBR can be calculated as:

$$\begin{cases} P_{ref}^{post} = i_d^{+,post}\left|V_r^{+,post}\right| \\ Q_{ref}^{post} = -i_q^{+,post}\left|V_r^{+,post}\right| \end{cases} \tag{4.23}$$

The post-fault positive-sequence current of the IBR is obtained by replacing $P_{ref}^{post}$ and $Q_{ref}^{post}$ in (4.17). Finally, the superimposed current of the IBR is calculated as $I_r^{+,post} - I_r^{+,pre}$.

The LVRT characteristics of IBRs depend on their control system and operational limits. Over the first few milliseconds following the fault onset, the transient behaviour of different types of IBRs might be slightly different. However, they can quickly fulfil their control targets in normal and fault conditions [3]. As a backup protection, a few hundred milliseconds after the fault onset are available for the method before making a trip decision. This is sufficiently long to let the IBR completely settle at its new quasi-steady-state operating modes as per its LVRT characteristics [2], [8]. The proposed method performs well with any LVRT characteristics of IBRs. The reason is that the method does not make any assumptions about the IBRs' LVRT characteristics but is directly fed by the functions $f^t(V)$ and $f^I(V)$ describing these characteristics. This will be verified by simulations in Subsection 4.5.4.

### 4.5.2 Fault Detection and Real-Time Implementation

A block diagram illustrating the real-time implementation of the method proposed for WABP with an integrated fault detection logic is shown in Figure 4.9. The inputs to the method are:

- The bus impedance matrix for forming $\boldsymbol{H}^{mon}$ and $\boldsymbol{H}^{unm}$,
- The power references and LVRT characteristics of unmonitored IBRs, and
- PMU data and time signal for establishing $\boldsymbol{m}$ and $\boldsymbol{m}^{mod}$.

The superimposed value for a phasor, let us say phasor $U$, at the current time $t$ is calculated as $U(t) - U\left(t^{pre}\right)$. In normal conditions, $t^{pre}$ is set to $t - \tau$. In this study, the parameter $\tau$ is assigned a value of 20 ms, accounting for the size of the data window employed for phasor estimation. Once a fault is detected, $t^{pre}$ is held at the fault inception time.

As shown in Figure 4.9, the value of $t^{pre}$ is the Output of an S&H block, whose function is described here. In the absence of the Hold signal, the S&H block directly delivers the Input signal, i.e., $t - \tau$, to the Output, i.e., $t^{pre}$. The S&H block samples and holds the Input signal at the rising edge of the Hold signal. It presents the held value of the Input signal as the Output signal as long as the Hold signal remains activated. The calculated *WSSR*s are used for generating the Hold signal. When there is no fault in the power system, the superimposed quantities and, consequently, all *WSSR*s for the candidate lines take negligible values. Following a fault,

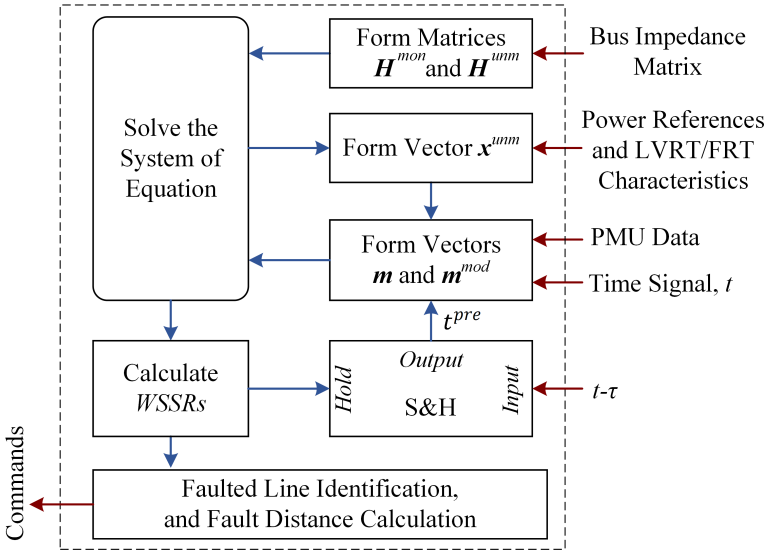


Figure 4.9: Block diagram of the proposed WABP method.

*WSSR*s for non-faulted lines drift away from zero, whilst the faulted line's *WSSR* remains quite negligible. This criterion is used to generate the Hold signal. In the proposed method, the Hold signal is generated once the maximum *WSSR* calculated is bigger than 1 and at least 5 times bigger than the minimum *WSSR*.

### 4.5.3 Conceptual Diagram

Figure 4.10 shows the flowchart of the proposed method. The steps that are to be taken to indicate the faulted line are as below:

*(i)* Unmonitored IBRs are initially disregarded in the superimposed circuit. As a result, the modified measurement vector $\boldsymbol{m}^{mod}$ becomes equal to $\boldsymbol{m}$ in the first step.

*(ii)* The vector $\boldsymbol{x}^{mon}$ is estimated by solving (4.14) using $\boldsymbol{m}^{mod}$ and $\boldsymbol{H}^{mon}$ in (2.8). The vector $\boldsymbol{m}^{mod}$ includes the current sources representing the candidate line, i.e., $\Delta J^{+}_{c,1}$and $\Delta J^{+}_{c,2}$.

*(iii)* The positive-sequence superimposed terminal voltages of unmonitored IBRs are obtained from (4.5).

*(iv)* The superimposed currents of unmonitored IBRs are calculated using (4.16) to (4.23) and arranged in the vector $\boldsymbol{x}^{unm}$.

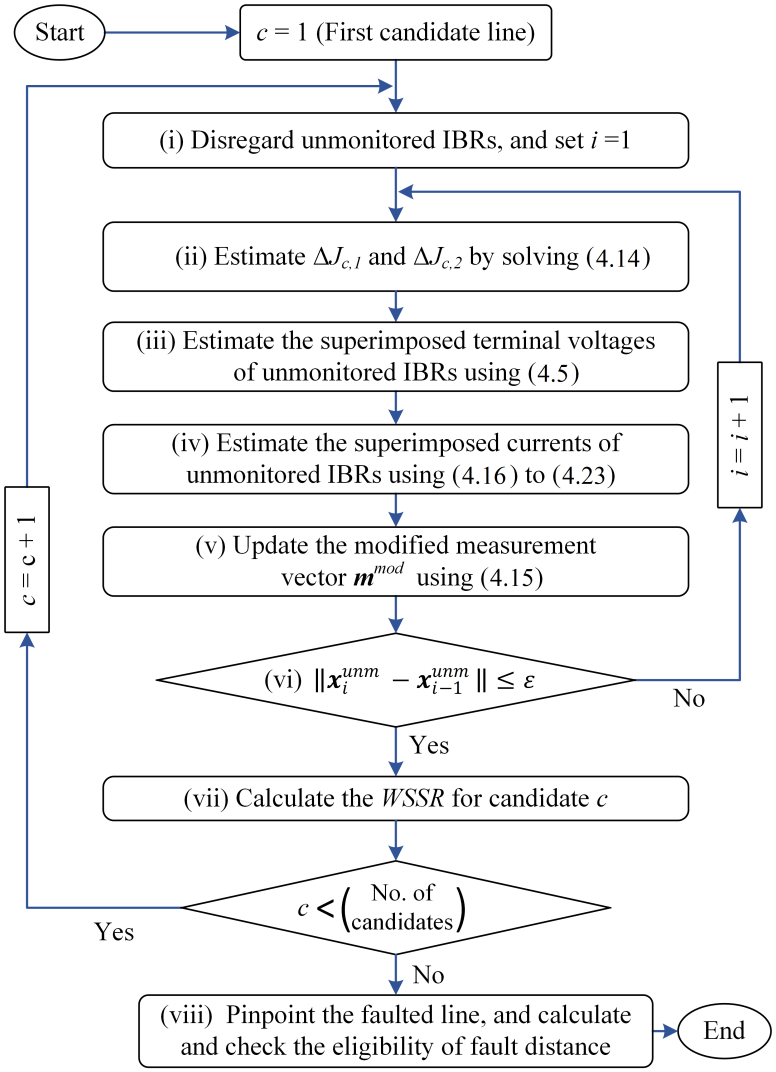


Figure 4.10: Flowchart of the proposed WABP method.

*(v)* The vector $\boldsymbol{m}^{mod}$ is updated by $\boldsymbol{x}^{unm}$ using (4.15).

*(vi)* The algorithm goes back to the first step to update the estimation of $\Delta J^{+}_{c,1}, \Delta J^{+}_{c,2}$, and the superimposed currents of unmonitored IBRs. To terminate the iteration, whose number is indicated by "$i$", the most recent estimation of the superimposed currents of unmonitored IBRs, i.e., $\boldsymbol{x}_i^{unm}$, are compared to that of the previous iteration, i.e., $\boldsymbol{x}_{i-1}^{unm}$. The iteration is terminated if the norm of $\left(\boldsymbol{x}_i^{unm} - \boldsymbol{x}_{i-1}^{unm}\right)$ is smaller than the specified tolerance, $\varepsilon = 10^{-6}$.

*(vii)* The *WSSR* of the candidate line is obtained using the $\boldsymbol{m}^{mod}$ and $\boldsymbol{H}^{mon}$ in (2.9).

Steps *(i)* to *(vii)* are conducted for every candidate line.

*(viii)* Finally, the line with the smallest *WSSR* is indicated as the faulted line. The fault distance on this line is also calculated to ensure that it lies within the acceptable range [0,1], thereby reinforcing the security of the method.

### 4.5.4 Performance Evaluation

Numerous fault cases are simulated on the IEEE 39-bus test system via the electromagnetic transient simulation tool in DIgSILENT PowerFactory. To examine the method's performance in the presence of renewables, IBRs with different numbers, locations, and penetration levels are added to the system. The profile shown in Figure 4.2 is considered for the time-voltage profile of all IBRs' LVRT characteristics. The locations of PMUs are usually determined to establish network observability [84]. Hence, the method of [84] is used to place 12 PMUs at buses 3, 5, 8, 11, 14, 16, 19, 23, 25, 27, 29, and 39. Part D of this subsection scrutinises the impact of PMU coverage and the system's full observability on the method's performance.

The method's general performance is studied for various fault types across the system with different fault resistance. Then, the method's accuracy for estimating the post-fault voltages and the superimposed currents of unmonitored IBRs is studied. The impact of sequential tripping of the faulted line's CBs and the computation time of the method are also discussed and evaluated. The method's performance is compared with two existing methods. Next, the impact of input errors on the method's performance is scrutinised. The method is then tested for partial network observability. The impact of various numbers, locations, and penetration levels of IBRs with different LVRT characteristics is also investigated.

To filter high-frequency components, a Butterworth filter is applied to the captured time-domain waveforms. The phasors of these waveforms are estimated after sampling them with a frequency of 2 kHz. Although very accurate phasor extraction methods, such as [64], can be utilised, simulations show that the method provides promising accuracy even using ordinary DFT. As defined in [68], the maximum acceptable TVE is $1\%$ for phasor measurements. Therefore, the phasors are contaminated with errors to have TVEs with random phase angles between 0 and $\pi$, and random amplitudes evenly distributed between $0\%$ and $1\%$. The method's performance with higher measurement errors is investigated in part C of this subsection.

Table 4.12: Locations, Size, and Settings of IBRs

| Location (Bus No.) | Nominal Power | Voltage Support Slope | Operating References |
|---|---|---|---|
| 1, 5, 7, 9, 12, 14, 15, 17, 24, 26 | 150MVA | 2 | $P_{ref} = 0.95$pu $Q_{ref} = 0.05$pu |
| 3, 4, 8, 11, 13, 16, 18, 21, 27, 28 | 200MVA | 4 | $P_{ref} = 0.9$pu $Q_{ref} = 0.1$pu |

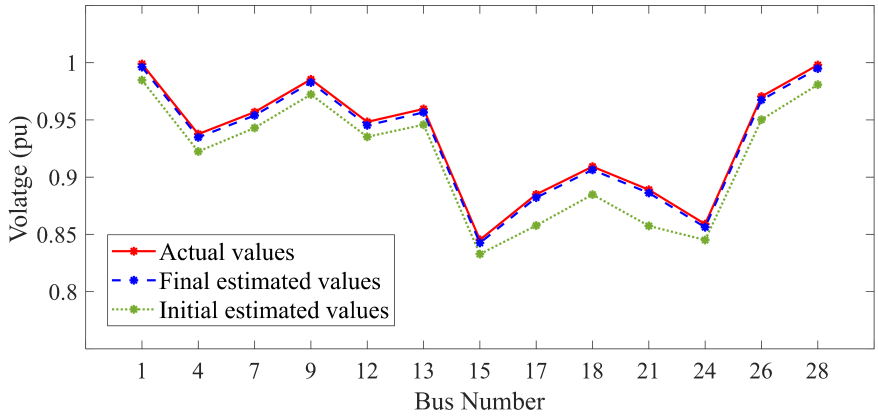


Figure 4.11: True values and estimates of post-fault voltages at non-monitored IBRs after a solid SLG fault at 5% of line 15-16.

### A. General Evaluation of the Proposed Method

Table 4.12 tabulates the locations, rated power, and control references/settings of the set of 20 IBRs considered. The unmonitored IBRs are taken into account by estimating their superimposed currents and modifying the measurement vector using (4.15). To achieve this, the post-fault terminal voltages of these IBRs are used to obtain their post-fault active and reactive power references by (4.19) to (4.23). Figure 4.11 shows the actual values, the initial estimated values ignoring unmonitored IBRs, and the final estimated values of the post-fault IBRs' terminal voltages at 80 ms following a solid single phase to ground (SLG) fault at 5% of line 15-16. As can be observed, the final estimations are very close to the true values. The TVEs between the estimated and true superimposed currents of the unmonitored IBRs are illustrated in Figure 4.12. The maximum TVE obtained is less than 5%, which shows the method's effectiveness for calculating the superimposed currents of unmonitored IBRs.

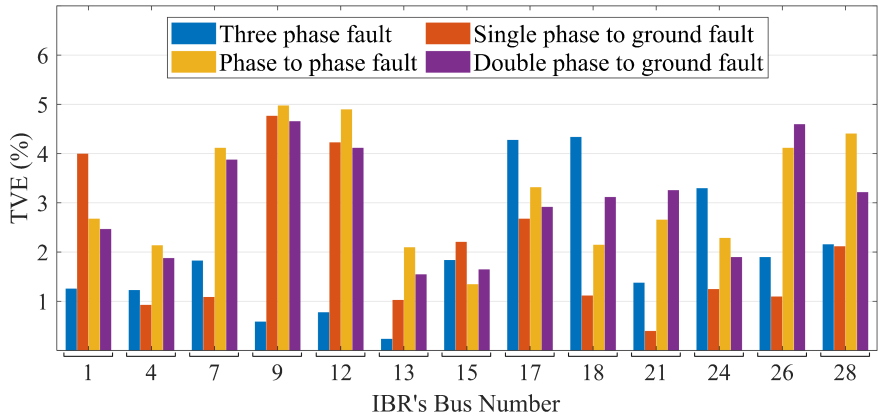


Figure 4.12: TVE (%) of the estimated superimposed current of IBRs following different faults at 5% of line 15-16.

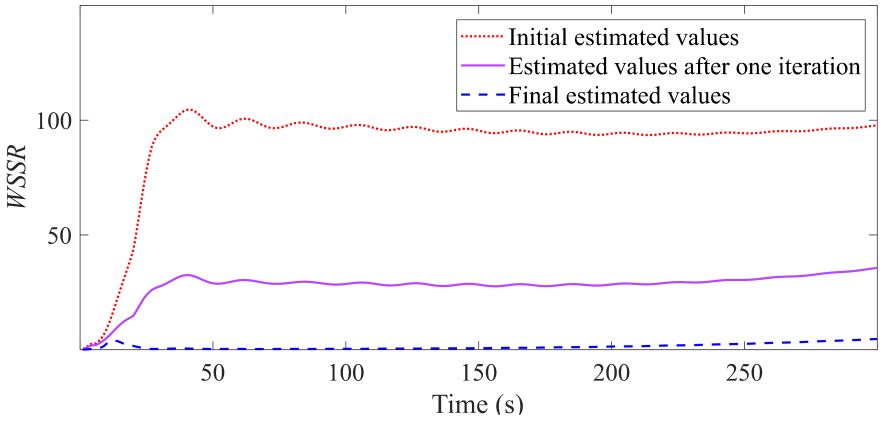


Figure 4.13: Initial and the final *WSSR* obtained for the faulted line over time after a solid SLG fault at 5% of line 15-16.

As explained, the fault current contributions of unmonitored IBRs are initially disregarded by the method. This initially introduces inaccuracies in the calculations and results in a larger value for the *WSSR* of the faulted line. In each iteration, the superimposed currents of unmonitored IBRs are estimated, updated, and used as the starting point of the next iteration. This iterative procedure aims to improve accuracy, as evidenced by smaller *WSSR* for the faulted line. If unmonitored IBRs are disregarded, the fault distance for the fault at 5% of the line length is calculated at 0.87%. However, this is obtained at 4.73% after applying the method.

Figure 4.13 shows the initial, after one iteration, and the final values obtained for the faulted line's *WSSR* over time. It can be seen that the faulted line's *WSSR* is noticeably reduced after incorporating the estimated superimposed currents of the unmonitored IBRs. This is very

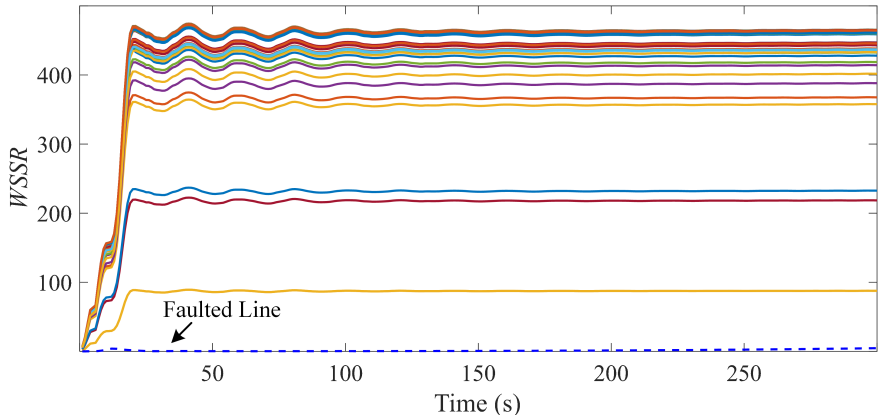


Figure 4.14: *WSSR*s obtained for all lines over time after a solid SLG fault at 5% of line 15-16.

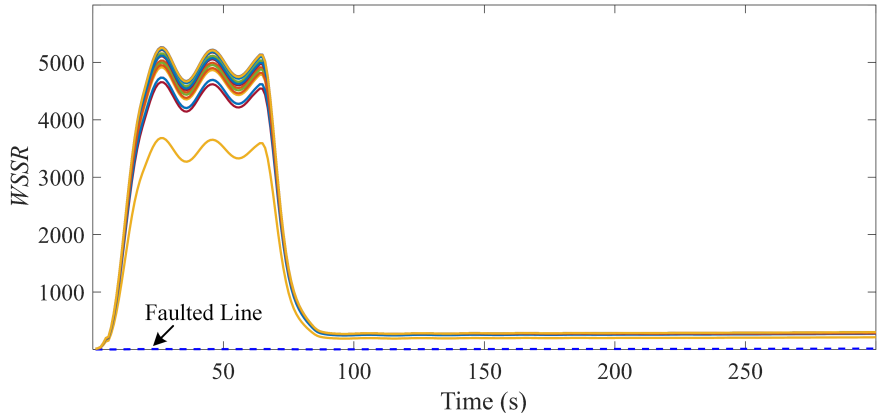


Figure 4.15: *WSSR*s obtained for all lines over time after a solid three-phase fault at 90% of line 8-9 with fast fault clearance from one side.

important as superimposed-circuit-based methods are all based upon *WSSR* indices to identify the faulted line. Figure 4.14 shows the *WSSR*s of all lines over time following the fault onset, in which the faulted line's *WSSR* is distinctly smaller than those of non-faulted lines.

Due to the operation of the local protections, the faulted line will get disconnected from one or both ends (single-pole or three-pole) shortly after the fault onset. In the proposed formulation, however, the faulted line is entirely substituted by two current sources. As a result, the proposed system of equations remains valid irrespective of the status of terminal CBs. To demonstrate this, the CB at bus 9 is opened 60 ms after the occurrence of a solid three-phase fault at 90% of line 8-9. Figure 4.15 shows the *WSSR*s obtained over time with this scenario. As can be observed, the *WSSR* of the faulted line is significantly lower than those of other lines be-

Table 4.13: Summary of Method's Performance for Different Faults

| Fault Type | Index | Prop. Method | | Method of [11] | | Method of [15] | |
|---|---|---|---|---|---|---|---|
| | | 0Ω | 25Ω | 0Ω | 25Ω | 0Ω | 25Ω |
| LLL* | LIFR (%) | 0.39 | 0.81 | 23.46 | 11.71 | 17.79 | 8.82 |
| | AFDE (%) | 0.46 | 0.71 | 14.54 | 9.25 | 11.12 | 6.23 |
| SLG* | LIFR (%) | 0.47 | 0.65 | 21.83 | 10.42 | 16.11 | 9.49 |
| | AFDE (%) | 0.45 | 1.01 | 17.16 | 12.78 | 16.13 | 5.41 |
| LL* | LIFR (%) | 0.45 | 0.78 | 19.01 | 11.35 | 14.98 | 9.66 |
| | AFDE (%) | 0.52 | 0.83 | 16.82 | 10.36 | 15.16 | 4.68 |
| DLG* | LIFR (%) | 0.37 | 0.97 | 19.89 | 10.71 | 15.81 | 8.14 |
| | AFDE (%) | 0.56 | 0.75 | 15.87 | 9.87 | 14.68 | 3.41 |

LLL: Three phase, SLG: Single phase to ground, LL: Phase to phase,
DLG: Double phase to ground.

fore and after the one-sided disconnection of the line. Therefore, the faulted line identification remains valid irrespective of the non-simultaneous CB opening.

Methods of [11] and [15] are applicable against all fault types and have better features compared to existing methods in the literature, as per the comprehensive review of the existing WABP methods in [12]. Thus, a performance comparison is presented for the proposed method and those of [11] and [15]. In this regard, various fault types are studied at 40 evenly distributed distances on every line with 0 Ω and 25 Ω of fault resistance. The *WSSR* index and the calculated fault distance are the criteria employed for the identification of the faulted line.

Simulations show that the precision of faulted-line identification is more affected by the fault current of IBRs following faults closer to substations. Hence, the results are only reported for faults within 0% to 20% and 80% to 100% of line lengths. Table 4.13 shows the obtained results in terms of average fault distance error (AFDE) and line identification failure rate (LIFR). The average fault distance obtained between 80 ms and 120 ms following the fault onset is used to calculate AFDE. The method's success rate in identifying the faulted line is more than 99% providing higher accuracy in the fault distance calculation. Disregarding the presence of IBRs results in a larger *WSSR* for the faulted line and introduces excessive errors in the fault distance calculations. These are the reasons that the existing methods lead to a noticeably lower success rate and accuracy as compared with the proposed method.

### B. Method's Computation Time

Once a sufficient number of PMU data is delivered to the control centre, WABP should promptly pinpoint the faulted line. Because of the linearity of the formulation, the *WSSR* indices can be calculated using a limited number of arithmetical operations. The product $\boldsymbol{S}^*\boldsymbol{R}^{-1}\boldsymbol{S}$ in (2.10) can be computed and saved in memory offline. Accordingly, the real-time calculation of the *WSSR* for every line in each iteration entails $Np(Np+1)$ multiplication and $(Np+1)(Np-1)$ addition operations, where $Np$ is the size of the measurement vector. Moreover, as per the extensive simulations conducted, the average number of iterations required for estimating the superimposed currents of unmonitored IBRs is 4. Using a PC with a processor of 2.8 GHz and RAM of 8 GB, the whole process for all lines, including the calculation of superimposed currents of unmonitored IBRs, takes less than 5 ms on average, which is eligible compared to communication latencies [97]. The technique introduced in [66] can be leveraged to further reduce the computation time. Reference [70] presents one of the most recent WABP methods for transmission systems. Contrary to the proposed, the method of [70] can only address asymmetrical faults on systems incorporating IBRs with certain basic LVRT characteristics. Running that method on the same test system takes around 50 ms using the same PC. This is ten times greater than the computation time required by the proposed method.

### C. Method's Sensitivity to Input Errors

The method's sensitivity to input errors is evaluated by simulating 200 arbitrary faults across the transmission grid with fault resistances between 0 Ω to 20 Ω. Phasors and parameters are contaminated with normally distributed errors of mean zero. The three-sigma criterion is used to report the error ranges. The procedure is repeated 500 times for each fault case with random input errors, and the obtained results are tabulated in Table 4.14. As can be seen, with up to 4% errors in the measurements, the method's failure rate remains less than 1%. The method's effectiveness in handling measurement errors is because the WLS method exploits the redundancy of the equations to minimise the overall effect of errors. Table 4.14 also summarises the results obtained with errors in the parameters of generators and transmission lines. As can be seen, the method's accuracy slightly decreases with larger parameter errors.

Table 4.14: Method's Sensitivity to Input Errors

| Error Source | Index | Error Range (%) | | | |
|---|---|---|---|---|---|
| | | $\pm 1$ | $\pm 2$ | $\pm 3$ | $\pm 4$ |
| Measured Phasors | LIFR (%) | 0.73 | 0.61 | 0.85 | 0.99 |
| | AFDE (%) | 0.49 | 0.54 | 0.66 | 0.78 |
| Generator Parameters | LIFR (%) | 0.59 | 0.64 | 0.74 | 0.92 |
| | AFDE (%) | 0.61 | 0.68 | 0.72 | 0.87 |
| Line Parameters | LIFR (%) | 0.79 | 0.97 | 1.44 | 1.96 |
| | AFDE (%) | 0.69 | 0.94 | 1.54 | 2.12 |

**D. Method's Sensitivity to PMU Coverage**

The proposed method is not reliant on the full observability of the system. It should be noted that the solvability of the system of equations derived for any candidate faulted line can be verified offline for any set of PMU measurements given [65]. This means the method does not rely upon specific PMU data. As explained, the modified system of equations (4.14) only includes two actual unknowns representing the faulted line. Theoretically, two PMU data with independent equations make (4.14) solvable. Thus, as per the multiplicity of PMU measurements in practice, missing a couple of PMU data is not likely to compromise the solvability of (4.14). However, the availability of a larger number of PMU data is considered an advantage, as it improves the method's accuracy and robustness against measurement errors [12].

The method's accuracy is evaluated for different numbers and locations of PMUs, while phasor measurements are contaminated with up to $1\%$ errors [97]. A total of 100 random PMU placements resulting in a unique solution for (4.14) are studied for a range of different numbers of PMUs. Figure 4.16 shows the LIFR and AFDE indices obtained for the same arbitrary 200 fault cases selected in the previous subsection. As can be observed, the method's reliability and accuracy are enhanced with larger numbers of PMUs. The results also confirm that the loss of a few PMU data does not have a noticeable adverse impact on the method's performance.

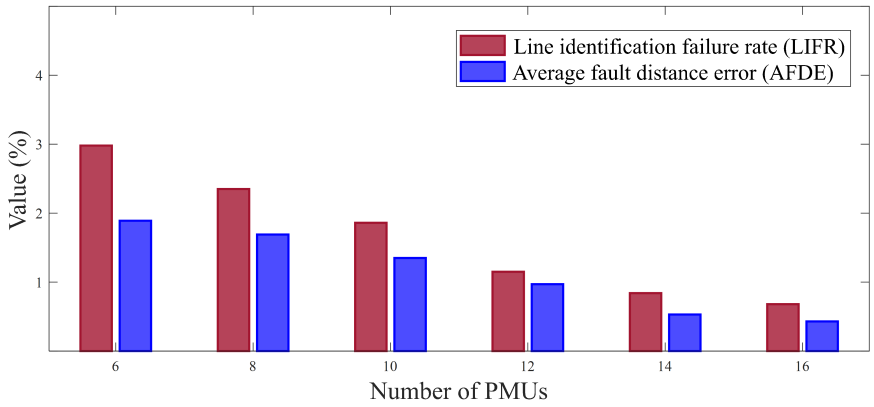


Figure 4.16: Method's sensitivity to the PMU coverage.

Table 4.15: Method's Sensitivity to IBR Penetration Levels and Distributions

| IBRs Penetration | Index | No. of IBRs | | | |
|---|---|---|---|---|---|
| | | 24 | 20 | 16 | 12 |
| 50% | LIFR (%) | 0.59 | 0.49 | 0.46 | 0.51 |
| | AFDE (%) | 0.56 | 0.51 | 0.53 | 0.59 |
| 65% | LIFR (%) | 0.64 | 0.55 | 0.51 | 0.58 |
| | AFDE (%) | 0.59 | 0.61 | 0.63 | 0.67 |
| 80% | LIFR (%) | 0.81 | 0.90 | 0.84 | 0.98 |
| | AFDE (%) | 0.65 | 0.67 | 0.62 | 0.72 |

### E. Impacts of IBRs

The proposed method performs well, irrespective of the number, location, and LVRT characteristics of IBRs. To demonstrate this, three different penetration levels are studied. The slope of the voltage support characteristic of IBRs, i.e., $f^I(V)$, is randomly selected between 2 and 6. A total of 100 random placements of IBRs are considered for each penetration level and number of IBRs. The nominal powers of IBRs are modified based on their number and desired penetration level. Table 4.15 reports the LIFR and AFDE indices obtained for the same 200 fault cases in part C of this subsection. It can be concluded that the method's performance is not noticeably affected by the penetration level, control settings, and location of IBRs.

## 4.6 Summary

A WABP method for transmission systems with high penetration of renewable energy sources was put forward in this chapter. An efficient technique was proposed to capture the behaviour of non-synchronous generations during faults based on their control strategies. The formulations were focused on well-established strategies of inverter-based resources in the Grid Codes and literature. The superimposed circuit technique was used for deriving an overdetermined system of linear equations with reference to the short-circuit fault in question. This results in robust fault location based upon the weighted sum of squared residuals concept. It was demonstrated that modelling all IBRs as unknown current sources may render the system of equations unsolvable.

The potential solvability issues in the negative-sequence circuit were minimised by modelling a limited number of IBRs as current sources. The rest of the IBRs in the negative-sequence circuit were modelled by an equivalent impedance according to their control strategies/settings and overcurrent limits. On the other hand, in the positive-sequence circuit, the solvability issues were avoided by excluding the currents of unmonitored IBRs (those without PMUs) from the set of unknowns. It was demonstrated that the presence of these IBRs can easily be taken into account using the *Substitution Theorem* and the IBRs' low-voltage ride-through (LVRT) characteristics.

The faulted line was readily identified by comparing the weighted sum of squared residuals calculated for candidate lines. The method requires neither full network observability nor any certain set of PMU data to function properly. These features make the proposed method flexible in the face of PMU data loss caused by communication latencies and PMU failures. The method can readily take into account different control strategies and LVRT characteristics imposed upon IBRs by the Grid Code. Extensive simulations conducted show that the proposed method is highly robust against factors such as measurement and parameter errors. The proposed method outperforms existing WABP methods in a wide variety of conditions examined. This is the case irrespective of the fault type, IBR penetration level, locations, control strategies, and LVRT characteristics.

# CHAPTER 5

## WABP Using Sparse/Delayed Synchronised/Unsynchronised PMU Measurements

## 5.1 Overview

To be practical, WABP must be able to make reliable decisions in near real-time. It must also be robust against the insufficiency of PMU data, various reporting rates of PMUs, communication failure, and latencies, and the loss of the time-synchronisation signal (LTSS). The WABP methods that require the availability of PMUs at certain locations can not be implemented in practice. Even if all buses are equipped with PMUs, these methods might fail in the case of a PMU malfunction or partial communication failure. Existing WAFL methods are not suitable for WABP due to technical difficulties attached to their nonlinear formulations and, thus, iterative solutions. These methods are computationally demanding and not flexible enough to deal with practical challenges. As they are essentially designed for offline calculations, the inherent attributes of these methods make them unsuitable for WABP.

Communication latency is a practical challenge faced by all real-time wide-area applications. Indeed, data associated with the same time instant from different PMUs are unlikely to be received simultaneously in the control centre [97]. This calls for defining a maximum wait time to make a decision based on the data received without having to wait for all data to arrive. Another technical difficulty, which is not addressed by the existing methods, is the possibility of having PMUs with different reporting rates. The proposed method accommodates sparse PMU coverage, PMU malfunction, and communication latencies/failures. This is because the method requires neither full network observability nor a fixed set of PMU data, which means a few delayed or missing PMU data can be tolerated.

A novel superimposed-circuit method is proposed in [11, 15, 66, 69] to address practical challenges associated with WABP. However, these methods are vulnerable to temporary LTSS. Building upon the previous methods, [13] reformulates the system of equations as a linear combination of current sources and angle drifts caused by LTSS. In this formulation, the coefficient matrix relies on the measurements, and the outcome can be highly affected by erroneous measurements. Moreover, the solution of this system requires inversions and multiplications of large matrices, which make the formulation computationally inefficient for real-time applications.

This chapter proposes a computationally efficient superimposed-circuit-based WABP method. An index is proposed to identify the faulted line by quantifying the mismatch degree between the observed and expected superimposed phasors. The proposed method works with measurements having different reporting rates and unsynchronised measurements without imposing a significant computational burden. It is robust against measurement and parameter errors and can identify the faulted line through a noniterative formulation regardless of the fault distance, type, and resistance. A simple yet effective technique is proposed to reduce the number of suspected lines as more PMU data is received in the control centre. This is continued until only one line remains, i.e., the faulted line, or the wait time is reached.

## 5.2 Proposed WABP Method

In this section, a coefficient vector relating the voltage and current measurements to the fault current is derived using transfer impedances between measurements and the FL [28]. The transfer impedances are a nonlinear function of the FL, which is not known a priori. Solving this system of equations leads to the exact FL on the faulted line, which is time-consuming. This research focuses on identifying the faulted line rather than unnecessarily spending so much time to find the exact FL on the faulted line. This highly expedites the decision-making process and is similar to what local protection techniques, such as directional overcurrent, differential, and distance protection do to protect transmission lines [2, 7, 8]. To achieve this, the coefficient vectors at two fixed locations on each line are calculated offline. To identify the faulted line, an index is calculated for these locations. This whole process is ultra-fast yet quite reliable, as will be demonstrated in the simulation section.

### 5.2.1 System of Equations for WABP

Let us assume a fault has occurred at distance $\alpha$ on line $i-j$ from bus $i$, as shown in Figure 5.1(a). The fault type determines the interconnection of sequence circuits [2]. Nonetheless, each sequence circuit can be independently analysed regardless of the fault type and resistance [15]. The superimposed circuit in sequence "$s$" is shown in Figure 5.1(b). This circuit only includes one nodal current injection at FL, i.e., $I_f^s$, representing the fault current in that sequence circuit. This is because synchronous generators can be modelled as constant impedances in the

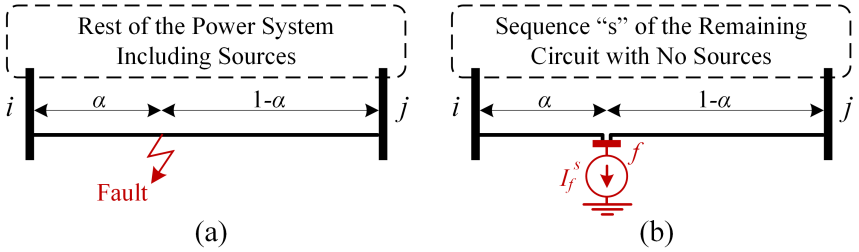


Figure 5.1: (a) Whole faulted circuit. (b) Superimposed circuit representation [16].

superimposed circuit over the time frame of interest [2, 11]. Regardless of the fault type, the fault current path is entirely replaced by the nodal current source $I_f^s$ in each sequence circuit. Thus, the fault resistance is not included in the bus impedance matrix. In this method, the distributed parameter model of the line is used for modelling transmission lines.

Let $\boldsymbol{Z}^s$ denote the pre-fault bus impedance matrix of the sequence circuit "$s$" and bus $f$ represent a virtual bus at the FL. The transfer impedance between a real bus, let us say bus $u$, and bus $f$ can be obtained as follows using entries of $\boldsymbol{Z}^s$, $\alpha$, and the distributed parameters of line $i-j$ [23]

$$Z_{u,f}^{T,s} = \frac{\frac{Z_{i,u}^s}{\sinh(\gamma_{ij}l_{ij}\alpha)} + \frac{Z_{j,u}^s}{\sinh(\gamma_{ij}l_{ij}(1-\alpha))}}{\frac{1}{\sinh(\gamma_{ij}l_{ij}\alpha)} + \frac{1}{\sinh(\gamma_{ij}l_{ij}(1-\alpha))} + \tanh\left(\frac{\gamma_{ij}l_{ij}}{2}\alpha\right) + \tanh\left(\frac{\gamma_{ij}l_{ij}}{2}(1-\alpha)\right)} \tag{5.1}$$

where $l_{ij}$ and $\gamma_{ij}$ denote the length and the propagation constant of the line, respectively. Based on the superimposed circuit representation during a fault on line $i-j$ in Figure 5.1(b), the superimposed voltage at an arbitrary bus $u$ satisfies the following equation

$$\Delta V_u^s = Z_{u,f}^{T,s} I_f^s \tag{5.2}$$

where $Z_{u,f}^{T,s}$ is the transfer impedance between bus $u$ and $f$ in the sequence circuit "$s$", where "$T$" is used to emphasise that $Z_{u,f}^{T,s}$ is different from the entries in the bus impedance matrix. The sending-end superimposed current of line $u$ - $v$, denoted by $\Delta J_{uv}$, can be obtained from

$$\Delta J_{uv}^s = C_{uv,f} I_f^s \tag{5.3}$$

where the derivation of $C_{uv}$ is obtained by (2.6). Regarding available PMU measurements, all

equations of types (5.2) and (5.3) together form an overdetermined system of equations as

$$\boldsymbol{m}^{\text{exp,s}} = \boldsymbol{h}_f^s I_f^s \tag{5.4}$$

where $\boldsymbol{m}^{\text{exp,s}}$ represents the expected superimposed measurement vector induced by the fault current $I_f^s$, and $\boldsymbol{h}_f^s$ denotes the coefficient vector between PMU locations and bus $f$ in the sequence circuit "$s$". Due to the time-invariant behaviour of synchronous machines in the negative-sequence circuit and its higher accuracy than the zero-sequence circuit, the negative-sequence circuit is used for asymmetrical faults, while the positive-sequence circuit is utilised for symmetrical faults. The amounts of negative-sequence components are used to detect asymmetrical faults, as detailed in [13]. For simplicity, the superscript "$s$" is dropped in the rest of the chapter.

### 5.2.2 Optimisation Problem for Identifying the Faulted Line

In the proposed method, the nonlinearity regarding the exact fault distance on the faulted line is avoided using the coefficient vectors for a limited number of fixed *fault location candidates* (*FLC*s). An index is calculated for every coefficient vector using the observed measurement vector. The index quantifies the *mismatch degree* (*MD*) between the expected and observed measurements, irrespective of the unknown fault current. Using this index, an optimisation problem is formulated to identify the faulted line by finding the *FLC* whose coefficient vector has the smallest *MD*.

The following optimisation problem can be solved to find the location of an event at which the expected measurement vector best matches the observed one.

$$\text{event location} = \underset{E\in\mathcal{E}}{\arg\min} \left( \left\| \boldsymbol{m} - \boldsymbol{m}^{\text{exp},E} \right\| \right) \tag{5.5}$$

where $\boldsymbol{m}$ represents the observed measurement vector, and $\varepsilon$ denotes the set of possible events at different locations. Further, $\boldsymbol{m}^{exp,E}$ is the expected measurement vector for event $E$ at a location. However, when $\varepsilon$ is restricted to a set of short circuit faults, (5.5) can be written as below by using (5.4) [101].

$$FLC^* = \underset{\forall FLC}{\arg\min} \left( \min_{I_f} \|\boldsymbol{m} - \boldsymbol{h}_{FLC} I_f\| \right) \tag{5.6}$$

where $FLC^*$ represents the identified $FLC$ which is the closest one to the actual FL. This optimisation problem can be readily solved using dot products. Let us consider two vectors $\boldsymbol{a}$ and $\boldsymbol{b}$ with elements of complex numbers. From linear algebra, it is well-known that the projection of $\boldsymbol{a}$ onto $\boldsymbol{b}$, i.e., $\text{proj}_{\boldsymbol{b}}\, \boldsymbol{a}$, is the vector that minimises $\|\boldsymbol{a} - \boldsymbol{b}k\|$, where $k$ is a complex scalar [102]. The projection of $\boldsymbol{a}$ onto $\boldsymbol{b}$ can be obtained from

$$\text{proj}_b\, \boldsymbol{a} = \underset{k}{\arg\min} \|\boldsymbol{a} - \boldsymbol{b}k\| = \left( \frac{\boldsymbol{a} \cdot \boldsymbol{b}}{\boldsymbol{b}, \boldsymbol{b}} \right)^* \tag{5.7}$$

where $(\cdot)^*$ represents the conjugate operator. Using (5.7), the actual value of $I_f$ in (5.6) can be disregarded. This is achieved by replacing $I_f$ with a complex scalar obtained by (5.7) that results in the best match between the observed and expected measurements for every $FLC$. In other words, the complex scalar minimises the objective function (5.6). This is advantageous because the fault current is an unknown variable in fault location formulations. Accordingly, the following index, which quantifies the minimum mismatch degree between the expected and observed phasors, is calculated regarding the coefficient vector of an $FLC$, i.e., $\boldsymbol{h}_{FLC}$.

$$MD_{m,h_{FLC}} = \left\| \boldsymbol{m} - \boldsymbol{h}_{FLC} \left( \frac{\boldsymbol{m} \cdot \boldsymbol{h}_{FLC}}{h_{FLC} \cdot h_{FLC}} \right)^* \right\| \tag{5.8}$$

Using these indices, the problem (5.6) can be written as

$$FLC^* = \underset{\forall FLC}{\arg\min} \left( MD_{m,h_{FLC}} \right) \tag{5.9}$$

Finally, the line associated with $FLC^*$ is identified as the faulted line. It is worth noting that the $MD$ calculated for an $FLC$ that is exactly located at the true FL, i.e., virtual bus $f$, would be ideally zero if measurements were error-free.

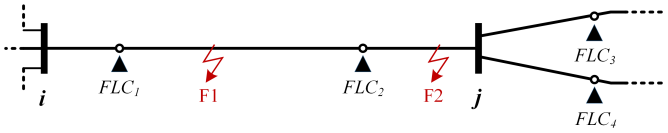


Figure 5.2: Location of *FLC*s on transmission lines [16].

### 5.2.3 Optimal Number and Locations of *FLC*s

The closer the *FLC* is to the true FL, the closer lies the vector $\boldsymbol{h}_{FLC}$ to $\boldsymbol{h}_f$. If an *FLC* does not exactly locate at the FL, its corresponding coefficient vector, i.e., $\boldsymbol{h}_{FLC}$, deviates from the actual fault coefficient vector $\boldsymbol{h}_f$. This means that if an *FLC* is not exactly at the true FL, its corresponding *MD* will be larger. As the faulted line and the fault distance are not known in advance, a trivial approach is to consider many *FLC*s on every line in the set of candidates in (5.9) so that one of the *FLC*s is placed very close to the actual FL. This approach, however, would not be computationally efficient for protection applications, especially in large-scale power systems. More importantly, the proposed WABP method aims to identify the faulted line rather than the exact FL on it. As will be explained later, two *FLC*s at proper locations on every line would be sufficient, providing that the *MD* calculated for at least one of the *FLC*s on the faulted line is smaller than those for all other *FLC*s, irrespective of the fault distance.

The proposed approach for locating the *FLC*s on every line is presented here. As shown in Figure 5.2, consider a fault, e.g., F1, between $FLC_1$ and $FLC_2$ on line $i-j$. This fault will be closer to either $FLC_1$ or $FLC_2$ than other *FLC*s at adjacent lines, regardless of their locations. As a result, the *MD* for $FLC_1$ or $FLC_2$ will be smaller than those for *FLC*s on the adjacent lines. Special considerations should be taken for a fault occurring within the end sections, i.e., between the $FLC_2$ and bus $j$. The *FLC*s around a common bus must be located so that their *MD*s for a fault at the common bus are equal. For example, the *FLC*s around bus $j$ should be located so that

$$MD_{m_j,h_{FLC_2}} = MD_{m_j,h_{FLC_3}} = MD_{m_j,h_{FLC_4}} \tag{5.10}$$

where $\boldsymbol{m}_j$ is the measurement vector induced by an arbitrary fault at bus $j$. In doing so, a fault on an end section, e.g., $F2$ in Figure 5.2, will be closer to the *FLC* on the faulted line, i.e., $FLC_2$. Thus, its corresponding *MD* will be smaller than *MD*s for *FLC*s on the adjacent lines, i.e., $FLC_3$ and $FLC_4$. Using (5.4), $\boldsymbol{m}_j$ can be written as $\boldsymbol{h}_j I_j$, in which $I_j$ represents the fault

current at bus $j$, and $\boldsymbol{h}_j$ is the coefficient vector at this bus. According to (5.8), it can be easily shown that

$$MD_{m_j,h_{FLC_k}} = |I_j| \cdot MD_{h_j,h_{FLC_k}} \tag{5.11}$$

where $|I_j|$ denotes the magnitude of the fault current at bus $j$.

Regardless of $|I_j|$, (5.10) can be written as (5.12) using (5.11).

$$MD_{\boldsymbol{h}_j,\boldsymbol{h}_{FLC_2}} = MD_{\boldsymbol{h}_j,\boldsymbol{h}_{FLC_3}} = MD_{\boldsymbol{h}_j,\boldsymbol{h}_{FLC_4}} \tag{5.12}$$

To locate the *FLC*s around bus $j$, first, the *MD*s between $\boldsymbol{h}_j$ and the coefficient vectors at distance $\beta$ from bus $j$ are calculated for all lines connected to this bus. The location corresponding to the coefficient vector giving the smallest *MD* is taken as the first *FLC*. Without loss of generality, let us assume that $FLC_2$ is determined in this step. Then, $FLC_3$ and $FLC_4$ are located so that (5.12) holds true. This procedure should be done for all buses. As a result, an *FLC* is located at each opposite end of every line. Figure 5.3 shows the flowchart of the process for locating *FLC*s across the system. This process will be further clarified using an example in part B of Subsection 5.3.5.

While the method does not place rigid limits on the value of $\beta$, it should be selected between 0 and 0.5 to ensure that one end section of any line does not overlap with its other end section. However, very small values for $\beta$ result in locating the *FLC*s very close to the common buses, thereby having almost similar coefficient vectors. This might impact the method's performance in correctly identifying the faulted line because of possible measurement and parameter errors. The impact of $\beta$ on the method's success rate on the IEEE 39-bus test system is scrutinised in part A of Subsection 5.3.5.

According to (5.12), all procedures for locating *FLC*s and calculating their coefficient vectors are conducted offline, thereby incurring no during-fault computational burden. Hence, the *MD* indices for every *FLC* using (5.8) can be quickly computed in near real-time. The proposed method proves to be faster than existing methods. A detailed analysis of the computational burden of the proposed method and the most recent existing method is presented in part D of Subsection 5.3.5.

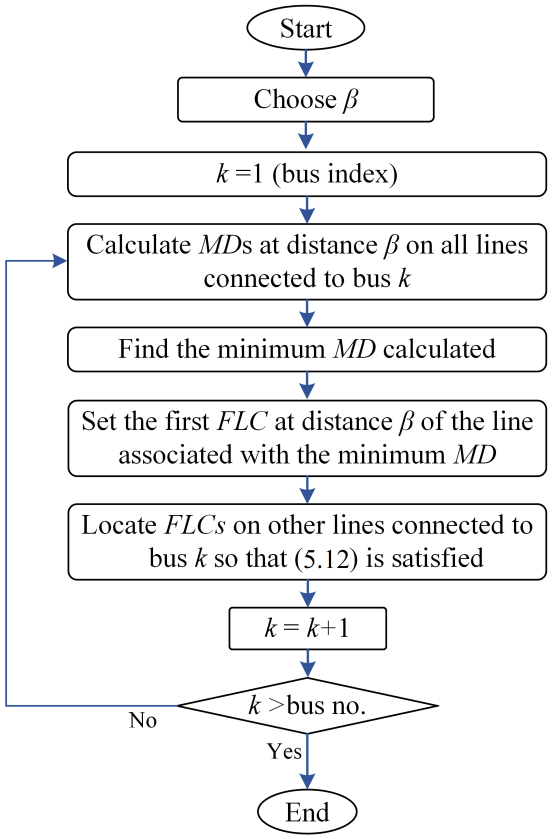


Figure 5.3: Flowchart of the procedure for locating *FLC*s on all lines.

## 5.3 Considerations for Practical Challenges

Wide-area methods are subject to bad data caused by device failures or cyber-attacks. The robustness against cyber-attacks can be enhanced using reliable encryption protocols. Moreover, the proposed indices are calculated based on the well-known least-squares method [102]. This allows for bad data detection approaches, e.g., the largest normalised residual test [80]. As the calculation of *MD*s is not dependent on any specific measurements, removing the equations associated with bad data will not render the formulation unsolvable.

The WABP formulation put forward in the previous section assumes that PMU data are all available. However, this assumption may not hold true in practice for different reasons, such as LTSS, sparse PMU coverage, communication failure, communication latencies, and having PMUs with different reporting rates. This section embeds effective solutions in the

method to ensure the success of WABP in the face of the challenges mentioned. In addition, the fault detection criteria and the interaction logic between the proposed method and the primary protection systems are detailed.

### 5.3.1 Loss of the Time-Synchronisation Signal

Unpredictable factors such as GPS antenna failure, atmospheric disturbances, electromagnetic interference, and cyberattacks may occasionally cause LTSS [22]. However, (5.8) can be utilised to calculate *MD*s with synchronised measurements only. Following an LTSS, the phase-angles of observed phasors will become unreliable. Nevertheless, unsynchronised measurements can still be incorporated into the WABP formulations by only considering their magnitudes. In doing so, the following index will be formed based only on the magnitudes of measurements as *MD* of magnitudes.

$$MD^{mag}_{\boldsymbol{m},\boldsymbol{h}_{FLC}} = \left\| |\boldsymbol{m}| - |\boldsymbol{h}_{FLC}| \cdot \frac{|\boldsymbol{m}| \cdot |\boldsymbol{h}_{FLC}|}{|\boldsymbol{h}_{FLC}| \cdot |\boldsymbol{h}_{FLC}|} \right\| \tag{5.13}$$

where the operator $|\cdot|$ extracts the magnitudes of the elements in a vector. Although the phase angles are not accurate with respect to each other following an LTSS, those provided by PMUs at a substation always remain aligned with respect to the same local time reference [79]. This means there is still useful information in the measurements that can be exploited.

At each bus, a GPS server receives GPS signals as a source to generate the time synchronisation signal. In the event of the loss of the GPS signal, the GPS server continues distributing time signals for the PMUs at that bus using an internal clock [79]. This could introduce a time drift from the accurate time signal of the GPS, which can become unacceptably large if the GPS signal is not restored. However, with or without the GPS signal, the time references for measurements associated with a bus remain the same [30, 79]. Accordingly, to model the impact of LTSS, phase-angles reported by PMUs at buses 1 to $N$ are added by unknown angle drifts, $\theta_1^{\text{LTSS}}, \ldots, \theta_N^{\text{LTSS}}$, respectively. In other words, if the observed measurement vector is sorted as $\boldsymbol{m} = [\boldsymbol{m}_1, \ldots, \boldsymbol{m}_p, \ldots, \boldsymbol{m}_N]$, in which $\boldsymbol{m}_p$ includes measurements associated with bus $p$, we have

$$\angle \boldsymbol{m}_p = \angle \boldsymbol{m}_p^{\text{exp}} + \overrightarrow{\mathbf{1}} \cdot \theta_p^{\text{LTSS}}, \quad 1 \leq \text{p} \leq Np \tag{5.14}$$

where the operator $\angle$ extracts the phase-angle of the elements in a vector. The vector $\boldsymbol{m}_p^{\text{exp}}$

stands for the expected PMU measurements at bus $p$, and $\overrightarrow{1}$ denotes a vector of ones. The vector $\boldsymbol{h}_f$ can also be sorted as $\boldsymbol{h}_f = [\boldsymbol{h}_{f,1}, \ldots, \boldsymbol{h}_{f,p}, \ldots, \boldsymbol{h}_{f,N}]$, where the vector $\boldsymbol{h}_{f,p}$ includes the elements of $\boldsymbol{h}_f$ that are associated with phasors reported by PMUs at bus $p$. As per (5.4), $\angle \boldsymbol{m}_p^{\text{exp}} = \angle \boldsymbol{h}_{f,p} + \overrightarrow{1} \cdot \angle I_f$. Thus, (5.14) can be written as

$$\angle \boldsymbol{m}_p - \angle \boldsymbol{h}_{f,p} = \overrightarrow{1} \cdot \left( \angle I_f + \theta_p^{\text{LTSS}} \right), \quad 1 \leq \text{p} \leq Np \tag{5.15}$$

The right side of (5.15) is a vector with identical elements for phasors associated with the same bus. Variance is a measure of the dispersion of samples in a data set from their mean. It is defined as the average of the squared deviations from the mean. It can be easily confirmed that the vector on the right side of (5.15) has a zero variance, ideally. Based on this property, the following index can be calculated as *MD* of angles for every *FLC*s regardless of the phase angle of the fault current, $\angle I_f$, and LTSS angle drifts.

$$MD^{ang}_{m,h_{FLC}} = \sum_{p=1}^{Np} \text{Var} \left( \angle \boldsymbol{m}_p - \angle \boldsymbol{h}_{FLC,p} \right) \tag{5.16}$$

Finally, the total mismatch degree is obtained using the normalised *MD*s of magnitudes and angles, i.e., $\overline{MD^{mag}_{m,h_{FLC}}}$ and $\overline{MD^{ang}_{m,h_{FLC}}}$. To normalise *MD*s at any time instant, these are divided by the maximum of the *MD*s calculated for that time instant. The share of $\overline{MD^{\text{mag}}_{m,h_{FLC}}}$ and $\overline{MD^{ang}_{m,h_{FLC}}}$ in the total *MD* can be set by two coefficients, $\mathcal{W}_1$ and $\mathcal{W}_2$, as follows

$$MD_{m,h_{FLC}} = \mathcal{W}_1 \cdot \overline{MD^{mag}_{m,h_{FLC}}} + \mathcal{W}_2 \cdot \overline{MD^{ang}_{m,h_{FLC}}} \tag{5.17}$$

Since the faulted line is identified with the minimum *MD*, dividing all *MDs* by the same scalar does not affect the results for the faulted-line identification. Thus, (5.18) can be reformulated as below by dividing both sides by $\mathcal{W}_2$.

$$MD_{\boldsymbol{m},\boldsymbol{h}_{FLC}} = W \cdot \overline{MD^{\text{mag}}_{m,h_{FLC}}} + \overline{MD^{ang}_{m,h_{FLC}}} \tag{5.18}$$

To investigate the impact of $W$ on the success rate of the method, a sensitivity analysis is presented in part A of Subsection 5.3.5.

### 5.3.2 Sparse PMU Coverage

Full network observability is not a prerequisite for the proposed method. Theoretically, the method could identify the faulted line using two PMU data at different locations, providing that the coefficient vectors for the *FLC*s on the faulted line are linearly independent of those on other lines. This is because the fault current can take any value that results in the least mismatch degree between the observed and expected measurements, as in (5.6) and (5.7). From linear algebra [102], the normalised dot product of two linearly dependent vectors is 1 . Based upon this fact, an index quantifying the mutual *dependence degree* $(DD)$ between different coefficient vectors, namely $\boldsymbol{h}_{FLC_u}$ and $\boldsymbol{h}_{FLC_w}$, can be obtained as

$$DD_{FLC_u,FLC_w} = \left| \frac{\boldsymbol{h}_{FLC_u}}{\|\boldsymbol{h}_{FLC_u}\|} \cdot \frac{\boldsymbol{h}_{FLC_W}}{\|\boldsymbol{h}_{FLC_W}\|} \right| \tag{5.19}$$

To account for rounding and parameter errors, it is better to define a security threshold for *DD*, e.g., 0.99, to confirm mutual dependency. Following a fault, the coefficient vectors with a *DD* of 1 will have the same *MD* with respect to the observed measurement vector. Therefore, if their *MD* is smaller than all other candidates, it would not be possible to distinguish the true faulted line between them. However, according to (5.8) and (5.9), the faulted line can be distinctly identified, provided that the coefficient vectors of the faulted line and those of other lines are not mutually dependent.

Unlike existing residual-based methods [11, 13, 15], sparse PMU measurements would never cause unsolvability and singularity issues. This is because there is no matrix inversion in the proposed formulation. Furthermore, all coefficient vectors and their mutual *MD*s can be readily computed offline using the bus impedance matrix and the selected locations for *FLC*s. Hence, prior to the fault onset in a power system with sparse PMU measurements, we know which lines can be uniquely identified if faulted. The lines corresponding to coefficient vectors with mutual *MD*s of 1 will all be identified as suspected lines if a fault occurs on any of them.

### 5.3.3 Communication Latency

As stated in [97], communication latencies may vary from a few milliseconds to even seconds for many reasons, e.g., routing, forwarding, error checking, equipment malfunctions, communication infrastructure limits, and cyber-attacks [103]. The unpredictable behaviour of com-

munication latencies makes it a major challenge to wide-area applications [22]. Hence, WABP should not be dependent on the availability of a fixed set of PMUs as their data might get lost or not received in the action time of WABP. This is not a problem with the proposed method, as it does not place rigid limits on the number and locations of PMUs. Indeed, removing the equations associated with missing/delayed PMU data will not render the WABP formulation unsolvable unless the remaining data are linearly dependent, which is rarely the case. Nevertheless, this might lead to having mutually dependent coefficient vectors, as the dimension of coefficient vectors is determined by the number of PMU data received.

The maximum number of PMU data lost that can be tolerated by the method to distinctly identify the faulted line depends on the faulted line and the locations of PMUs whose data has been successfully collected. For any combinations of received PMU data, however, all *MD*s between different coefficient vectors can be computed offline by (5.19). Thus, for any scenario of loss of PMU data, the system operator would know which lines can be distinctly identified and which lines have the same *MD* if a fault occurs on any of them.

In the desired action time for WABP, the superimposed circuit in Figure 5.1 remains valid. One phasor reported before and one after the fault onset would be enough to obtain the superimposed quantities employed in the system of equations (5.4) [13]. Thus, the method can run properly with PMUs having different reporting rates. The method can function correctly irrespective of the exact time instant at which the phasors have been measured and time-tagged as long as they are within the timeframe of interest for the WABP.

Figure 5.4 illustrates the performance of the proposed method in the presence of communication latencies, which will be further verified by simulations in part E of Subsection 5.3.5. Timelines of time tags and reception time instants of four data, denoted by D1 to D4, with different reporting rates, are shown in Figure 5.4(a). The solid timeline represents the sampling time instant at which the corresponding data are time-tagged by a PMU, while the dashed one shows the time instant at which the data are received at the control centre. Each measured sample and its corresponding received data are numbered by a superscript from 0 onwards. Figure 5.4(b) shows the assumed mutual *MD*s between coefficient vectors for $FLC_1, FLC_2$, and $FLC_3$ on lines L1, L2, and L3, respectively, over time. Assuming that a fault occurs at $t = t_f$, the first post-fault sample $\mathrm{D1}^1$ is received at $t = t_l$. However, as per (5.19), coefficient vectors with merely one element are always linearly dependent, which means they will have a

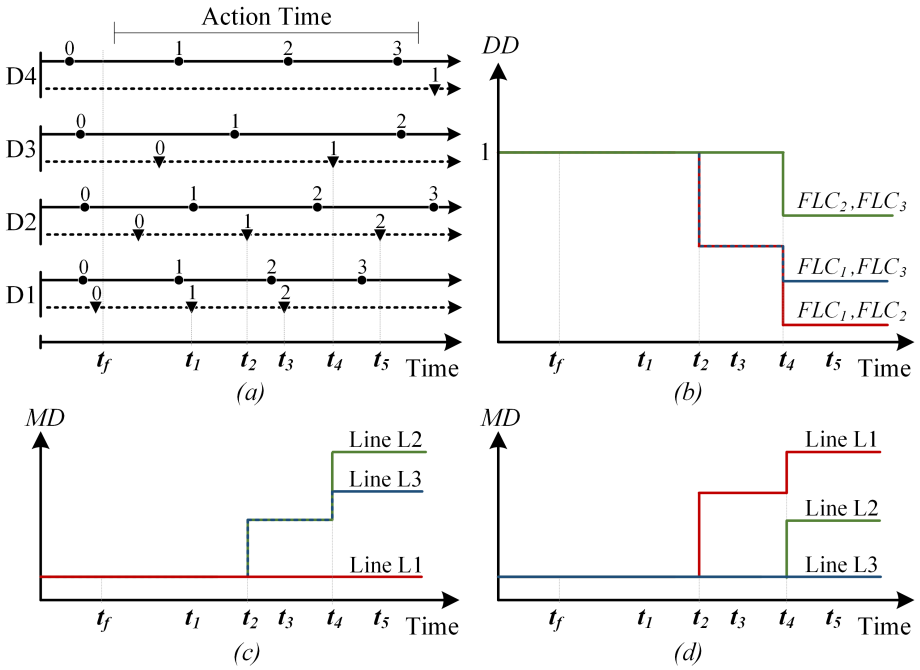


Figure 5.4: (a) Timelines of time-tags and receiving time instant. (b) Mutual *DD*s between coefficient vectors. (c). Calculated *DD*s following a fault on line L1. (d) Calculated *DD*s following a fault on line L3 [16].

*DD* of 1 until $t = t_2$, at which the sample $\mathrm{D2}^1$ is received. As explained, all previous samples of other data received in the action time can be utilised together with new samples.

Having received $\mathrm{D2}^1$, the dimensions of coefficient vectors become two. In this condition, the coefficient vectors of $FLC_2$ and $FLC_3$ are assumed to be linearly dependent, whereas $FLC_I$ is assumed independent of the formers. That is why $DD_{FLC2,FLC3}$ is 1 , and $DD_{FLC1,FLC2}$ and $DD_{FLC1,FLC3}$ are less than 1 after $t = t_2$ until the reception of new data at $t = t_4$. Next, the data sample $\mathrm{D}^1$ is received at $t = t_4$. Consequently, the dimension of coefficient vectors becomes three. Now, they all are assumed to be mutually independent, which is why all mutual *DD*s become less than 1 from $t = t_4$ onwards. In this example, data D4 is not received during the desired action time because of communication failure, so it is not used in the formulation. It is worth noting that at $t = t_3$ and $t = t_5$, the values of D1 and D2 are updated by $\mathrm{D1}^2$ and $\mathrm{D2}^2$, respectively. This, however, does not affect the dimension of the coefficient vectors and the values of *DD*s, but it helps to update *MD*s regarding minor variations of post-fault phasors.

For the scenario described for mutual *DD*s between coefficient vectors, the resulting *MD*s

for a fault on lines L1 and L3 will be as shown in Figures 5.4(c) and 5.4(d), respectively. Until $t = t_2$ in both cases, the *MD*s are the same and remain the minimum because all coefficient vectors are mutually dependent. As can be seen in Figure 5.4(c), for a fault on line L1, the *MD*s of L2 and L3 increase and depart from that of L1 after $t = t_2$. Hence, the faulted line can be discriminately identified from other candidates following $t = t_2$ using only data D1 and D2.

As shown in Figure 5.4(d), for a fault on lines L3 (or L2) between time $t = t_2$ and $t = t_4$, line L1 is excluded from the suspected lines, thus having both L2 and L3 suspected. Although the faulted line is not distinctly identified, the shortage of input data between $t = t_2$ and $t = t_4$ will not render the WABP formulations unsolvable. Instead, valuable information can be derived from the received data to limit the number of suspected lines. Subsequently, more lines can be excluded from the suspected lines by receiving new data. This approach is continued in the action time until only one line remains in the set of suspected lines, e.g., time $t_4$ following the fault onset on L3 in this example. Hence, the faulted line can be correctly identified before the reception of all data, e.g., data D4.

### 5.3.4 Fault Detection and Interaction with Primary Protection

As detailed in part D of Subsection 5.3.5, the computation time of the method is in the order of a few milliseconds. Therefore, the method can continuously run in the control centre to calculate mismatch degrees of magnitudes ($MD^{\text{mag}}$) of all lines using (5.13). In normal conditions, the superimposed quantities and, thus, all $MD^{mag}$ are negligible. After a short circuit fault, mismatch degrees of non-faulted lines move away from zero, while that of the faulted line remains negligible. A fault is detected once both criteria below are met:

- The maximum $MD^{\text{mag}}$ is bigger than a threshold.
- The ratio between the maximum and the minimum $MD^{\text{mag}}$ exceeds another threshold.

In the proposed method, these thresholds are 1 and 5, respectively. One should not use mismatch degrees of phase-angles ($MD^{ang}$) for fault detection because angles of the negligible superimposed quantities during normal conditions are unreliable.

Due to indefinite communication latencies [97], wide-area protection is not typically aimed at providing primary protection but backup protection. However, owing to the low computation burden, the proposed method can be employed in the primary protection system if the communication latencies are limited to tens of milliseconds. Receiving an overriding signal from the

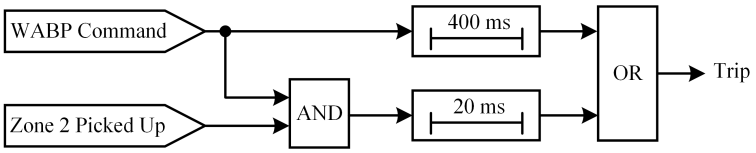


Figure 5.5: Tripping logic of the proposed method [16].

control centre can be extremely helpful in reducing the intentional time delays applied to guarantee the coordination between relays and/or to ensure the fault is within the intended reach.

The main aim of WABP methods is to come into effect in case the primary protection has failed to operate. Thus, a few hundred milliseconds are available to ensure sufficient PMU data have been received at the control centre. The time setting of the method for acting as stand-alone backup protection can be the same as that of the local backup protection relays, e.g., 300-500 ms for transmission level [2, 8]. This time delay ensures that sufficient PMU data has been delivered to the control centre so that the WABP method can decisively pinpoint the faulted line. It should be noted that the WABP command is only sent to the identified faulted line. As a result, the WABP does not take action on the healthy lines.

Figure 5.5 shows the tripping logic incorporating the command generated by the proposed method into the primary protection. In this logic, the WABP commands are used as a permissive signal for permissive overreaching transfer trip protection [7, 8]. Following the reception of a WABP command at a line terminal, the line's circuit breaker is tripped after 20 ms, provided that the primary distance relay is correctly operating and has picked up in its zone 2. This allows for fast fault clearance over 100% of the line length. Moreover, in case of failure/misoperation of the local relay, the method will act as stand-alone backup protection by tripping the circuit breaker after 400 ms from the fault onset.

### 5.3.5 Performance Evaluation

The performance of the proposed method is evaluated by conducting more than 200,000 simulations on the IEEE 39-bus test system with 34 lines. First, the general performance of the method is evaluated for various fault types/resistance at different locations with synchronised and unsynchronised measurements. Next, the sensitivity of the method to inaccuracies in line/generator parameters and measurement errors is scrutinised. Then, the computational burden of the method is compared with that of the most recent method. Finally, the method's

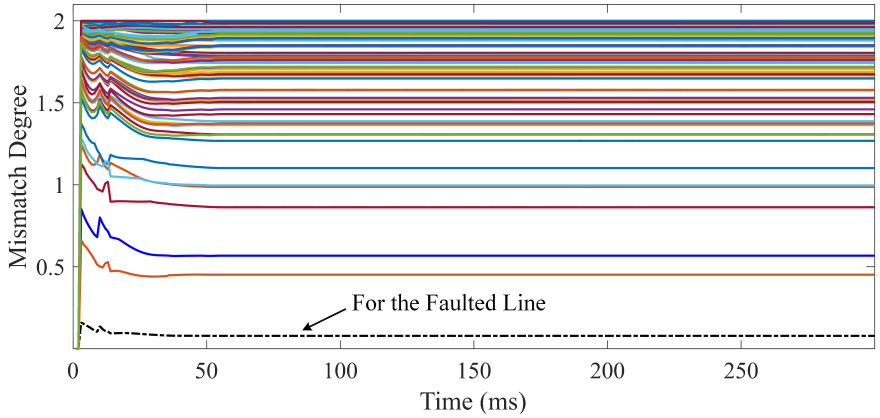


Figure 5.6: Mismatch degrees following a 1-ph-g fault at 20% of line 21-22 [16].

performance in the face of communication latencies and sparse PMU coverage is studied.

These waveforms obtained by DIgSILENT PowerFactory are first filtered by an anti-aliasing Butterworth filter and then sampled with frequency 2 kHz. Finally, the phasors are extracted using the DFT. If higher accuracy is desired, more effective phasor extraction methods, e.g., the complete PMU model in [64], could be used.

To consider compliance specifications of PMUs, magnitude and angle error bounds are combined into a single quantity known as total vector error (TVE) [97]. The IEEE standard for synchrophasor measurements establishes a criterion of 1% for the TVE [97]. Thus, PMU data are manipulated to have a random TVE between 0% and 1% in all conducted simulations. In doing so, a TVE with an evenly distributed random magnitude between 0% and 1% and a random angle between 0 and $2\pi$ is applied to all phasors. The performance of the proposed method for measurements with higher TVEs is studied in part C of this subsection.

### A. General Evaluation of the Proposed Method

The proposed WABP method is first examined through a few arbitrarily selected examples. Buses 3, 5, 8, 11, 14, 16, 19, 23, 25, 27, 29, and 39 are equipped with PMUs. Figure 5.6 shows the normalised *MD*s for all *FLC*s for up to 300 ms after a solid 1-ph-g fault at 20% of line 21-22, where *FLC*s are located with the ratio $\beta$ of 0.1. The coefficient $W$ in (5.18) is chosen at 1. As can be seen, The *MD* corresponding to the *FLC* on the faulted line closer to the actual FL is the smallest with sufficient distinction among that of other lines.

Table 5.1: Success Rate (%) of the Proposed WABP Method

| Fault Type | Synchronised meas. | | | | Unsynchronised meas. | | | |
|---|---|---|---|---|---|---|---|---|
| | 0Ω | 20Ω | 50Ω | 100Ω | 0Ω | 20Ω | 50Ω | 100Ω |
| Symmetrical | 99.74 | 99.69 | 99.52 | 99.31 | 99.18 | 99.07 | 98.92 | 98.75 |
| Asymmetrical | 99.68 | 99.54 | 99.26 | 99.07 | 99.51 | 99.34 | 99.11 | 98.98 |

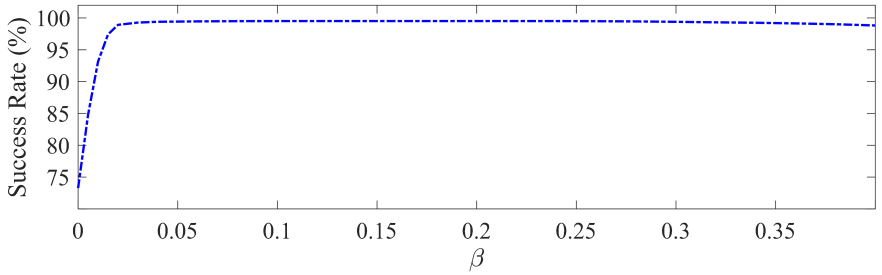


Figure 5.7: Sensitivity of the proposed method to the value of $\beta$ [16].

https://www.overleaf.com/project/64540d4eab632cfeb2eff2e0

The general performance of the proposed method is examined through various fault types at 20 evenly distributed distances on every line with fault resistances of 0 Ω, 20 Ω, 50 Ω, and 100 Ω. Table 5.1 reports the success rate of the proposed method in identifying the faulted line with synchronised and unsynchronised measurements at 60 ms following the fault onset ignoring communication latencies. In this study, $\beta$ and $W$ are set at 0.1 and 1, respectively. The method's sensitivity to $\beta$ and $W$ will also be studied in this subsection. To make measurements unsynchronised, the angles of the phasors associated with each PMU are all added with a random angle drift between 0 and $2\pi$. It can be seen from Table 5.1 that the method is highly successful in faulted line identification irrespective of the fault distance, type, and resistance.

Simulations show that the method is rarely unsuccessful for a few faults very close to a bus in areas with poor PMU coverage. Following a fault very close to a bus without a PMU, the difference between the *MD*s calculated for the *FLC*s around that bus could be quite small. Therefore, input errors might lead to wrong identification of the faulted line. Specifically, the proposed method only failed for a few fault cases at distance 2% of lines 7-8 and 26-27.

The location of *FLC*s is determined by the ratio $\beta$. Here, the sensitivity of the method to $\beta$ is scrutinised. Figure 5.7 shows the success rate of the proposed method with different values

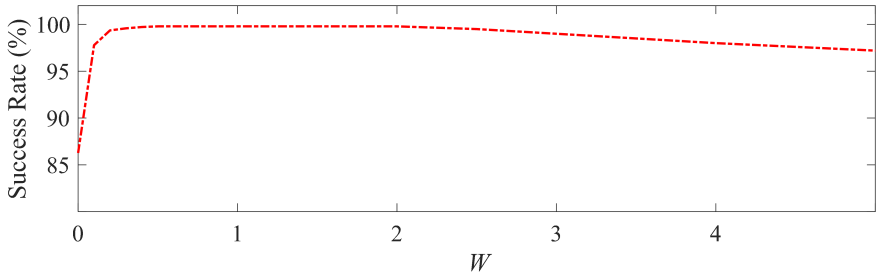


Figure 5.8: Sensitivity of the proposed method to the value of $W$ [16].

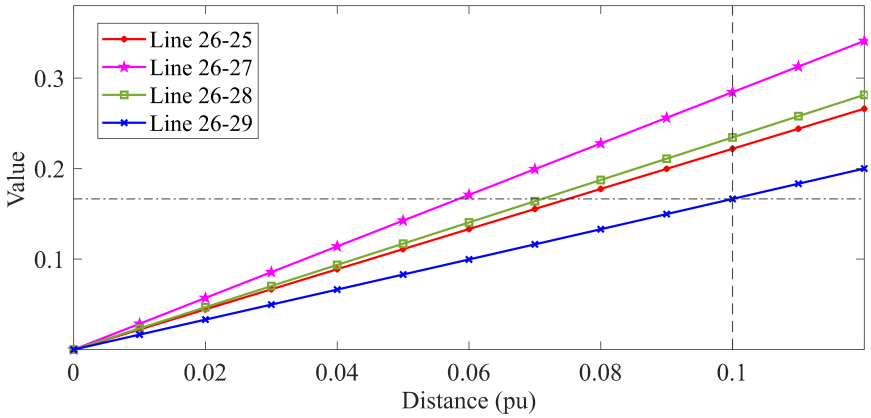


Figure 5.9: Mismatch degree between the coefficient vector at bus 26 and the coefficient vectors at distance 0 to 0.12 pu on all lines connected to bus 26 [16].

of $\beta$ for all fault cases studied in Table 5.1, while the weighting coefficient $W$ is set at 1. As can be seen, the method is not noticeably impacted by $\beta$ in the range [0.03,0.4]. However, too small and very large values for $\beta$ could impair the performance of the method.

The sensitivity of the method with unsynchronised measurements to $W$ is also scrutinised. Figure 5.8 shows the success rate for different values of $W$, with $\beta$ set at 0.1. As can be seen, the success rate of the proposed method is more than 99% for $W$ between 0.3 and 2. The success rate drops to 86% if *MD*s are calculated with either $\overline{MD^{\text{mag}}}$ or $\overline{MD^{ang}}$ only by setting $W \gg 1$ and $W = 0$ in (5.18), respectively.

### B. Procedure for Locating *FLC*s

The procedure for locating *FLC*s around bus 26 is detailed here. Figure 5.9 shows the *MD*s between the coefficient vector at bus 26 and the coefficient vectors at distances 0 to 0.12 pu on all lines connected to this bus. Let us assume $\beta$ is set at 0.1. The location at distance 0.1 on line

Table 5.2: WABP Sensitivity to Measurement and Parameter Errors

| Type of Error | Error Range (%) | | | | |
|---|---|---|---|---|---|
| | $\pm$ 1 | $\pm$ 2 | $\pm$ 3 | $\pm$ 4 | $\pm$ 5 |
| With Measurement Err. | 99.55% | 99.40% | 99.34% | 99.11% | 98.75% |
| With Parameter Err. | 99.36% | 99.18% | 99.07% | 98.72% | 98.33% |

26-29 that gives the smallest *MD* is taken as the first *FLC*. Then, other *FLC*s on lines 26-25, 26-27, and 26-28 are located at distances 0.075, 0.058, and 0.071 on the respective lines so that they have the same *MD* as the selected *FLC* on line 26-29 to satisfy (5.12).

### C. Sensitivity to Measurement and Parameter Errors

This subsection studies the impact of measurement and parameter errors on the performance of the proposed method. To this end, 100 arbitrary faults are applied across the power system. For reporting success rates in Table 5.2, each fault case is repeated 1,000 times for every error range with evenly distributed random errors. The method functions correctly for more than 98.75% and 98.33% of the cases with up to 5% errors in measurements and parameters, respectively.

The method proves to be quite robust against measurement and parameter errors. However, excessive errors in the bus impedance matrix can impair its performance. According to the GB Grid Code, the minimum dependability index of protection systems must be 99%. As reported in Table 5.2, the method is more than 99% successful with reasonable input errors. For example, in IEEE standard C37.118.1, the TVE of PMU measurements is mandated to be less than 1% [97]. In this section, however, larger input errors are only investigated to demonstrate the robustness of the proposed WABP method against excessive measurement/parameter errors.

### D. Computational Burden

All coefficient vectors are computed offline, with no impact on the real-time computational burden of the proposed method. Table 5.3 details the step-by-step number of summation and multiplication operations needed for obtaining the *MD* of a coefficient vector, in which $N_p$ and $N_{pmu}$ denote the number of measurements and PMUs, respectively. In the last row of the table,

Table 5.3: The Computation Burden of Every Mismatch Degree

| Equation | Operation | No. of Mul. | No. of Sum |
|---|---|---|---|
| (5.13) | $x1 = \|\boldsymbol{m}\|.\|\boldsymbol{h}\|$ | $N_p$ | $N_p$ |
| | $x2 = \|\boldsymbol{h}\|.\|\boldsymbol{h}\|$ | $N_p$ | $N_p$ |
| | $\boldsymbol{x3} = \|\boldsymbol{h}\|(x1/x2)$ | $N_p + 1$ | 0 |
| | $MD^{\text{mag}} = \|\|\boldsymbol{m}\| - \boldsymbol{x3}\|$ | $N_p$ | $2N_p$ |
| (5.16) | $\boldsymbol{y1} = \angle\boldsymbol{m} - \angle\boldsymbol{h}$ | 0 | $N_p$ |
| | $y2 =$ mean $(\angle\boldsymbol{m} - \angle\boldsymbol{h})$ | $N_{pmu}$ | $N_p$ |
| | $MD^{\text{ang}} = \|\boldsymbol{y1} - \overrightarrow{\mathbf{1}} \cdot y2\|^2$ | $N_p$ | $2N_p$ |
| (5.18) | Norm. $MD^{\text{mag}}$ and $MD^{ang}$ | $2N_p$ | 0 |
| | $MD = W \cdot \overline{MD^{\text{mag}}} + \overline{MD^{ang}}$ | $N_p$ | $N_p$ |
| | Total | $8N_p + N_{pmu} + 1$ | $9N_p$ |

since $N_p$ is bigger than $N_{pmu} + 1$ in power systems, $N_{pmu} + 1$ is replaced by $N_p$. As a result, the total time needed for calculating all *MD*s, i.e., $T_{\text{total}}$ , is constrained as

$$T_{\text{total}} < 9N_p \left(T_{mul} + T_{\text{sum}}\right) \times N_{FLC} \tag{5.20}$$

where $N_{FLC}$ is the number of *FLC*s, and $T_{mul}$ and $T_{\text{sum}}$ are the time needed for conducting a multiplication and summation operation, respectively. As described in Subsection 5.2.3 the proposed method requires only two *FLC*s on every transmission line. Therefore, the total computation time of all *MD*s can be obtained by replacing $N_{FLC}$ in (5.20) by $2N_L$, where $N_L$ represents the number of transmission lines. Thus, the total time needed for calculating all mismatch degrees is

$$T_{\text{total}} < 18N_L N_p \left(T_{mul} + T_{\text{sum}}\right) \tag{5.21}$$

where $N_L$ and $N_p$ denote the number of transmission lines and measurements, and $T_{mul}$ and $T_{sum}$ are the time needed for a multiplication and summation operation, respectively.

Table 5.4: Computation Time of the Proposed and Existing Methods

| Measurement Type | Synchronised meas. | | Unsynchronised meas. | |
|---|---|---|---|---|
| References | [13] | Prop. | [13] | Prop. |
| 48 measurements<br>34 lines | 20 ms | $< 1$ ms | 50 ms | $< 1$ ms |
| 1000 measurements<br>200 lines | 150 ms | 6 ms | 8400 ms | 10 ms |

It is worth noting that computation time refers to the time needed to make a decision after receiving the PMU data at the control centre and does not account for communication latencies. The existing wide-area fault location methods, such as [23, 25, 43], use computationally expensive nonlinear and iterative approaches for fault location. The most recent WABP method presented by the authors in [13] utilises a noniterative closed-form linear formulation for WABP. That method is, however, computationally demanding compared to the proposed method, especially with unsynchronised measurements. This is because of several transpositions, multiplications, and inversions operations on large matrices in the real-time operation during faults included in [13]. The computation times of the proposed method and [13] with synchronised and unsynchronised measurements for two different power systems are reported in Table 5.4. In this study, a personal computer with a 2.8 GHz processor and 8 GB of RAM is employed. As can be seen, due to the huge computation time, the method [13] would not be advantageous for large power systems with unsynchronised measurements.

**E. Sparse PMU Coverage and Communication Latencies**

As described earlier, the proposed method does not require full network observability or specific PMU placements. Therefore, missing PMU data could be well tolerated. Having said this, however, delayed/missing PMU data or sparse PMU coverage might result in having some *FLC*s with linearly dependent coefficient vectors. As a result, lines with mutually dependent coefficient vectors will be all suspected if a fault occurs on any of them. Even so, the proposed method can identify the faulted line or limit the number of suspected lines based on partially received PMU data. The set of suspected lines may be refined after receiving more data.

Table 5.5: Time-Tags and Delivery Time Instant at Control centre

| PMU's bus | 3 | 8, 11 | 19 | 16 | 25, 29 | 14, 23 | 27 | 5, 39 |
|---|---|---|---|---|---|---|---|---|
| Time-tag | 40 ms | 45 ms | 55 ms | 60 ms | 70 ms | 75 ms | 85 ms | 90 ms |
| Delivery | 60 ms | | 80 ms | | 100 ms | | 120 ms | |

To demonstrate the above point, different communication latencies are assumed for every PMU. To make matters worse, it is assumed that only one post-fault phasor sample is delivered to the control centre from each PMU. Table 5.5 lists the time instant after the fault onset at which PMU data are time-tagged and received at the control centre. Figure 5.10 depicts the *MD*s of all sending-side *FLC*s following a solid 1-ph-g fault at 20% of line 21-22 for up to 150 ms. It can be observed that between 60 ms and 80 ms following the fault onset, the *MD*s belonging to lines 21-22, 22-23, 23-24, and 21-16 are identical and less than all other *MD*s. This means that after collecting data from only three PMUs, the number of suspected lines reduces from 34 to 4. The suspected lines are updated by receiving new data so that between 80 ms and 100 ms, the *MD*s corresponding to non-faulted lines rise, while the *MD* of the *FLC* on the faulted line 21-22 remains the smallest. As a result, line 21-22 is identified as the faulted line using only five PMUs at buses 3, 8, 11, 16, and 19.

As shown in Figure 5.11, the trend of *MD*s can also be verified by the trend of mutual *DD*s. The mutual *DD*s between coefficient vectors of line 21-22 and adjacent lines are all 1 between 60 ms and 80 ms, thereby having the same *MD*s over this period. From 80 ms onwards, the mutual *DD*s drop below 1, resulting in discriminative *MD*s to identify the faulted line.

A comprehensive performance evaluation in the face of communication latencies is conducted here. As described, the calculation of the proposed *MD*s is not dependent on specific measurements. Hence, the method can also be utilised in regional control centres by using only regional measurements as long as the bus impedance matrix is available at these centres. Effective methods such as [89] can be used for accurately estimating the parameters of power system components. These parameters can be utilised to calculate the bus impedance matrix, as detailed in [74]. According to the formulation put forward, the bus impedance matrix of the whole network model is used for the regional implementation of the method. However, the

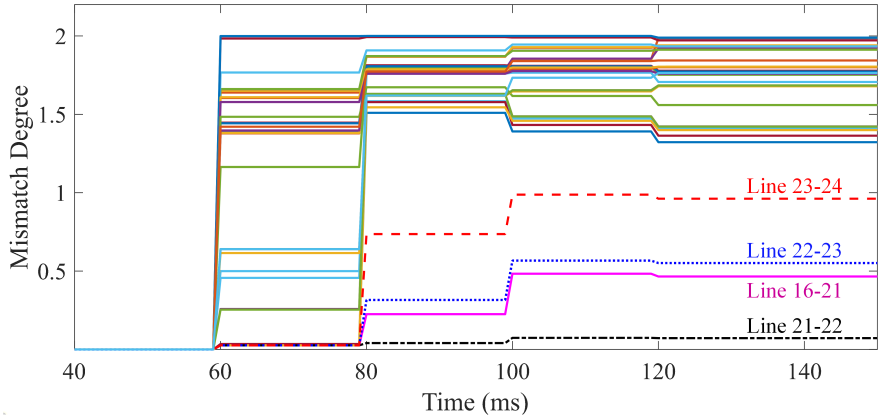


Figure 5.10: Calculated mismatch degrees following a 1-ph-g fault at 20% of line 21-22 considering communication latencies [16].

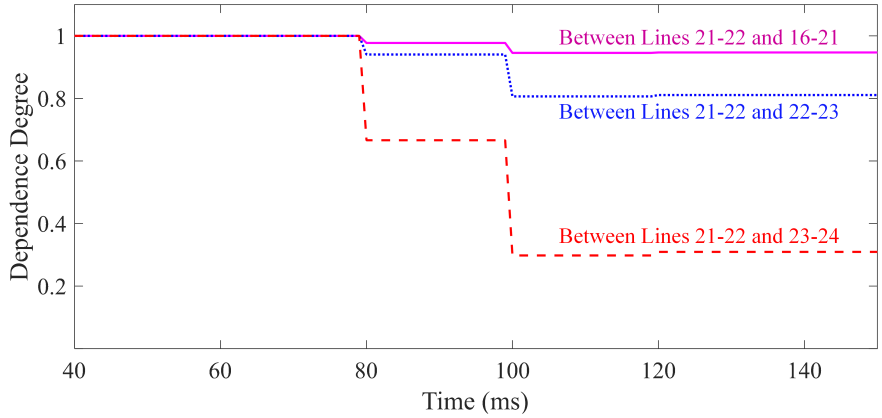


Figure 5.11: Dependence degrees between the faulted line 21-22 and lines 16-21, 22-23, and 23-24 with communication latencies [16].

network model can be efficiently limited to a smaller area whose boundaries are observed by PMUs. This technique has recently been proposed and successfully tested in [15].

To evaluate the method's performance with regional-based calculations versus the centralised large area-based calculations, the test system has been divided into three regions with respect to its geographical characteristics, as shown in Figure 5.12. The proposed method in each regional control centre is assumed to only use data from PMUs installed in that region. Communication latencies can be reduced by dividing a large area into small regions. Thus, in the simulations conducted, communication latencies between PMUs in each region and their associated regional control centre are assumed to be smaller than those between PMUs and the

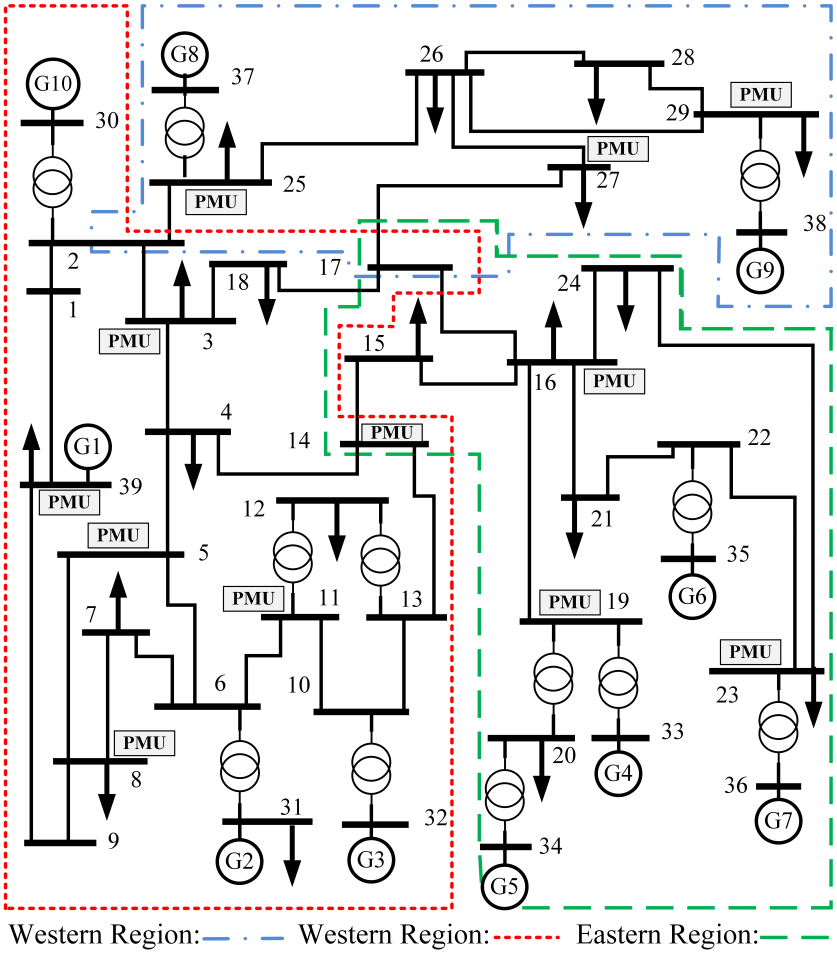


Figure 5.12: Single line diagram of the 39-bus test system divided into three regions [15].

central large-area control centre. Accordingly, regional communication latencies are assumed to have normal distributions with mean 40 ms and standard deviation 10 ms, whereas these for large-area communication are 100 ms and 30 ms, respectively [104].

The same set of 100 arbitrary faults used in part C of this subsection is applied and each fault case is repeated 1,000 times considering random communication latencies for every 12 PMUs. Figure 5.13 shows the distributions of decision time instants after the fault onset with centralised and regional calculations (in the Western region). The average decision time by the method with centralised calculation is around 115 ms after the fault onset. Although the regional centre only uses 6 PMUs, the average decision time is reduced to 61 ms because of smaller communication latencies within the region. The distribution of the number of PMUs

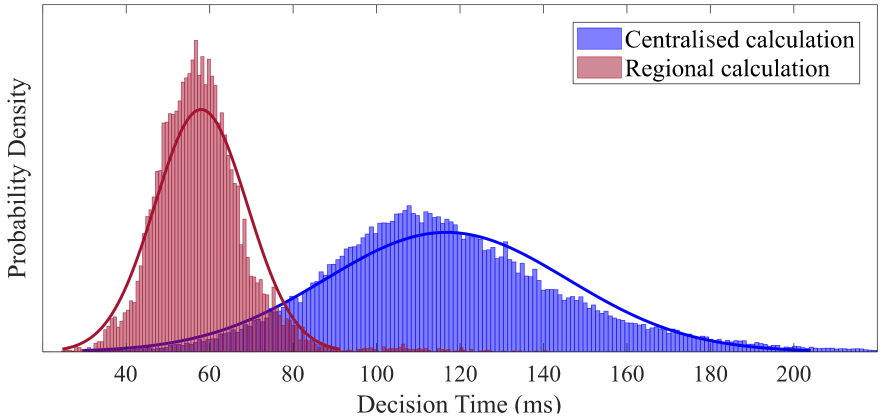


Figure 5.13: Distribution of time instants at which the faulted line is identified [16].

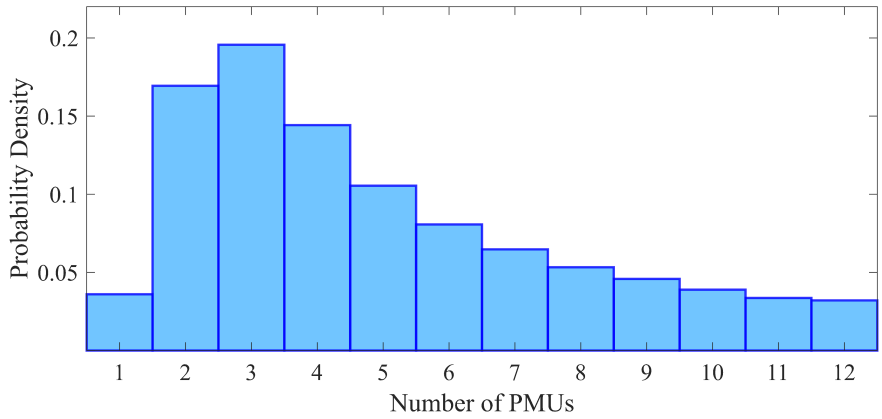


Figure 5.14: Distribution of the number of PMUs whose data are received at the control centre once the faulted line is distinctly identified [16].

whose data are received before making a decisive decision with centralised calculations is shown in Figure 5.14. The average number of PMUs used to make the final decision is only 5. More importantly, these are not predetermined PMUs but those whose data have been received early enough.

### F. Sensitivity to the Presence of Renewables

The presence of renewables has not been addressed by the proposed method. However, due to their smaller fault current contributions compared to those from synchronous generators, low penetration of renewables does not noticeably impair the method's performance. The method's sensitivity to different penetration levels of renewables is studied by adding 20 wind turbines

Table 5.6: Performance of the Proposed WABP in the Presence of Renewables

| Fault Type | IBR Penetration Level (%) | | | | |
|---|---|---|---|---|---|
| | 10 | 20 | 40 | 60 | 80 |
| Symmetrical | 99.13% | 98.75% | 97.66% | 96.13% | 94.43% |
| Asymmetrical | 99.17% | 99.01% | 98.16% | 97.27% | 96.11% |

with the same nominal powers at buses 1, 3, 4, 5, 7, 8, 9, 11, 12, 13, 14, 15, 16, 17, 18, 21, 24, 26, 27, and 28. To model different penetration levels, the nominal powers of renewables are modified based on the desired penetration level. The total active power generation in the system is maintained constant by reducing the synchronous generation. IBRs are assumed to have low-voltage ride-through capabilities defined in the GB Gird Codes. Table 5.6 reports the method's success rate for different fault types across the system in the presence of renewables with various penetration levels. As expected, high penetration of renewables slightly reduces the success rate of the proposed method.

## 5.4 Summary

A WABP method using sparse synchronised/unsynchronised phasor measurements was put forward in this chapter. A computationally efficient formulation was developed to identify the faulted line by quantifying the mismatch degree between the expected and observed superimposed phasors. The impact of unknown angle drifts caused by a temporary loss of the time-synchronisation signal was cancelled out from the formulations. This remarkably reduces the computational burden induced to cope with unsynchronised measurements compared to the existing methods. An index was introduced to determine whether the faulted line can be uniquely identified with any sets of PMU data received. Extensive simulation studies conducted confirm that the method performs well in the presence of communication latencies/failures with PMUs of different reporting rates.

The method is robust against measurement/parameter errors and can quickly identify the faulted line regardless of the fault distance, type, and resistance. The linearity and simplicity of

the derived formulations remove concerns over convergence speed and help to overcome practical challenges such as sparse PMU coverage and communication latencies/failures. Moreover, since no matrix inversion is involved, sparse PMU measurements do not result in unsolvability and singularity issues. These features are beyond the capability of the existing WABP methods.

# CHAPTER 6

Conclusion

## 6.1 Final Remarks

In conclusion, this thesis has brought attention to important viewpoints, introduced innovative methods, and explored previously overlooked areas in the field of WABP, as summarised below

- **Chapters 2** presented a comprehensive study of the superimposed-circuit methodology and its utilisation for WABP. It underscored the considerable potential of this methodology as a robust approach to effectively tackle system-wide practical challenges encountered in real-world scenarios. Moreover, it was also shown that the superimposed-circuit methodology can provide the indispensable prerequisites of WABP that must be met to ensure their practical applicability.

- **Chapter 3** delved into a specific aspect of the superimposed circuit methodology for WAFL/WABP. It was shown that there is a one-to-one equivalence between the responses of the superimposed circuit with and without the faulted line. This means that it is not even needed to replace the faulted line with suitable current sources based on the *Substitution Theorem*. To support the validity of the proposed technique, a proposition was put forward and subsequently proven. This technique reduces the computational burden involved in calculating the bus impedance matrices for each candidate line. The reduced computational burden offered by the proposed technique increases the chances of the uptake of such methods by system operators.

- **Chapter 3** also demonstrated that the distribution of superimposed errors has a considerable impact on the accuracy of WABP/WAFL schemes using the least-squares method. In order to optimise the utilisation of the weighted least-squares method, a comprehensive study was conducted to determine the mean and variance of superimposed errors. By incorporating the derived weight matrix into the formulation, the obtained results exhibit significantly higher accuracy compared to other methods in the literature. The linearity of the formulation and the thorough mathematical derivations of superimposed errors contribute to the feasibility of applying established techniques for detecting bad data.

- **Chapter 4** scrutinised the impact of the high penetration of RESs on the accuracy of existing WABP. It was shown that the presence of RESs is not negligible for WABP methods, yet their consideration can make the WABP formulations nonlinear. Two WABP

methods were presented for transmission systems with a high penetration of RESs while maintaining the formulation linear. These methods utilise the negative- and positive-sequence circuits, respectively, to capture the behaviour of IBRs during faults, based on their control strategies. The proposed methods provide robust faulted line identification based on the concept of the weighted sum of squared residuals. The proposed methods do not require full network observability or a certain set of PMU data to function properly. Additionally, the proposed method can accommodate different control strategies and Low LVRT characteristics imposed upon IBRs by the Grid Codes. It has been demonstrated that the proposed method offers significant advantages over existing methods when applied to transmission systems with a high penetration of renewable energy sources. Thanks to the foregoing advantages, the author believes that the proposed methods are a step forward in the context of promoting and encouraging practical implementations of WABP.

- **Chapter 5** introduced a novel method for WABP utilizing sparse synchronised/ unsynchronised phasor measurements. It was shown that unknown angle drifts caused by TLSS can be removed from the set of WABP equations. This significantly reduces the computational burden associated with unsynchronised measurements compared to existing methods. In this regard, a computationally efficient formulation was developed in order to identify the faulted line by quantifying the mismatch between the expected and observed superimposed phasors. Additionally, the derived formulations exhibit linearity and simplicity, thereby addressing concerns regarding convergence speed and overcoming practical challenges such as sparse PMU coverage and communication latencies/failures. This is because the absence of matrix inversion in the method allows for the resolution of unsolvability and singularity issues. Extensive simulation studies confirm the effectiveness of the proposed method in the presence of TLSS, communication latencies/failures, and PMUs with differing reporting rates. Thanks to the robustness against practical challenges, low-demanding nature, and low data requirements, the proposed method has great potential for employment in practical real-time applications.

## 6.2 Suggestions for Future Works

In consideration of the findings and limitations of this study, several suggestions are offered for future research endeavours in this field.

- Besides short circuit faults on transmission lines, the superimposed-circuit methodology can also be utilised for identifying other types of contingencies, such as generation outages [47, 105] and line outages [14] in the power system. An extension of this research study should focus on integrating the identification of all forms of contingencies into an universal wide-area event identification scheme. Ideally, this wide-area event identification scheme should be capable of identifying multiple events occurring almost at the same time. These include but are not limited to multiple generation outages, the outage of an overloaded line following a generation outage, or asymmetrical faults.

- The proposed WABP methods, like other wide-area methods, may be affected by issues like device failures or cyber-attacks, leading to bad data. Conventional techniques commonly used for identifying bad data, such as LNRT, may not be effective when dealing with complex scenarios involving multiple interacting and conforming bad data. In these cases, measurement errors can align in such a way that fundamental circuit equations such as KCL and KVL still hold [81]. These hard-to-detect bad data could be deliberately injected into the wide-area measurements as part of cyberattacks. Consequently, the development of more robust encryption protocols and enhanced methods for identifying bad data are becoming increasingly indispensable in the context of wide-area applications. As an extension of this study, it is suggested to incorporate an effective bad data detection method into the proposed WABP methods.

- One of the main practical challenges associated with superimposed-circuit-based methods is their dependence on the accuracy of the network bus impedance matrix. The reliability of the results obtained from these methods hinges on the accuracy of the bus impedance matrix. Inaccuracies in the bus impedance matrix can arise from errors in the impedance model of electrical components or discrepancies between the reported and actual topologies of the power system. Although the proposed method is highly robust against parameter errors, it is sensitive to topology errors. Thus, it is imperative for future

research to explore the impact of topology errors on these methods. Furthermore, the development of a technique to identify and rectify significant errors in the bus impedance matrix using PMU data would be highly advantageous.

- The indices in the proposed superimposed-circuit-based WABP methods in this thesis are obtained using weighted least-squares methods. Simulations show that the methods are highly robust against input errors. However, excessive input errors could degrade the performance of the proposed method. Kalman filter is an algorithm commonly used for estimating the state of a dynamic system based on noisy observations. It is particularly useful in situations where there is uncertainty or noise in the measurements. The filter works by combining previous system state information with new measurements to obtain an optimal estimate of the current system state. It takes into account the system dynamics, measurement noise, and the covariance of the state/measurement errors. As an extension of this study, it is suggested to incorporate Kalman filter in the proposed WABP methods, which could hugely improve the robustness of the methods against input errors.

Cutting-edge research is needed to address the research gaps pointed out above. The superimposed-circuit methodology is a powerful tool with the potential to address many of the challenges associated with wide-area event identification. The authors believe this research direction can open the door for advancing wide-area event identification, thus facilitating their uptake by system operators.

# APPENDIX A

dq-Frame Transformation

In a two-axis stationary frame, the space phasor of three arbitrary waveform signals, e.g. $f_a(t)$, $f_b(t)$, and $f_c(t)$ with a summation of zero, is represented as follows:

$$\overline{F}(t) = F_\alpha(t) + jF_\beta(t) \tag{A.1}$$

In which:

$$\begin{bmatrix} F_\alpha(t) \\ \\ F_\beta(t) \end{bmatrix} = \frac{2}{3} \begin{bmatrix} 1 & -\frac{1}{2} & -\frac{1}{2} \\ \\ 0 & \frac{\sqrt{3}}{2} & -\frac{\sqrt{3}}{2} \end{bmatrix} \begin{bmatrix} F_a(t) \\ \\ F_b(t) \\ \\ F_c(t) \end{bmatrix} \tag{A.2}$$

Equation $(A.2)$ can be graphically shown in a complex stationary plane as in Figure A.1, where $\theta(t)$, $\omega(t)$, and $F(t)$ are the instantaneous phase angle, frequency, and magnitude of the three-phase signals, respectively [46]. The space phasor of a balanced three-phase sinusoidal signal rotates at an instantaneous angular velocity of $\omega(t)$ in $\alpha\beta$ frame with a constant magnitude. Therefore, its projections on $\alpha$ and $\beta$ axes oscillate over time.

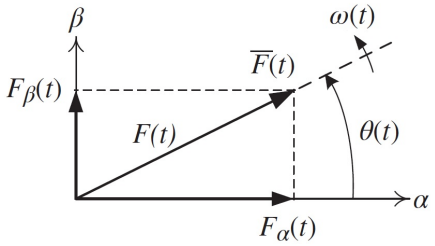


Figure A.1: Space phasor in stationary reference frame [46].

As shown in Figure A.2, a Cartesian frame that rotates at the instantaneous angular velocity, $\omega_r(t)$, is introduced. If $\omega_r(t)$ is set equal to the instantaneous angular velocity of $\overline{F}(t)$, the projections of the phasor on the orthogonal axes of the rotating dq-frame will be time-invariant.

The two-dimensional dq-frame is a helpful tool to convert the problem of controlling three sinusoidal waveforms to the problem of regulating two DC signals. In this regard, the relation between the projection of $\overline{F}(t)$ on orthogonal axes of stationary and rotating reference frames in the positive sequence network is represented through Park transformation as follows:

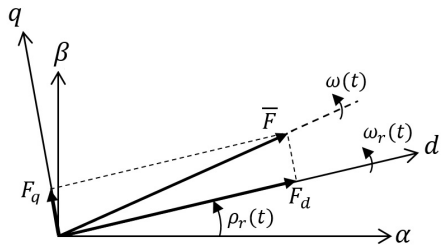


Figure A.2: Space phasors in rotating dq-frame [46].

$$\begin{bmatrix} F_d^p \\ \\ F_q^p \end{bmatrix} = \begin{bmatrix} cos(\rho_r(t)) & sin(\rho_r(t)) \\ \\ -sin(\rho_r(t)) & cos(\rho_r(t)) \end{bmatrix} \begin{bmatrix} F_\alpha^p(t) \\ \\ F_\beta^p(t) \end{bmatrix} \tag{A.3}$$

For the negative sequence network, another rotating reference frame that rotates clockwise at the same angular velocity $\omega_r(t)$ is considered. The projection of $\overline{F}(t)$ in the negative sequence network on orthogonal axes of stationary and rotating reference frames are correlated as bellow:

$$\begin{bmatrix} F_d^n \\ \\ F_q^n \end{bmatrix} = \begin{bmatrix} cos(\rho_r(t)) & -sin(\rho_r(t)) \\ \\ sin(\rho_r(t)) & cos(\rho_r(t)) \end{bmatrix} \begin{bmatrix} F_\alpha^n(t) \\ \\ F_\beta^n(t) \end{bmatrix} \tag{A.4}$$

# BIBLIOGRAPHY


[1] A. G. Phadke and J. S. Thorp, *Computer relaying for power systems*. John Wiley & Sons, 2009.

[2] S. H. Horowitz, A. G. Phadke, and C. F. Henville, *Power system relaying*. John Wiley & Sons, 2022.

[3] A. Yazdani and R. Iravani, *Voltage-sourced converters in power systems: modeling, control, and applications*. John Wiley & Sons, 2010.

[4] V. Terzija, G. Valverde, D. Cai, P. Regulski, V. Madani, J. Fitch, S. Skok, M. M. Begovic, and A. Phadke, "Wide-area monitoring, protection, and control of future electric power networks," *Proceedings of the IEEE*, vol. 99, no. 1, pp. 80–93, 2010.

[5] P. M. Anderson, C. F. Henville, R. Rifaat, B. Johnson, and S. Meliopoulos, *Power system protection*. John Wiley & Sons, 2022.

[6] L. Ramesh, S. Chowdhury, and S. Chowdhury, "Wide area monitoring protection and control - a comprehensive application review," in *10th IET International Conference on Developments in Power System Protection (DPSP 2010). Managing the Change*, pp. 1–4, 2010.

[7] G. Ziegler, *Numerical distance protection: principles and applications*. John Wiley & Sons, 2011.

[8] J. L. Blackburn and T. J. Domin, *Protective relaying: principles and applications*. CRC press, 2015.

[9] V. Telukunta, J. Pradhan, A. Agrawal, M. Singh, and S. G. Srivani, "Protection challenges under bulk penetration of renewable energy resources in power systems: A review," *CSEE journal of power and energy systems*, vol. 3, no. 4, pp. 365–379, 2017.

[10] O. H. Gupta, M. Tripathy, and V. K. Sood, *Protection Challenges in Meeting Increasing Electric Power Demand*. Springer, 2021.

[11] S. Azizi and M. Sanaye-Pasand, "A straightforward method for wide-area fault location on transmission networks," *IEEE Transactions on Power Delivery*, vol. 30, no. 1, pp. 264–272, 2014.

[12] S. Azizi, M. R. Jegarluei, J. S. Cortés, and V. Terzija, "State of the art, challenges and prospects of wide-area event identification on transmission systems," *International Journal of Electrical Power & Energy Systems*, vol. 148, p. 108937, 2023.

[13] S. Azizi, G. Liu, A. S. Dobakhshari, and V. Terzija, "Wide-area backup protection against asymmetrical faults using available phasor measurements," *IEEE Transactions on Power Delivery*, vol. 35, no. 4, pp. 2032–2039, 2019.

[14] S. Azizi, M. R. Jegarluei, A. M. Kettner, and A. S. Dobakhshari, "Wide-area line outage monitoring by sparse phasor measurements," *IEEE Transactions on Power Systems*, 2022.

[15] S. Azizi and M. Sanaye-Pasand, "From available synchrophasor data to short-circuit fault identity: Formulation and feasibility analysis," *IEEE Transactions on Power Systems*, vol. 32, no. 3, pp. 2062–2071, 2016.

[16] M. R. Jegarluei, P. Aristidou, W. Fernandes, and S. Azizi, "Wide-area backup protection using sparse synchronized/unsynchronized pmu measurements," *IEEE Transactions on Power Delivery*, 2023.

[17] A. S. Dobakhshari, "Wide-area fault location of transmission lines by hybrid synchronized/unsynchronized voltage measurements," *IEEE Transactions on Smart Grid*, vol. 9, no. 3, pp. 1869–1877, 2016.

[18] C. Halliday, "Visualization of real-time system dynamics using enhanced monitoring (visor)," 2018.

[19] K. W. Jones, P. Pourbeik, G. Kobet, A. Berner, N. Fischer, F. Huang, J. Holbach, M. Jensen, J. O'Connor, M. Patel, *et al.*, "Impact of inverter based generation on bulk power system dynamics and short-circuit performance," *Task Force on Short-Circuit and System Performance Impact of Inverter Based Generation, Tech. Rep. PES-TR68*, 2018.

[20] S. M. Brahma and A. A. Girgis, "Development of adaptive protection scheme for distribution systems with high penetration of distributed generation," *IEEE Transactions on power delivery*, vol. 19, no. 1, pp. 56–63, 2004.

[21] A. Haddadi, M. Zhao, I. Kocar, U. Karaagac, K. W. Chan, and E. Farantatos, "Impact of inverter-based resources on negative sequence quantities-based protection elements," *IEEE Transactions on Power Delivery*, vol. 36, no. 1, pp. 289–298, 2020.

[22] G. Feng and A. Abur, "Fault location using wide-area measurements and sparse estimation," *IEEE Transactions on Power Systems*, vol. 31, no. 4, pp. 2938–2945, 2015.

[23] A. S. Dobakhshari, "Fast accurate fault location on transmission system utilizing wide-area unsynchronized measurements," *International Journal of Electrical Power & Energy Systems*, vol. 101, pp. 234–242, 2018.

[24] Q. Jiang, X. Li, B. Wang, and H. Wang, "Pmu-based fault location using voltage measurements in large transmission networks," *IEEE transactions on power delivery*, vol. 27, no. 3, pp. 1644–1652, 2012.

[25] N. Kang and Y. Liao, "Double-circuit transmission-line fault location with the availability of limited voltage measurements," *IEEE transactions on power delivery*, vol. 27, no. 1, pp. 325–336, 2011.

[26] X. Tong, X. Wang, R. Wang, F. Huang, X. Dong, K. M. Hopkinson, and G. Song, "The study of a regional decentralized peer-to-peer negotiation-based wide-area backup protection multi-agent system," *IEEE Transactions on Smart Grid*, vol. 4, no. 2, pp. 1197–1206, 2013.

[27] M. Chen, H. Wang, S. Shen, and B. He, "Research on a distance relay-based wide-area backup protection algorithm for transmission lines," *IEEE Transactions on Power Delivery*, vol. 32, no. 1, pp. 97–105, 2016.

[28] P. V. Navalkar and S. A. Soman, "Secure remote backup protection of transmission lines using synchrophasors," *IEEE Transactions on Power Delivery*, vol. 26, no. 1, pp. 87–96, 2010.

[29] P. Kundu and A. K. Pradhan, "Synchrophasor-assisted zone 3 operation," *IEEE Transactions on Power Delivery*, vol. 29, no. 2, pp. 660–667, 2013.

[30] J. Ma, C. Liu, and J. S. Thorp, "A wide-area backup protection algorithm based on distance protection fitting factor," *IEEE Transactions on Power Delivery*, vol. 31, no. 5, pp. 2196–2205, 2015.

[31] S. Gajare, J. G. Rao, O. Naidu, and A. K. Pradhan, "Wide-area measurement system-based supervision of protection schemes with minimum number of phasor measurement units," *Philosophical Transactions of the Royal Society A: Mathematical, Physical and Engineering Sciences*, vol. 375, no. 2100, p. 20160295, 2017.

[32] J. Ma, J. Li, J. S. Thorp, A. J. Arana, Q. Yang, and A. G. Phadke, "A fault steady state component-based wide area backup protection algorithm," *IEEE Transactions on Smart Grid*, vol. 2, no. 3, pp. 468–475, 2011.

[33] W. Li and M. Wang, "Identifying overlapping successive events using a shallow convolutional neural network," *IEEE Transactions on Power Systems*, vol. 34, no. 6, pp. 4762–4772, 2019.

[34] M. K. Neyestanaki and A. M. Ranjbar, "An adaptive pmu-based wide area backup protection scheme for power transmission lines," *IEEE Transactions on Smart Grid*, vol. 6, no. 3, pp. 1550–1559, 2015.

[35] M. Eissa, M. E. Masoud, and M. M. M. Elanwar, "A novel back up wide area protection technique for power transmission grids using phasor measurement unit," *IEEE Transactions on Power Delivery*, vol. 25, no. 1, pp. 270–278, 2009.

[36] Z. He, Z. Zhang, W. Chen, O. P. Malik, and X. Yin, "Wide-area backup protection algorithm based on fault component voltage distribution," *IEEE Transactions on Power Delivery*, vol. 26, no. 4, pp. 2752–2760, 2011.

[37] J. Zare, F. Aminifar, and M. Sanaye-Pasand, "Synchrophasor-based wide-area backup protection scheme with data requirement analysis," *IEEE Transactions on Power Delivery*, vol. 30, no. 3, pp. 1410–1419, 2014.

[38] S.-S. Mirhosseini and M. Akhbari, "Wide area backup protection algorithm for transmission lines based on fault component complex power," *International Journal of Electrical Power & Energy Systems*, vol. 83, pp. 1–6, 2016.

[39] M. Majidi, M. Etezadi-Amoli, and M. S. Fadali, "A sparse-data-driven approach for fault location in transmission networks," *IEEE Transactions on Smart Grid*, vol. 8, no. 2, pp. 548–556, 2015.

[40] G. Gajjar and S. Soman, "Auto detection of power system events using wide area frequency measurements," in *2014 Eighteenth National Power Systems Conference (NPSC)*, pp. 1–6, IEEE, 2014.

[41] Y. Yuan, Y. Guo, K. Dehghanpour, Z. Wang, and Y. Wang, "Learning-based real-time event identification using rich real pmu data," *IEEE Transactions on Power Systems*, vol. 36, no. 6, pp. 5044–5055, 2021.

[42] M. Biswal, S. M. Brahma, and H. Cao, "Supervisory protection and automated event diagnosis using pmu data," *IEEE Transactions on power delivery*, vol. 31, no. 4, pp. 1855–1863, 2016.

[43] Z. H. Rather, Z. Chen, P. Thøgersen, P. Lund, and B. Kirby, "Realistic approach for phasor measurement unit placement: Consideration of practical hidden costs," *IEEE Transactions on Power Delivery*, vol. 30, no. 1, pp. 3–15, 2014.

[44] R. Ma, S. Basumallik, and S. Eftekharnejad, "A pmu-based data-driven approach for classifying power system events considering cyberattacks," *IEEE Systems Journal*, vol. 14, no. 3, pp. 3558–3569, 2020.

[45] H. Li, Z. Ma, and Y. Weng, "A transfer learning framework for power system event identification," *IEEE Transactions on Power Systems*, vol. 37, no. 6, pp. 4424–4435, 2022.

[46] N. Chaudhuri, B. Chaudhuri, R. Majumder, and A. Yazdani, *Multi-terminal direct-current grids: Modeling, analysis, and control*. John Wiley & Sons, 2014.

[47] S. Azizi, M. R. Jegarluei, A. S. Dobakhshari, G. Liu, and V. Terzija, "Wide-area identification of the size and location of loss of generation events by sparse pmus," *IEEE Transactions on Power Delivery*, vol. 36, no. 4, pp. 2397–2407, 2020.

[48] J. J. Chavez, N. V. Kumar, S. Azizi, J. L. Guardado, J. Rueda, P. Palensky, V. Terzija, and M. Popov, "Pmu-voltage drop based fault locator for transmission backup protection," *Electric Power Systems Research*, vol. 196, p. 107188, 2021.

[49] S. R. Samantaray *et al.*, "A differential voltage-based wide-area backup protection scheme for transmission network," *IEEE Systems Journal*, vol. 16, no. 1, pp. 520–530, 2021.

[50] H. K. Zadeh and Z. Li, "Phasor measurement unit based transmission line protection scheme design," *Electric Power Systems Research*, vol. 81, no. 2, pp. 421–429, 2011.

[51] S. Azizi, M. Sanaye-Pasand, and M. Paolone, "Locating faults on untransposed, meshed transmission networks using a limited number of synchrophasor measurements," *IEEE Transactions on Power Systems*, vol. 31, no. 6, pp. 4462–4472, 2016.

[52] Y. Liao, "Fault location for single-circuit line based on bus-impedance matrix utilizing voltage measurements," *IEEE Transactions on Power Delivery*, vol. 23, no. 2, pp. 609–617, 2008.

[53] A. Meghwani, J. Sreenath, S. Srivastava, S. Chakrabarti, and A. Sharma, "Robust event detection using synchrophasor assisted forecasting-aided state estimation," in *2019 IEEE Power & Energy Society General Meeting (PESGM)*, pp. 1–5, IEEE, 2019.

[54] G. Zhang, X. Tong, Q. Hong, X. Lu, and C. D. Booth, "A novel fault isolation scheme in power system with dynamic topology using wide-area information," *IEEE Transactions on Industrial Informatics*, vol. 18, no. 4, pp. 2399–2410, 2021.

[55] Y.-K. Wu, Z.-T. Lin, T.-C. Lee, T.-Y. Hsieh, and W.-M. Lin, "Adaptive setting and simulation of distance protection relay in a long transmission system connected to an offshore wind farm," *Journal of Clean Energy Technologies*, vol. 4, no. 6, pp. 401–407, 2016.

[56] A. Hooshyar, M. A. Azzouz, and E. F. El-Saadany, "Distance protection of lines emanating from full-scale converter-interfaced renewable energy power plantsâ€"part ii: Solution description and evaluation," *IEEE Transactions on Power Delivery*, vol. 30, no. 4, pp. 1781–1791, 2014.

[57] J. Barati, S. G. Seifossadat, and M. Joorabian, "A new adaptive coordination scheme of distance relays in dfig-based wind farm collector lines and transmission line compensated by statcom," *International Transactions on Electrical Energy Systems*, vol. 31, no. 12, p. e13205, 2021.

[58] X. Xie, Y. Zhan, H. Liu, W. Li, and C. Wu, "Wide-area monitoring and early-warning of subsynchronous oscillation in power systems with high-penetration of renewables," *International Journal of Electrical Power & Energy Systems*, vol. 108, pp. 31–39, 2019.

[59] S. Biswal, S. D. Swain, R. D. Patidar, A. K. Bhoi, and O. P. Malik, "Integrated wide-area backup protection algorithm during stressed power system condition in presence of wind farm," *Arabian Journal for Science and Engineering*, vol. 46, no. 10, pp. 9363–9376, 2021.

[60] Y. Fang, K. Jia, Z. Yang, Y. Li, and T. Bi, "Impact of inverter-interfaced renewable energy generators on distance protection and an improved scheme," *IEEE Transactions on Industrial Electronics*, vol. 66, no. 9, pp. 7078–7088, 2018.

[61] K. Jia, Z. Yang, Y. Fang, T. Bi, and M. Sumner, "Influence of inverter-interfaced renewable energy generators on directional relay and an improved scheme," *IEEE Transactions on Power Electronics*, vol. 34, no. 12, pp. 11843–11855, 2019.

[62] M. Popov, J. Chavez, E. M. Carrasco, M. T. V. Martínez, S. B. Vicente, D. López, S. Azizi, and V. Terzija, "Enhancing distance protection performance in transmission systems with renewable energy utilization," in *2020 IEEE PES Innovative Smart Grid Technologies Europe (ISGT-Europe)*, pp. 181–185, IEEE, 2020.

[63] M. A. U. Khan, Q. Hong, A. Egea-Àlvarez, A. Dyśko, and C. Booth, "A communication-free active unit protection scheme for inverter dominated islanded microgrids," *International Journal of Electrical Power & Energy Systems*, vol. 142, p. 108125, 2022.

[64] P. Romano and M. Paolone, "Enhanced interpolated-dft for synchrophasor estimation in fpgas: Theory, implementation, and validation of a pmu prototype," *IEEE Transactions on Instrumentation and Measurement*, vol. 63, no. 12, pp. 2824–2836, 2014.

[65] M. R. Jegarluei, J. S. Cortés, S. Azizi, and V. Terzija, "Wide-area event identification in power systems: A review of the state-of-the-art," in *2022 International Conference on Smart Grid Synchronized Measurements and Analytics (SGSMA)*, pp. 1–7, IEEE, 2022.

[66] M. R. Jegarluei, A. S. Dobakhshari, and S. Azizi, "Reducing the computational complexity of wide-area backup protection in power systems," *IEEE Transactions on Power Delivery*, vol. 37, no. 3, pp. 2421–2424, 2022.

[67] A. S. Dobakhshari and A. M. Ranjbar, "A novel method for fault location of transmission lines by wide-area voltage measurements considering measurement errors," *IEEE Transactions on smart grid*, vol. 6, no. 2, pp. 874–884, 2014.

[68] A. S. Dobakhshari, S. Azizi, M. Paolone, and V. Terzija, "Ultra fast linear state estimation utilizing scada measurements," *IEEE Transactions on Power Systems*, vol. 34, no. 4, pp. 2622–2631, 2019.

[69] M. R. Jegarluei, T. E. El-Gorashi, J. M. Elmirghani, and S. Azizi, "A generalized closed-from solution for wide-area fault location by characterizing the distributions of superimposed errors," *IEEE Transactions on Power Delivery*, vol. 37, no. 6, pp. 5484–5487, 2022.

[70] M. R. Jegarluei, P. Aristidou, and S. Azizi, "Wide-area backup protection against asymmetrical faults in the presence of renewable energy sources," *International Journal of Electrical Power & Energy Systems*, vol. 144, p. 108528, 2023.

[71] M. R. Jegarluei, A. S. Dobakhshari, M. Popov, V. Terzija, and S. Azizi, "Pmu-based backup protection in the presence of inverter-based resources," in *International Conference on Energy Technologies for Future Grids (ETFG)*, pp. 1–6, IEEE, 2023.

[72] J. Bird, *Electrical circuit theory and technology*. Routledge, 2017.

[73] C. D. Meyer, *Matrix analysis and applied linear algebra*, vol. 71. Siam, 2000.

[74] J. J. Grainger and W. D. Stevenson Jr, *Power system analysis*. McGraw-Hill series in electrical and computer engineering, 1994.

[75] H. Saadat *et al.*, *Power system analysis*. Mc- Graw-Hill, 2002.

[76] M. M. Saha, J. J. Izykowski, and E. Rosolowski, *Fault location on power networks*. Springer Science & Business Media, 2009.

[77] N. Tleis, *Power systems modelling and fault analysis: theory and practice*. Elsevier, 2007.

[78] A. Johns and S. Jamali, "Accurate fault location technique for power transmission lines," in *IEE Proceedings C (Generation, Transmission and Distribution)*, vol. 137, pp. 395–402, IET, 1990.

[79] W. Yao, Y. Liu, D. Zhou, Z. Pan, M. J. Till, J. Zhao, L. Zhu, L. Zhan, Q. Tang, and Y. Liu, "Impact of gps signal loss and its mitigation in power system synchronized measurement devices," *IEEE Transactions on Smart Grid*, vol. 9, no. 2, pp. 1141–1149, 2016.

[80] A. Abur and A. G. Exposito, *Power system state estimation: theory and implementation*. CRC press, 2004.

[81] A. S. Dobakhshari, V. Terzija, and S. Azizi, "Normalized deleted residual test for identifying interacting bad data in power system state estimation," *IEEE Transactions on Power Systems*, vol. 37, no. 5, pp. 4006–4016, 2022.

[82] A. M. Kettner and M. Paolone, "On the properties of the power systems nodal admittance matrix," *IEEE Transactions on Power Systems*, vol. 33, no. 1, pp. 1130–1131, 2017.

[83] M. Sipser, "Introduction to the theory of computation," *ACM Sigact News*, vol. 27, no. 1, pp. 27–29, 1996.

[84] S. Azizi, A. S. Dobakhshari, S. A. N. Sarmadi, and A. M. Ranjbar, "Optimal pmu placement by an equivalent linear formulation for exhaustive search," *IEEE Transactions on Smart Grid*, vol. 3, no. 1, pp. 174–182, 2012.

[85] S. Sarri, M. Pignati, P. Romano, L. Zanni, and M. Paolone, "A hardware-in-the-loop test platform for the performance assessment of a pmu-based real-time state estimator for active distribution networks," in *2015 IEEE Eindhoven PowerTech*, pp. 1–6, IEEE, 2015.

[86] J. De La Ree, V. Centeno, J. S. Thorp, and A. G. Phadke, "Synchronized phasor measurement applications in power systems," *IEEE Transactions on smart grid*, vol. 1, no. 1, pp. 20–27, 2010.

[87] M. M. Saha, J. Izykowski, and E. Rosolowski, *Fault location on power networks*, vol. 2. Springer, 2010.

[88] L. Zanni, A. Derviškadić, M. Pignati, C. Xu, P. Romano, R. Cherkaoui, A. Abur, and M. Paolone, "Pmu-based linear state estimation of lausanne subtransmission network: Experimental validation," *Electric Power Systems Research*, vol. 189, p. 106649, 2020.

[89] A. S. Dobakhshari, M. Abdolmaleki, V. Terzija, and S. Azizi, "Online non-iterative estimation of transmission line and transformer parameters by scada data," *IEEE Transactions on Power Systems*, vol. 36, no. 3, pp. 2632–2641, 2020.

[90] X. Song, Y. Wang, W. Hu, and Z. Wang, "Three reference frame control scheme of 4 wire grid-connected inverter for micro grid under unbalanced grid voltage conditions," in *2009 Twenty-Fourth Annual IEEE Applied Power Electronics Conference and Exposition*, pp. 1301–1305, IEEE, 2009.

[91] H. Aji, M. Ndreko, M. Popov, and M. A. van der Meijden, "Investigation on different negative sequence current control options for mmc-hvdc during single line to ground ac faults," in *2016 IEEE PES innovative smart grid technologies conference Europe (ISGT-Europe)*, pp. 1–6, IEEE, 2016.

[92] V. FNN, "Vde-ar-n 4120: Technische regeln fur den anschluss von kundenanlagen an das hochspannungsnetz und deren betrieb (tar hochspannung)," *VDE-Verlag, Berlin*, 2018.

[93] M. Nagpal and C. Henville, "Impact of power-electronic sources on transmission line ground fault protection," *IEEE Transactions on Power Delivery*, vol. 33, no. 1, pp. 62–70, 2017.

[94] "The grid code, national grid electricity system operator limited," tech. rep., Available: https://www.nationalgrideso.com/document/162271/download, 2022.

[95] B. H, H. M, K. H.D., R. R, S. U, and V. J, "Network and system rules of the german transmission system operators," tech. rep., Verband der Netzbetreiber, Germany, Tech. Rep., 2007.

[96] V. d. E. E. I. VDE, "Technical requirements for the connection and operation of customer installations to the high voltage network (tar high voltage)," tech. rep., VDE-AR-N-4130, 2018.

[97] "Ieee standard for synchrophasor measurements for power systems," in *IEEE Std C37.118.1*, IEEE, 2011.

[98] R. Kabiri, D. G. Holmes, and B. P. McGrath, "Control of active and reactive power ripple to mitigate unbalanced grid voltages," *IEEE Transactions on Industry Applications*, vol. 52, no. 2, pp. 1660–1668, 2015.

[99] F. Ghassemi and M. Perry, "Review of voltage unbalance limit in the gb grid code cc. 6.1. 5 (b)," *National Grid, Report*, pp. 14–58, 2014.

[100] F. C. Schweppe and J. Wildes, "Power system static-state estimation, part i: Exact model," *IEEE Transactions on Power Apparatus and systems*, no. 1, pp. 120–125, 1970.

[101] J. E. Tate and T. J. Overbye, "Line outage detection using phasor angle measurements," *IEEE Transactions on Power Systems*, vol. 23, no. 4, pp. 1644–1652, 2008.

[102] H. Anton, *Elementary Linear Algebra 9 th Edition.* Wiley 2003 Support material (s)(vcs, acs, etc). Study guide (s)(if â€¦, 1987.

[103] C. Huang, F. Li, T. Ding, Y. Jiang, J. Guo, and Y. Liu, "A bounded model of the communication delay for system integrity protection schemes," *IEEE Transactions on Power Delivery*, vol. 31, no. 4, pp. 1921–1933, 2016.

[104] M. Chenine and L. Nordström, "Investigation of communication delays and data incompleteness in multi-pmu wide area monitoring and control systems," in *2009 International*

*Conference on Electric Power and Energy Conversion Systems,(EPECS)*, pp. 1–6, IEEE, 2009.

[105] J. S. Cortés, M. R. Jegarluei, P. Aristidou, K. Li, and S. Azizi, "Size/location estimation for loss of generation events in power systems with high penetration of renewables," *Electric Power Systems Research*, vol. 219, p. 109242, 2023.